NBS TECHNICAL NOTE 1015

U.S. DEPARTMENT OF COMMERCE/National Bureau of Standards

Design of a Reflection Apparatus for Laser Beam Profile Measurements

NATIONAL BUREAU OF STANDARDS

The National Bureau of Standards[1] was established by an act of Congress on March 3, 1901. The Bureau's overall goal is to strengthen and advance the Nation's science and technology and facilitate their effective application for public benefit. To this end, the Bureau conducts research and provides: (1) a basis for the Nation's physical measurement system, (2) scientific and technological services for industry and government, (3) a technical basis for equity in trade, and (4) technical services to promote public safety. The Bureau's technical work is performed by the National Measurement Laboratory, the National Engineering Laboratory, and the Institute for Computer Sciences and Technology.

THE NATIONAL MEASUREMENT LABORATORY provides the national system of physical and chemical and materials measurement; coordinates the system with measurement systems of other nations and furnishes essential services leading to accurate and uniform physical and chemical measurement throughout the Nation's scientific community, industry, and commerce; conducts materials research leading to improved methods of measurement, standards, and data on the properties of materials needed by industry, commerce, educational institutions, and Government; provides advisory and research services to other Government agencies; develops, produces, and distributes Standard Reference Materials; and provides calibration services. The Laboratory consists of the following centers:

Absolute Physical Quantities[2] — Radiation Research — Thermodynamics and Molecular Science — Analytical Chemistry — Materials Science.

THE NATIONAL ENGINEERING LABORATORY provides technology and technical services to the public and private sectors to address national needs and to solve national problems; conducts research in engineering and applied science in support of these efforts; builds and maintains competence in the necessary disciplines required to carry out this research and technical service; develops engineering data and measurement capabilities; provides engineering measurement traceability services; develops test methods and proposes engineering standards and code changes; develops and proposes new engineering practices; and develops and improves mechanisms to transfer results of its research to the ultimate user. The Laboratory consists of the following centers:

Applied Mathematics — Electronics and Electrical Engineering[2] — Mechanical Engineering and Process Technology[2] — Building Technology — Fire Research — Consumer Product Technology — Field Methods.

THE INSTITUTE FOR COMPUTER SCIENCES AND TECHNOLOGY conducts research and provides scientific and technical services to aid Federal agencies in the selection, acquisition, application, and use of computer technology to improve effectiveness and economy in Government operations in accordance with Public Law 89-306 (40 U.S.C. 759), relevant Executive Orders, and other directives; carries out this mission by managing the Federal Information Processing Standards Program, developing Federal ADP standards guidelines, and managing Federal participation in ADP voluntary standardization activities; provides scientific and technological advisory services and assistance to Federal agencies; and provides the technical foundation for computer-related policies of the Federal Government. The Institute consists of the following centers:

Programming Science and Technology — Computer Systems Engineering.

[1]Headquarters and Laboratories at Gaithersburg, MD, unless otherwise noted; mailing address Washington, DC 20234.
[2]Some divisions within the center are located at Boulder, CO 80303.

Design of a Reflection Apparatus for Laser Beam Profile Measurements

Eric G. Johnson, Jr.

Electromagnetic Technology Division
National Engineering Laboratory
National Bureau of Standards
Boulder, Colorado 80303

U.S. DEPARTMENT OF COMMERCE, Juanita M. Kreps, Secretary

Jordan J. Baruch, Assistant Secretary for Science and Technology

NATIONAL BUREAU OF STANDARDS, Ernest Ambler, Director

Issued July 1979

NATIONAL BUREAU OF STANDARDS TECHNICAL NOTE 1015
Nat. Bur. Stand. (U.S.), Tech. Note 1015, 124 pages (July 1979)
CODEN: NBTNAE

U.S. GOVERNMENT PRINTING OFFICE
WASHINGTON: 1979

For sale by the Superintendent of Documents, U.S. Government Printing Office, Washington, D.C. 20402

Stock No. 003-003-02103-2 Price $4.00 (Add 25 percent additional for other than U.S. mailing)

TABLE OF CONTENTS

DESIGN OF A REFLECTION APPARATUS FOR LASER BEAM PROFILE MEASUREMENTS*

Eric G. Johnson, Jr.

Measurement of both the irradiance and phase front (the beam profile) in real time from the output of a laser has interest for control of that beam and for efficient energy and economic design of the source and the resulting optical systems. The National Bureau of Standards (NBS) has begun a program to build a unit that can measure, at numerous wavelengths from 1.06 μm to 10.6 μm, a selected spatial sample of the beam profile. This device would have the following features: (1) The different carrier wavelengths use the same apparatus by changing two mirrors. (2) The beam profile is sampled simultaneously with no time-shift distortions. (3) The output data streams documenting the sampled beam profile are continuous and are distorted only by the finite number and the time constants of the detectors. (4) The phase-front information is generated before the detectors create the data streams. (5) The apparatus uses mirrors and a reflection hologram that is computer generated. (6) The unit is calibrated piecewise over the range of relative phase and irradiances for each pair of neighboring sampling holes which are 5 mm apart. (7) The resulting calibrated unit can measure profiles near 10 cm in diameter with phase-front variations of less than 5 wavelengths. (8) The expected response time for measurements as controlled by the electronics is of the order of several tens of nanoseconds.

The design analysis reported here includes: (1) the theory which uses Fourier optics concepts with off-axis reflections and rough surfaces to provide the basis for accurate computer simulation of laser beams; (2) the program, BEAM, which generates the expected behavior of the apparatus under variation of laser wavelength, physical dimensions for curvatures, hologram structure, and changes in positions of the various components; (3) the simulation results which demonstrate the expected characteristics for the apparatus; and (4) the key element in the apparatus, namely the reflection hologram, which requires discussion of the design, construction, and testing of this element.

The Hartmann plate method is described briefly so that a comparison between it and the holographic method can be made. The comparison shows why the holographic method is best for a standard for irradiance and phase-front measurements.

Key words: Beam profile; calibrated system; holography; irradiance; laser diagnostics; phase front.

INTRODUCTION

A previous publication [1] has documented the background for beam profile measurements and has indicated the basis of the holographic method. Here we develop the design details for a reflection system. This technical note presents sequentially the concepts and results necessary to estimate for selected accuracy the allowed range of irradiance levels and phase-front variation for an apparatus using the holographic method. This presentation format has been chosen to give the reader the option either for scanning each section for a sense of the design or for studying the analysis in detail in order to construct a similar apparatus.

---

*Funded in part by the Calibration Coordination Group (CCG) under contract No. 78-109.

The design development, grouped as nine sections, begins in section 2 with a general description of the apparatus and an operation synopsis. The remaining sections detail, in turn, particular points of the design process. We indicate those points below--one for each paragraph.

In section 3, we derive the necessary improvements to the scalar theory for coherent wave propagation under the Fourier optics approximation with due consideration for the surface character of the mirrors and the hologram and for the effects due to off-axis illumination of these optics.

In section 4, we describe the computer program generated from these corrected formulas so the reader can copy and use this program. This program allows a reader to simulate the apparatus before construction. There are numerous adjustment parameters for a given apparatus. It is impossible to select the correct version; rather, we arbitrarily select certain convenient choices and then adjust the remaining parameters to make the design as accurate as possible.

In section 5, with the computer program as given, we apply this capability to study one possible configuration for the 10.6 μm wavelength. Here we select the arbitrary parameters and adjust the remaining parameters to get the optimum system. The numerous quantitative results show what can happen. These results range from alignment with an HeNe laser to sensitivity studies from variation of parameters such as wavelength, equipment dimensions, and curvatures of the mirrors.

Because the apparatus is expected to be used at wavelengths in addition to 10.6 μm and because 1.06 μm has significant use, in section 6 we repeat the process described in the previous section for 1.06 μm wavelength. These results should give the designer a clear picture of how to use the holographic method over a range of wavelengths.

Because these simulations have developed large blocks of apparently unrelated information, in section 7 we extract key results from sections 5 and 6 to establish a pictorial sense for the ideal operations, given these results. Additional simulations are performed here to drive home the capabilities and limits of this apparatus.

Normally in construction of a complex apparatus, there is great interest in the electronics of the device. Here the action of the optics on the laser radiation is more important; therefore, in section 8 we present the details for the surface hologram. This item is a key optical component for successful operation of the apparatus. We discuss the ideal concepts and the practical limitations such as allowed variation of the carrier frequency (wavelength), beam splitting efficiencies, and implications about the ultimate accuracies of the apparatus for beam profile measurements.

To complete the design, we indicate the equipment that can be bought and its approximate cost. Section 9 contains specifications for the equipment. We identify the necessary custom machining for the apparatus. The section also contains a summary on the detector unit which must be custom built. In subsection 9.3 we define some options for construction of the detector unit.

In section 10, we conclude the design phase for the reflection unit by summarizing the estimated cost for construction of the apparatus and by discussing other bottom line issues such as what is the expected accuracy of the device and why the unit is the best system for a standard of beam profile measurements compared with other techniques.

To provide a clear comparison between the holographic and the Hartmann plate methods, we briefly describe in the appendix what the Hartmann plate unit would do for the same design conditions as already detailed for the holographic method.

2. AN OVERVIEW OF THE BASIC APPARATUS

We define the reflection apparatus using the background terminology and concepts described in technical note [1] as a basis for the discussion in this section. In figure 2.1, a block diagram indicates the key optical stages for the unit. We describe the actions of each stage going from the prefilter to the array of detectors in the cross-correlation plane. The construction details and technical limits of the apparatus are relegated to section 9 and its subsections. The details of the hologram are in section 8.

The prefilter has an array of holes with a beam sampling pattern as shown in figure 2.2. The field of view of the apparatus is fixed as a circle 10 cm in diameter. Each hole spatially samples the incident radiation to get a laser beam, 1 mm in diameter, which then undulates through the apparatus. To visualize the action by each stage of the apparatus, we trace in the paragraphs below what happens to one beam, exiting from an arbitrary hole in the prefilter.

The prefilter is located at approximately one focal length (mirror 1) in front of the first Fourier transform mirror. The beam from a single hole in the prefilter becomes an Airy pattern with a flat phase front at approximately one focal length (mirror 1) after the reflection off this mirror.

The magnifying telescope has two mirrors which correctly scale this Airy pattern to the reflection pattern on the hologram. Mirror 2 has its radii of curvature changed to match the wavelength of the incident radiation. The nominal position of this mirror is one focal length (mirror 2) after the Fourier plane of mirror 1. The position of mirror 3 is one focal length (mirror 2) plus one focal length (mirror 3) after the mirror 2.

The properly matched Airy pattern, again with a flat phase front, at the hologram is approximately one focal length (mirror 3) after mirror 3. The surface hologram splits each Airy pattern into a single reflected beam plus eight diffracted beams exiting in a square array all of which diverge around the reflected beam.

The Fourier transform done by mirror 4, located one focal length (mirror 4) after the hologram, causes the resulting nine beams to form a three-by-three array of spots in the Fourier plane of mirror 4, namely one focal length (mirror 4) after this mirror.

Because the detector array has physical constraints that will prevent a match to the pattern at this last Fourier transform, mirror 5 magnifies and images the resulting spot pattern onto a detector array at the cross-correlation plane. Figure 2.3 shows the expected pattern when all holes in the prefilter are illuminated and the wavelength of the carrier frequency is properly matched to the curvatures of the five mirrors. The detector array has a detector at each spot that has only one or two beams contributing to the irradiance on the detector. If maximum accuracy in real time is needed, then there are detectors at the spots which have four-beams contributing to the irradiance at that spot. (At this stage, all phase-front details can be ignored.) Each detector measures the resulting laser power in its intersected spot to produce electrical signals. These signals represent the needed information about the original beam profile at the prefilter plane once the apparatus has been calibrated properly (see [1]).

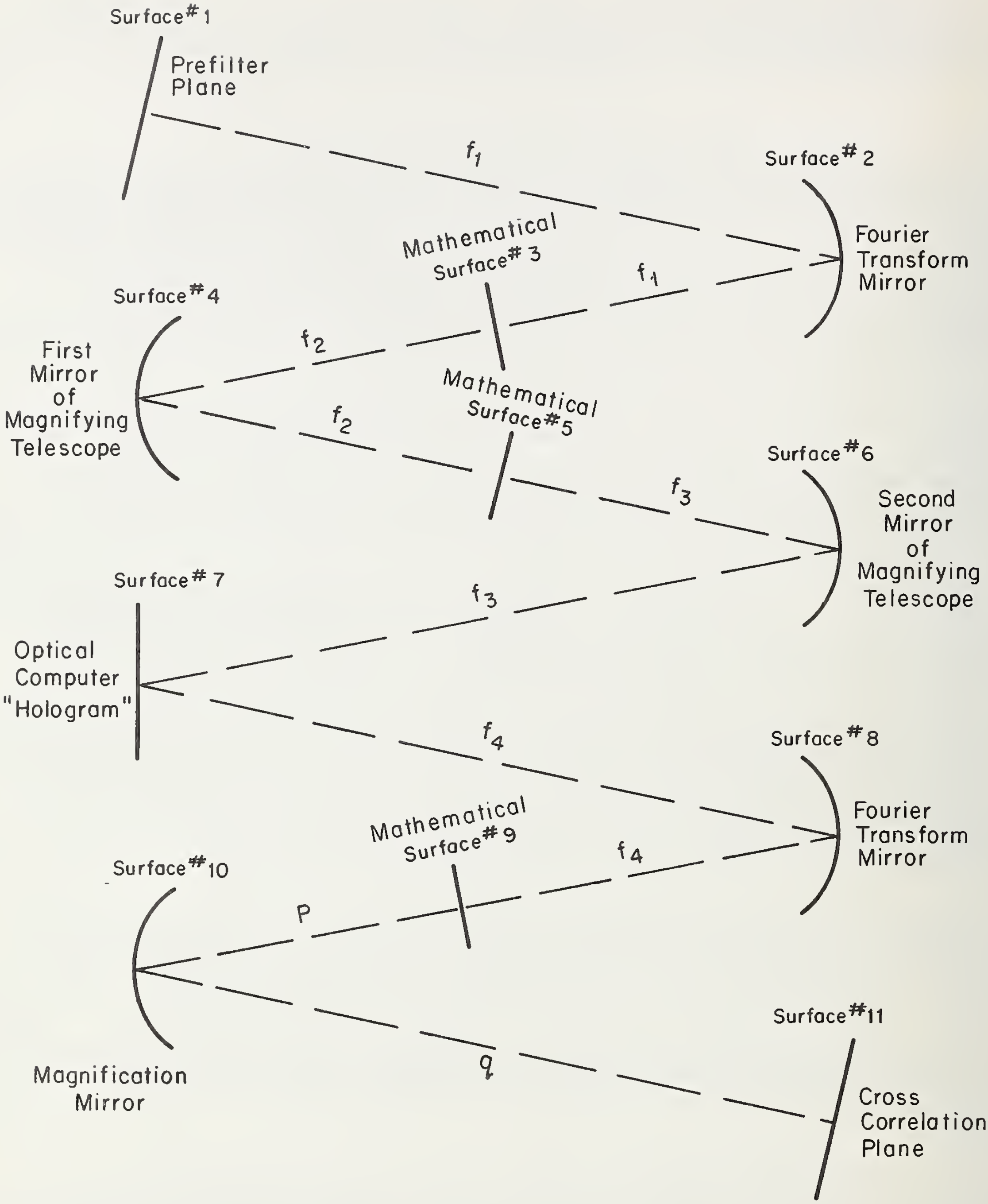

Figure 2.1. Beam profile measuring apparatus using reflection optics (not to scale).

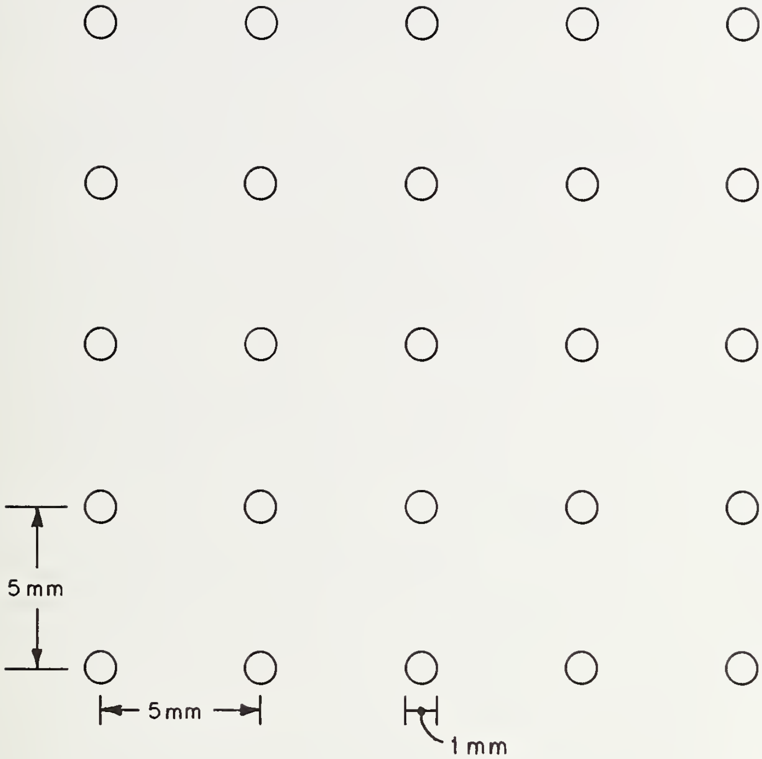

Figure 2.2. Beam sampling pattern in the prefilter plane.

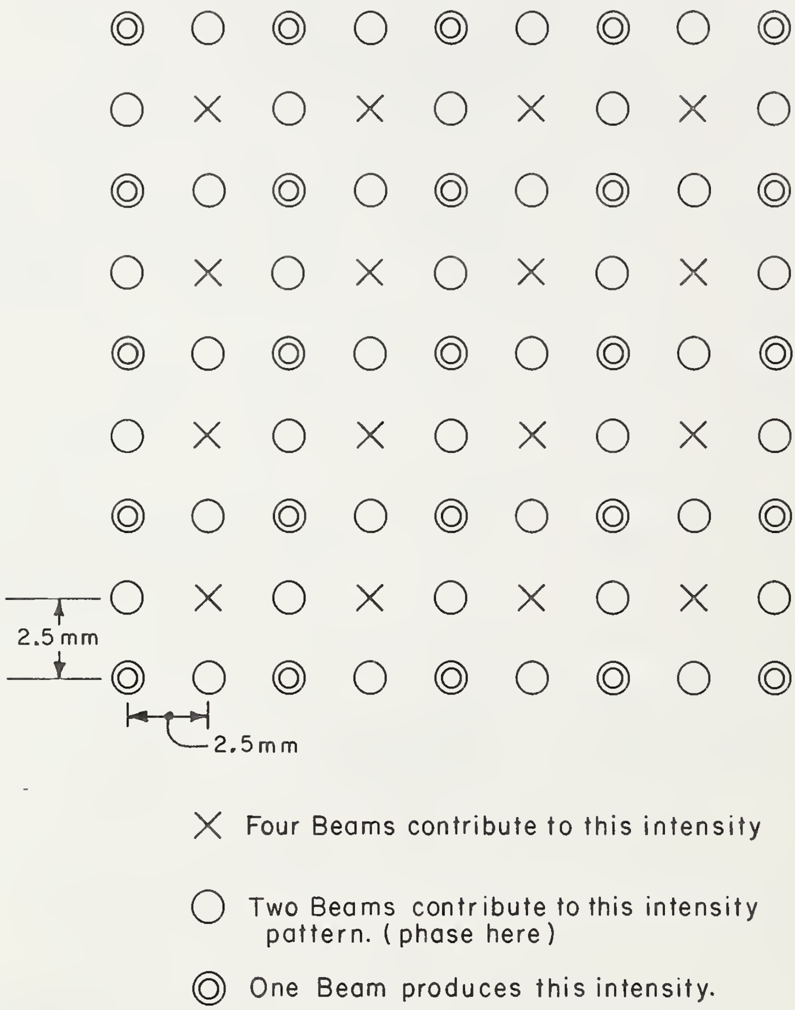

Figure 2.3. Resulting spot pattern in the cross-correlation plane.

3. PRELIMINARY ANALYSIS FOR THE THEORY ACCOUNTING FOR FIRST-ORDER ASTIGMATISM

To deduce the appropriate corrections to the theory of Fourier optics, we must get the proper integral equations to start the approximation sequence. Unlike the usual approximations for Fourier optics, here the source surfaces are not necessarily plane; they can be curved surfaces such as mirrors and bumpy surfaces such as holograms. To reflect this fact, the starting integral equation for approximation is formulated in general coordinates. (NOTE: The polarization features of laser radiation are ignored. See the conclusions in section 10 about this point.)

To make this development specific to the actual apparatus, we follow and define the surfaces illustrated in figure 3.1. Here they are labeled with $\ell = 1$ being the prefilter surface shown in figure 2.1, $\ell = 2$ being the surface of mirror 1, etc. Surfaces 3, 5, and 9 are convenient mathematical surfaces. Here the laser radiation continues without reflection to the next surface. Surfaces 1 and 11 also have no reflections; the rest reflect and may modify both the phase front and the irradiance of a beam. The b_ℓ quantifies the distance along the optical axis of the center laser beam between surfaces ℓ and $\ell + 1$. This diagram assumes the optical axis reflects at a constant angle θ from the normal of each reflecting surface. Obviously, the real apparatus would not do this; therefore, errors arise in the final apparatus from this failure. We ignore this situation and accept that the errors can be minimized by proper adjustments of each mirror. The nonreflecting surfaces are all perpendicular to the optical axis, and the global x, y, and z coordinates for this apparatus have positive z pointing to the right, positive x pointing toward the top of the page, and positive y pointing perpendicular out of the page. Finally, the origin of this coordinate system is at the center of the prefilter. The optical axis of the apparatus is defined by a laser beam exiting from a hole at the center of the prefilter and undulating off the mirrors and hologram until it is captured by the detector that is centered relative to the other detectors at surface 11.

Given the above definitions, we now develop the improved theory accounting for lowest-order astigmatism. To reduce the details in this derivation, we gather key notions from different references so that the resulting corrected, but still approximate, theory is plausible.

For the exact theory for laser radiation, we should use Maxwell's equations. The publication [1] and papers referenced by it establish that the scalar wave equation is adequate for many uses of laser radiation, namely almost plane-wave conditions and no significant polarization effects. Unfortunately, these discussions are primarily transmission analyses where the optical axis is not bent. Because we have reflections, we select the Fresnel equations from [2] when the electric field has only a y component. The other polarization case, namely the magnetic field has only a y component, is ignored in this discussion. The apparatus can be adjusted and calibrated for either polarization condition. However, once the unit has been adjusted for one polarization condition, that adjustment will not apply exactly to the other condition. Small errors in the measured results will occur which are caused by changes in the polarization state of the incident laser beam. Thus, we must select only linearly polarized beams if we are to get results of maximum accuracy. Most uses can accept these small errors.

Figure 3.2 shows the consequence of the reflection to the right from one medium to a second for a plane wave. The mathematical details for the phase functions are:

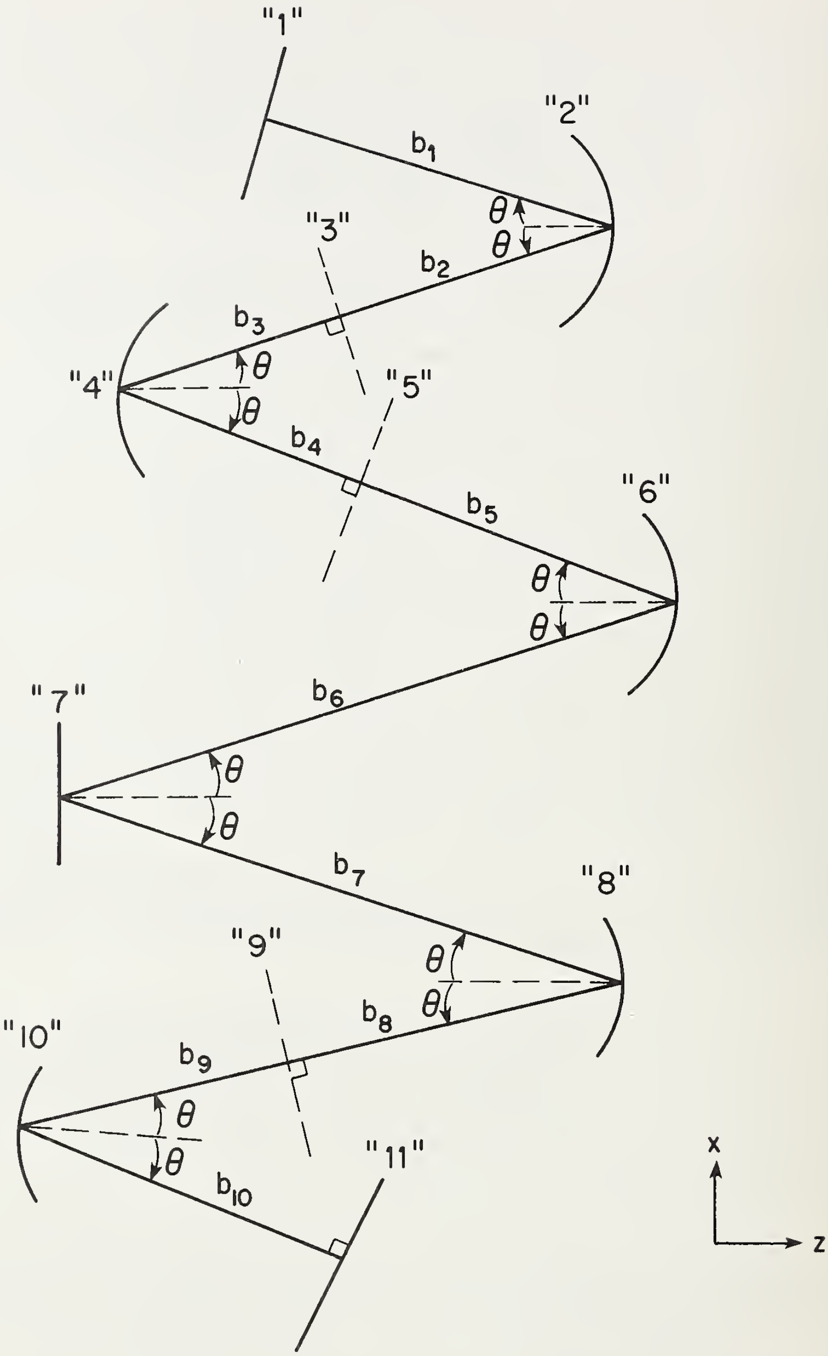

Figure 3.1 The "Surfaces" of the Holographic Apparatus
There are Eleven Such Surfaces

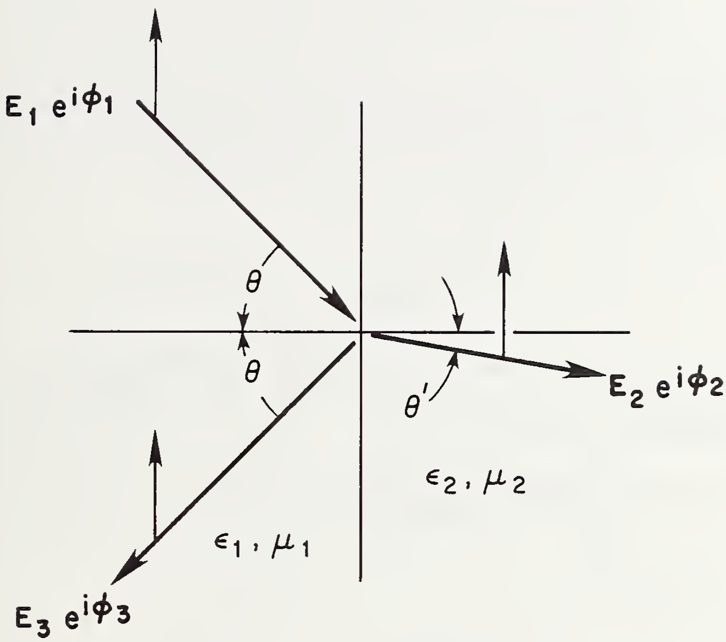

Figure 3.2 The case of plane wave reflection to the right with electric field parallel to reflecting surface

$$\phi_1 = k_1[-(x - x_1) \sin \theta + (z - z_1) \cos \theta],$$

$$\phi_2 = k_1[-(x - x_1) \sin \theta - (z - z_1) \cos \theta], \text{ and}$$

$$\phi_3 = k_2[-(x - x_1) \sin \theta' + (z - z_1) \cos \theta'], \tag{3.1}$$

where:

$$k_1 \equiv k\sqrt{\varepsilon_1\mu_1}\ , \ k_2 \equiv k\sqrt{\varepsilon_2\mu_2}\ , \ n_{21} \sin \theta' = \sin \theta, \ n_{21} = \sqrt{\varepsilon_2\mu_2/\varepsilon_1\mu_1}\ ,$$

and x_1 and z_1 are the coordinates of the origin for the reflection between the two mediums. The mathematical details for the strength of the electric fields are:

$$E_2 = 2 \cos \theta\, E_1/(\cos \theta + n_{21} \cos \theta'), \text{ and}$$

$$E_3 = -E_1(n_{21} \cos \theta' - \cos \theta)/\ n_{21} \cos \theta' + \cos \theta). \tag{3.2}$$

If we have a perfect reflector, that implies $n_{21} = \infty$; hence, $E_2 = \theta' = 0$ and $E_3 = -E_1$. For convenience in this analysis, we assume $u_1\varepsilon_1 = 1$ for propagation in air and set $k_1 = k$ in our subsequent discussion.

Figure 3.3 shows the consequence of the reflection to the left from one medium to a second for a plane wave. The mathematical details for the phase functions are:

$$\phi_a = k[-(x -x_a) \sin \theta - (z - z_a) \cos \theta],$$

$$\phi_b = k[-(x - x_a) \sin \theta + (z - z_a) \cos \theta], \text{ and}$$

$$\phi_c = k_2[-(x - x_a) \sin \theta' + (z - z_a) \cos \theta']. \tag{3.3}$$

The strengths of these electric fields are the same form as before for all values of n_{21}. Here x_a and z_a are the corresponding coordinates for the origin of this reflection.

From the above results for the ideal reflector, we note three points that are used in the scalar theory analysis.

1. The reflected term has a sign change regardless of the direction of the incident beam.

2. For incident wave propagation to the right, the derivative of the reflected term evaluated at $z = z_1$ and normal to that surface is:

$$\frac{d}{dz}(E_3) = -k \cos \theta\, E_3 = k \cos \theta\, E_1.$$

(Here this derivative is toward the reflecting surface.)

3. For incident wave propagation to the left, the normal derivative of the reflected term at $z = z_a$ is:

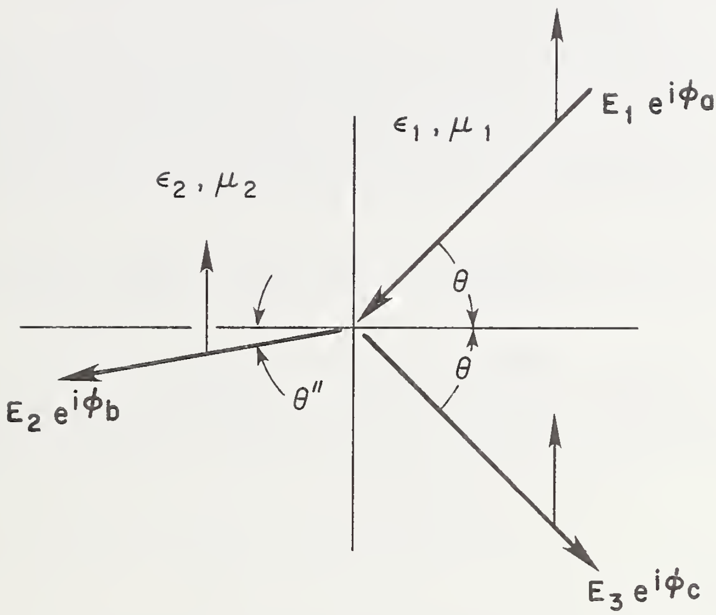

Figure 3.3 The case of plane wave reflection to the left with electric field parallel to reflecting surface

$$\frac{d}{dz}(E_3) = k \cos\theta\, E_3 = -k \cos\theta\, E_1.$$

(Here this derivative is away from the reflecting surface.)

If we make the convention that the normal derivative is away from the reflecting surface into the volume surrounded by these surfaces and make slight notational changes, we have the reflected electric field (ψ_R) related to the incident electric field (ψ_I) as $\psi_R = -\psi_I$ at each surface and the normal derivative as $\nabla_n \psi_R = -k \cos\theta\ \psi_I$ at each surface.

We are ready now to develop the appropriate scalar theory for off-axis reflections. We indicate briefly and somewhat cryptically the approximation sequence in the paragraphs that follow. For more background on this sequence, see [3] for the generalized coordinates, [4] for the Green's function, [5] for various details on aberrations, and [6] for discussion of the Fourier optics approximations.

We get the integral equation first for the scalar theory assuming harmonic time dependence. The scalar function ψ is defined by the Helmholtz equation as:

$$(\nabla^2 + k^2)\ \psi = 0. \tag{3.4}$$

To construct the transfer integral, we use Green's function method, where:

$$(\nabla^2 + k^2)\ G = -4\pi\delta(r - r_o)$$

with the solution

$$G = \exp(ikF)/F, \tag{3.5}$$

where

$$F = [(x - x_o)^2 + (y - y_o^2) + (z - z_o)^2]^{1/2}. \tag{3.6}$$

The integral equation is:

$$\psi(r) = \int dS[-G\ \nabla_n\ \psi(r_o) + \psi(r_o)\ \nabla_n\ G]/4\pi, \tag{3.7}$$

where ∇_n is the operator for normal derivative in r_o coordinates to the surface pointing into the volume. The surface surrounds the volume, and the origin for Green's function singularity is within this surface integration. The range of r is entirely within this volume and this surface. The range of r_o is the surface only.

To make the integral equation useful for simple modeling of the apparatus requires approximations. Basically, the vector features of the electric field is unimportant either left or right between the surfaces shown in figure 3.1. This condition means that the r coordinate is far from the r_o coordinates and that the characteristic phase function is like the plane wave shown in eq (3.1). These facts permit simplification of eq (3.7). For example, the reflected wave leaving a surface at the left and the incident wave ψ_I arriving at that same surface are related as:

$$\psi(r) = ik \cos\theta \int dS\, G\, \psi_I(r_o)/2\pi. \qquad (3.8)$$

In the case where the surface, S, has only transmission through the surface that is normal to the incident beam, the exit beam is related to the incident beam as:

$$\psi(r) = -ik \int dS\, G\, \psi_I(r_o)/2\pi\ . \qquad (3.9)$$

The propagation from right to left is the same form for this apparatus. We can rewrite eqs (3.8) and (3.9) to the form for each surface of the apparatus as:

$$\psi_{\ell+1} = -C_\ell \int du_\ell\, dv_\ell\, A_\ell\, \psi_\ell\, \exp(ikF_\ell)/i\lambda b_\ell, \qquad (3.10)$$

where

$$F_\ell = [(x_{\ell+1} - x_\ell)^2 + (y_{\ell+1} - y_\ell)^2 + (z_{\ell+1} - z_\ell)^2]^{1/2}. \qquad (3.11)$$

Here x_ℓ, y_ℓ, and z_ℓ are the coordinates of the ℓth surface. They are constrained by the surface coordinates u_ℓ and v_ℓ according to the form shown in the next subsection. The surface orientation factor C_ℓ and the surface aperture function A_ℓ are defined as:

$$\begin{aligned} C_\ell &= \cos\theta \qquad \text{for } \ell = 2, 4, 6, 7, 8, 10 \\ &= -1 \qquad\quad \text{for } \ell = 1, 3, 5, 9, 11, \text{ and} \end{aligned} \qquad (3.12)$$

$$A_\ell = \exp[-(u_\ell^2 + v_\ell^2)/p_\ell^2]. \qquad (3.13)$$

The factor A_ℓ is added to original equations to simulate the effects of aperturing by the finite mirrors. This Gaussian form is chosen for convenience and has no major significance beyond the fact that it permits explicit integration of eq (3.10) when the beam is Gaussian and when the F_ℓ has been approximated appropriately. The p_ℓ is the effective width of this Gaussian aperture.

The b_ℓ factor in eq (3.10) is the propagation distance between surfaces at the optical axis; this term is very large compared to any distances due to curvatures and bumps in these two surfaces. Therefore, we can replace the nonphase term F_ℓ by b_ℓ in eq (3.5).

We have completed the initial development of the integral equation for the apparatus. In subsection 3.1 we put in the explict local coordinates for this analysis so that we can extract the lowest-order correction for astigmatism as shown in subsection 3.4. To make the computer program listing convenient, we define a collection of formulas in subsection 3.2. Because we wish to develop various holograms, we note the modulation process at surface 7 in subsection 3.3. In subsection 3.4 we generate three classes of formulas with the necessary corrections for astigmatism [7,8]. We derive: first, the Fourier transform with its associated conditions on curvatures and placement of the mirror; second, the imaging relations by a single mirror with its associated conditions; and third, the formulas that describe coefficients for Gaussian beam propagation through the apparatus. As the final exercise of this section, we apply these results in subsections 3.5.1 and 3.5.2 to the

actual alignment of the apparatus for two beam shapes, namely Gaussian and an initially uniform spot, respectively. This discussion is presented here because the concepts also apply to the computer simulations for fixing the position of the optics. Using the same technique documents how close to ideal the system is before it is constructed.

3.1 The Local Coordinates for the Eleven Surfaces of the Apparatus

In this subsection we develop the local coordinates so that the F_ℓ can be expanded in b_ℓ to reflect the Fourier optics approximation.

The mirror surfaces in the apparatus are approximated here by parabolas defined by curvature functions, h_ℓ, with different radii of curvature possible for the u_ℓ and v_ℓ coordinates, respectively. This means that the actual mirrors with spherical or elliptical surfaces will have some aberrations due to their nonparabolic features. These effects are minimized by proper adjustment of all b_ℓ and by correct placement of the detectors in the cross-correlation plane. For convenience, we use $C1 \equiv \cos\theta$ and $S1 \equiv \sin\theta$ throughout this analysis and in the computer listing. The functional forms for the x_ℓ, y_ℓ, and z_ℓ in terms of local coordinates are:

$$x_\ell = -S1\left(\sum_{j=1}^{\ell-1} b_j\right) + u_\ell |C_\ell| ,$$

$$y_\ell = v_\ell, \text{ and}$$

$$z_\ell = h_\ell + S_\ell g_\ell u_\ell + C1\left(\sum_{j=1}^{\ell-1} b_j S_j\right) . \tag{3.14a}$$

The curvature functions are:

$$h_\ell = (u_\ell^2/d_\ell + v_\ell^2/e_\ell)/2, \tag{3.14b}$$

where the radii of curvatures, d_ℓ and e_ℓ, are less than zero for those left-side mirrors and greater than zero for those right-side ones shown in figure 3.1. Those flat surfaces are simulated by the required curvatures being very large positive numbers. The expression $|C_\ell|$ means the absolute magnitude of C_ℓ is used. The remaining parameters S_ℓ and g_ℓ are defined respectively as:

$$\begin{aligned} S_\ell &= 1 \quad \text{for } \ell = 1, 4, 5, 7, 10, 11 \\ &= -1 \quad \text{for } \ell = 2, 3, 6, 8, 9 \end{aligned} \tag{3.15}$$

and

$$\begin{aligned} g_\ell &= S1 \quad \text{for } \ell = 1, 3, 5, 9, 11 \\ &= 0 \quad \text{for } \ell = 2, 4, 6, 7, 8, 10. \end{aligned} \tag{3.16}$$

In addition, but not shown in eqs (3.14), surface 7 can have a term in z_7 that represents a bumpy surface. This would be added to the h_7 term. For convenience in

subsequent analysis, this term is ignored until subsection 3.3.

To develop the practical transfer function, we now restructure F_ℓ. First note:

$$x_{\ell+1} - x_\ell = W_\ell - S1\ b_\ell,$$

where

$$W_\ell \equiv u_{\ell+1} \left| C_{\ell+1} \right| - u_\ell \left| C_\ell \right| ,$$

$$y_{\ell+1} - y_\ell = v_{\ell+1} - v_\ell \text{ , and}$$

$$z_{\ell+1} - z_\ell = r_\ell + C1(b_\ell S_\ell),$$

where

$$r_\ell = t_\ell + h_{\ell+1} - h_\ell \text{ , and}$$

$$t_\ell \equiv S_{\ell+1}\ g_{\ell+1}\ u_{\ell+1} - S_\ell g_\ell u_\ell .$$

Thus F_ℓ becomes:

$$F_\ell^{\ 2} = b_\ell^{\ 2} + 2b_\ell\ H_\ell + K_\ell \ ,$$

where

$$H_\ell \equiv r_\ell s_\ell C1 - W_\ell\ S1 \text{ , and}$$

$$K_\ell \equiv (v_{\ell+1} - v_\ell)^2 + r_\ell^{\ 2} + W_\ell^{\ 2} \ .$$

The Fourier optics approximation has F_ℓ changed so that only the first three terms in a Laurent series in b_ℓ need be kept. In this case:

$$F_\ell \simeq b_\ell + H_\ell + T_\ell/2b_\ell \ , \tag{3.18}$$

where H_ℓ is as before and

$$T_\ell \equiv K_\ell - H_\ell^{\ 2} = (v_{\ell+1} - v_\ell)^2 + (W_\ell C1 + t_\ell\ S1\ S_\ell)^2. \tag{3.19}$$

The t_ℓ term is an r_ℓ term; however, the Fourier optics approximation neglects the h_ℓ terms in eq (3.19). In contrast, we do not and must not neglect these terms in H_ℓ of eq (3.18), which represent the lowest-order action by each mirror in the apparatus.

3.2 Some Definitions of Terms for Each Surface Used by the Computer Program

This subsection converts the notation and some formulas of the previous subsection to derive as briefly as possible new expressions that use notation and symbols in the computer language BASIC. This exercise simplifies the identification process in the computer program listed in subsection 4.2 and eliminates the extensive subscripting in these equations which makes typing and transcription difficult. During this conversion, there are expressions that mix the two notations. For example, note that an asterisk symbolizes multiplication. It will be present most places except when the local coordinates u_ℓ and v_ℓ are shown in the formulas. The expression "↑" symbolizes exponentiation. It is used when there is squaring of the number. General exponential operations are shown as EXP(X). In this discussion, $\ell \equiv$ L, and $\ell + 1 \equiv$ L1. The imaginary $i = \sqrt{-1}$ is <u>not</u> defined in BASIC; therefore, it is just inserted as needed. We define Z(L) $\equiv \psi_\ell$ as the field function.

$$Y(L) \equiv \mathrm{EXP}\left(\begin{array}{l} D(1,L) + iD(2,L) + u_\ell[D(3,L) + iD(4,L)] \\ + v_\ell[D(5,L) + iD(6,L)] + u_\ell^2[D(7,L) + iD(8,L)] \\ + v_\ell^2[D(9,L) + iD(10,L)] + u_{\ell+1}[E(1,L) + iB(2,L)] \\ + v_{\ell+1}[E(3,L) + iE(4,L)] + u_{\ell+1}^2[E(5,L) + iE(6,L)] \\ + v_{\ell+1}^2[E(7,L) + iE(8,L)] + u_\ell\ u_{\ell+1}[E(9,L) + iE(10,L)] \\ + v_\ell\ v_{\ell+1}[E(11,L) + iE(12,L)] \end{array}\right) \tag{3.20a}$$

is the transfer function between surface L and L1. The D and E are arrays of real numbers fixing this function. Using the array C, we can define:

$$Z(L) \equiv \mathrm{EXP}\left(\begin{array}{l} C(1,L) + iC(2,L) + u_\ell[C(3,L) + iC(4,L)] \\ + v_\ell[C(5,L) + iC(6,L)] + u_\ell^2[C(7,L) + iC(8,L)] \\ + v_\ell^2[C(9,L) + iC(10,L)] \end{array}\right), \tag{3.20b}$$

if the beam profile is Gaussian throughout the apparatus. Otherwise, Z(L) is not simply defined. In any case, eq (3.10) becomes in this notation:

$$Z(L1) = \int du_\ell \, dv_\ell \; Y(L)*Z(L) \; . \qquad (3.20c)$$

To use eqs (3.20) we must fix the D, E, and C set of parameters in terms of the previous definitions. We define:

$$\begin{array}{lll} B(1,L) = 1 & \text{for } L = 1, 5, 7, 11 & \\ \ -1 & \phantom{\text{for } L =}\ 3, 6, 9 & \\ \ 0 & \phantom{\text{for } L =}\ 2, 4, 8, 10 & (3.21) \end{array}$$

$$\begin{array}{lll} B(2,L) = 1 & \text{for } L = 4, 7, 10, 11 & \\ \ -1 & \phantom{\text{for } L =}\ 2, 6, 8 & \\ \ 0 & \phantom{\text{for } L =}\ 1, 3, 5, 9 & (3.22) \end{array}$$

$$\begin{array}{lll} B(3,L) = 1 & \text{for } L = 1, 3, 5, 6, 7, 9, 11 & \\ & \phantom{\text{for } L =}\ 2, 4, 8, 10 & (3.23) \end{array}$$

$$\begin{array}{lll} B(4,L) = 1 & \text{for } L = 2, 4, 6, 7, 8, 10, 11 & \\ & \phantom{\text{for } L =}\ 1, 3, 5, 9 & (3.24) \end{array}$$

$$\begin{array}{lll} B(5,L) \equiv C_\ell = C1 & \text{for } L = 2, 4, 6, 7, 8, 10 & \\ \ -1 & \phantom{\text{for } L =}\ 1, 3, 5,9, 11 & (3.25) \end{array}$$

$$\begin{array}{lll} B(6,L) \equiv S_\ell = 1 & \text{for } L = 1, 4, 5, 7, 10, 11 & \\ \ -1 & \phantom{\text{for } L =}\ 2, 3, 6, 8, 9. & (3.26) \end{array}$$

With eqs (3.21) to (3.26), we can define:

$$H_\ell \equiv C1*[B(1,L)\; h_{\ell+1} - B(2,L)\; h_\ell]$$

$$-S1*[B(3,L)\; u_{\ell+1} - B(4,L)\; u_\ell] \; ,$$

and

$$T_\ell \equiv \left(ABS[B(5,L1)]\; u_{\ell+1} - ABS[B(5,L)]\; u_\ell\right) \uparrow 2 + (v_{\ell+1} - v_\ell) \uparrow 2. \qquad (3.27)$$

More definitions are:

$A(1,L) \equiv K/(2d_\ell)$ as curvature factor for x coordinate,

$A(2,L) \equiv K/(2e_\ell)$ as curvature factor for y coordinate,

$A(3,L) \equiv -1/p_\ell^2$ as the Gaussian aperturing factor, and

$A(4,L) \equiv b_\ell$ as the distance between surfaces L and L1.

(We arbitrarily set A(4,11) = 1.) K is the wave number.

In the definitions of D and E, it is convenient to use T1 = K/[2*A(4,L)] during this generation of each surface coefficient. Thus D and E are:

$$D(1,L) = LN \left[ABS[B(5,L)]*T1/\pi\right],$$

$$D(2,L) = (\pi/2)*SN[B(5,L)] ,$$

$$D(3,L) = D(5,L) = D(6,L) = 0 ,$$

$$D(4,L) = K*S1*B(4,L) ,$$

$$D(7,L) = D(9,L) = A(3,L) ,$$

$$D(8,L) = T1*[B(5,L) \uparrow 2] - C1*B(2,L)*A(1,L) ,$$

$$D(10,L) = T1 - C1*B(2,L)*A(2,L) ,$$

$$E(I,L) = 0 \quad \text{for } I = 1, 3, 4, 5, 7, 9, \text{ and } 11.$$

$$E(2,L) = -K*S1*B(3,L) ,$$

$$E(6,L) = T1*[B(5,L1) \uparrow 2] + C1*B(1,L)*A(1,L1) ,$$

$$E(8,L) = T1 + C1*A(2,L1)*B(1,L) ,$$

$$E(10,L) = -2*T1*ABS[B(5,L1)*B(5,L)] , \text{ and}$$

$$E(12,L) = -2*T1 . \tag{3.28}$$

Above, SN(X) means the sign of X, ABS(X) means the absolute value of X, and LN(X) means the $\log_e(X)$.

The D(2,L) should contain +K*A(4,L). This factor is common to all beams going through the apparatus; therefore, it cannot be measured here. This fact makes it unimportant. Retaining this term in D(2,L) would generate large numbers which can produce significant and unnecessary round-off errors in subsequent computations.

There remain additional definitions that are used in the computer program BEAM. It assumes Gaussian beam propagation and is listed in subsection 4.2. When Z(L) is Gaussian, we define the complex numbers:

$$A1 = C(1,L) + D(1,L) + i[C(2,L) + D(2,L)] ,$$

$$A2 = C(3,L) + D(3,L) + i[C(4,L) + D(4,L)] ,$$

$$A3 = C(5,L) + D(5,L) + i[C(6,L) + D(6,L)] ,$$

$$A4 = C(7,L) + D(7,L) + i[C(9,1) + D(8,L)] ,$$

$$A5 = C(9,L) + D(9,L) + i[C(10,L) + D(10,L)] ,$$

$$A6 = E(1,L) + i\ E(2,L) ,$$

$$A7 = E(3,L) + i\ E(4,2) ,$$

$$A8 = E(5,L) + i\ E(6,L) ,$$

$$A9 = E(7,L) + i\ E(8,L) ,$$

$$A10 = E(9,L) + i\ E(10,L) \text{ , and}$$

$$A11 = E(11,L) + i\ E(12,L) . \tag{3.29}$$

With these definitions, the integrand in eq (3.20) becomes:

$$Y(L)*Z(L) = EXP \left(\begin{array}{l} A1 + u_\ell\ A2 + v_\ell\ A3 + u_\ell^2\ A4 \\ + v_\ell^2\ A5 + u_{\ell+1}\ A6 + v_{\ell+1}\ A7 \\ + u_{\ell+1}^2\ A8 + v_{\ell+1}^2\ A9 \\ + u_{\ell+1}\ u_\ell\ A10 + v_\ell\ v_{\ell+1}\ A11 \end{array} \right) . \tag{3.30}$$

We now integrate eq (3.20) to find Z(L1) for this case. Here eq (3.30) can be written in the form:

$$EXP\ [A4*(u_\ell - G2) \uparrow 2 + G3 + A5*(v_\ell - G5) \uparrow 2] ,$$

where

$$G2 = (A2 + u_{\ell+1}\ A10)/(-2*A4) ,$$

$$G5 = (A3 + v_{\ell+1}\ A11)/(-2*A5) \text{ , and}$$

$$G3 = A1 + u_{\ell+1}\ A6 + v_{\ell+1}\ A7 + u_{\ell+1}^2\ A8 + v_{\ell+1}^2\ A9$$

$$- (A2 + u_{\ell+1}\ A10) \uparrow 2/(4*A4) - (A3 + v_{\ell+1}\ A11) \uparrow 2/(4*A5). \tag{3.31}$$

The integration over u_ℓ and v_ℓ gives:

$$Z(L1) = (\pi/\sqrt{A4*A5}\ ) \ EXP(G3) \ . \tag{3.32}$$

For the computer program, we separate the complex numbers and place all terms into the exponential so the C array can be defined for the L1 surface.

We write:

$$F(1) = C(7,L) + D(7,L) \ ,$$

$$F(2) = C(8,L) + D(8,L) \ ,$$

$$F(3) = C(9,L) + D(9,L) \ ,$$

$$F(4) = C(10,L) + D(10,L) \ ,$$

$$R1 = F(1)*F(3) - F(2)*F(4) \ ,$$

$$R2 = F(1)*F(4) + F(3)*F(2), \text{ and}$$

$$R3 = SQR(R1 \uparrow 2 + R2 \uparrow 2) \ . \tag{3.33}$$

(Here SQR(X) is $\sqrt{X}$.)

Note that a separation into polar coordinates for the complex numbers gives:

$$A4*A5 = R3*EXP(i\ R6)$$

where

$$COS(R6) = R4 = R1/R3 \ , \text{ and}$$

$$SIN(R6) = R5 = R2/R3 \ .$$

Here the exponential form for π/SQR(A4*A5) = EXP(R8 + i R9), where:

$$R9 = -R6/2 \ , \text{ and}$$

$$R8 = LN[\pi/SQR(R3)] \ .$$

The phase term

$$\begin{aligned} R6 &= SIN^{-1}\ (R5) && \text{if } R4 > 0 \\ &= \pi - SIN^{-1}\ (R5) && \text{if } R4 < 0 \\ &= SN(R5)*\pi/2 && \text{if } R4 = 0 \ . \end{aligned} \tag{3.34}$$

The numbers C(I,L1) are related to the A1, etc., by the relationships:

$C(1,L1) + iC(2,L1) = R8 + iR9 + A1 - A2 \uparrow 2/(4*A4) - A3 \uparrow 2/(4*A5),$

$C(3,L1) + iC(4,L1) = A6 - (A2*A10)/(2*A4),$

$C(5,L1) + iC(6,L1) = A7 - (A3*A11)/(2*A5),$

$C(7,L1) = iC(8,L1) = A8 - A10 \uparrow 2/(4*A4),$ and

$$C(9,L1) + iC(10,L1) = A9 - A11 \uparrow 2/(4*A5). \qquad (3.35)$$

Separation of A6 throughA9 into real and imaginary is simple. See eq (3.29). The expression

$$-A_x*A_y/(4*A_z) \qquad (3.36)$$

requires a computer subroutine. With control parameters J1, J3, J5, and J7 that are shown for each eq (3.36) expression in the computer program (here J2 = J1+1, J4 = J3+1, and J6 = J5+1), we get:

$A_x = F(5) + i\ F(6)$,

$A_y = F(7) + i\ F(7)$, and

$A_z = F(9) + i\ F(10).$

Here:

$F(5) = C(J1,L) + D(J1,L)$, and

$F(6) = C(J2,L) + D(J2,L)$, if J7 = 1 or 2.

$F(5) = E(J1,L)$, and

$F(6) = E(J2,L)$, if J7 = 3.

Here:

$F(7) = C(J3,L) + D(J3,L)$, and

$F(8) = C(J4,L) + D(J4,L)$ if J7 = 1.

$F(7) = E(J3,L)$, and

$F(8) = E(J4,L)$, if J7 = 2 or 3.

Finally,

$F(8) = C(J5,L) + D(J5,L)$, and

$F(9) = C(J6,L) + D(J6,L).$

The multiplications defined in eq (3.36) are completed by using:

$$Q1 = F(5)*F(7) - F(6)*F(8) ,$$

$$Q2 = F(5)*F(8) + F(6)*F(7) ,$$

$$Q3 = F(9) \uparrow 2 + F(10) \uparrow 2 ,$$

$$Q5 = -F(9)/Q3 ,$$

$$Q6 = F(10)/Q3 ,$$

$$Q7 = (Q1*Q5 - Q2*Q6)/4 \text{ , and}$$

$$Q8 = (Q1*Q6 + Q5*Q2)/4, \tag{3.37}$$

where finally we define:

$$Q7 + i\ Q8 = -A_x*A_y/(4*A_z). \tag{3.38}$$

The above completes for the computer program the definitions that are needed in the remaining subsections 3.3, 3.4, and 3.5. There will be further definitions used in the computer program which will be defined in subsections 4.1 and 4.2.

3.3 Surface Phase and Amplitude Modulation Effects

Surface 7 in figure 3.1 is a reflector with a bumpy surface modifying the ideal plane. This unit acts as a hologram to split each incident beam into eight additional diffracted beams and into one reflected beam. To represent this bumpy surface, we add a term to the integral in eq (3.20) for the description of the field at surface 8. Thus:

$$Z(8) = \int du\ dv\ F(u,v)*Y(7)*Z(7), \tag{3.39}$$

where the surface function correcting for deviation from a plane surface of reflection is:

$$F(u,v) = EXP[-i\ 2*K*C1*h(u,v)] . \tag{3.40}$$

Here the local coordinates of surface 7 are abbreviated to:

$$u \equiv u_7 \quad \text{and } v \equiv v_7 .$$

One simple mathematical example of h is:

$$h(u,v) = s[\sin(u*S7) + \sin(v*T7)] , \tag{3.41}$$

where s is the variation from the plane front for surface 7 in μm units. A possible value for s is 0.084 μm. Notice that the S7 and T7 can be different. They are proportional to the spatial frequencies for u and v, respectively.

To identify the individual beams generated by this bumpy surface given in eq (3.41), we expand eq (3.40) to show the explicit relative directions for the diffracted beams from each reflected incident beam. Thus we have:

$$F(u,v) = \sum_{m=-\infty}^{\infty} \sum_{m=-\infty}^{\infty} J_m(z)\, J_n(z)\, EXP(iD) \tag{3.42}$$

where z = -2*K*C1*s, and the beam diffraction indicator is:

$$D \equiv m*u*S7 + n*v*T7 \;. \tag{3.43}$$

We will discuss more general examples of h in section 8. Here they are selected by practical fabrication issues. In many cases, eq (3.42) can be generalized to:

$$F(u,v) = \sum_{m,n=-\infty}^{\infty} EXP[G(m,n)]\, EXP(iD), \tag{3.44}$$

where G(m,n) are complex numbers giving the phase shift and the strength of the beam diffracted from the reflected beam. The order m corresponds to the u coordinate and the order n corresponds to the v coordinate.

The ideal hologram for the reflection apparatus would have the G(m,n) show the following form. All G(m,n) would equal $-\infty$ except when $|m|, |n| < 2$. In section 8, we discuss ways to realize this ideal.

The example shown by eq (3.41) can approach the ideal situation when z = -0.1. This happens if the wavelength is 10.6 μm and the amplitude of the bumpy surface has s = 0.084 μm. The Bessel functions become:

$$J_0(z) = 0.998 \;,$$

$$J_1(z) = -J_{-1}(z) = -0.050 \;, \text{ and}$$

$$J_2(z) = J_{-2}(z) = 0.001 \;.$$

The rest are less than 0.001 and can be neglected in one percent precision measurements. This example shows that the:

$$J_{|n|}(z) \sim 0 \qquad \text{for } |n| \geq 2 \;.$$

Therefore, there are operationally nine beams generated by the single incident beam. The m = n = 0 case represents the pure reflected beam. The four cases, namely m = 0, n = $\pm$1, or m = $\pm$1, n = 0, represent the diffracted beams that can generate the spot formed by two beams. These are shown in figure 2.3. To get this condition, we scale S7 and T7 relative to the optics of the apparatus and to the wavelength of the laser radiation. The remaining diffracted beams contribute to the spots shown in figure 2.3 as the spots with four beams contributing.

3.4 The Development of the Practical Transfer Functions Between Surfaces

In subsection 3.2 we generated in eq (3.20) the formula for the Fourier optics approximation when only one surface process acts on the laser beam. When a mirror generates a transform or image, it is a two-surface process. These are shown in references [1] and [9] for the simpler on-axis case. This section defines the off-axis case.

In the reflection apparatus, we have definite surfaces for each mirror of interest. In all cases, we assume that these surfaces in front of and after a given mirror are plane and that their surface normals are either parallel or at an angle θ to the surface normal of the mirror. Each circumstance uses appropriate values of B(5,L) in eq (3.25). Because the actual formulas are complex, we only indicate the algebraic form with many definitions of convenience. The reader should use a computer to generate from these equations a code that constrains the parameters of the apparatus. In the discussion below we assume the arrays D and E are defined in eq (3.28). We presume that the values of the arrays are known, and in this section we deduce the constraints on these values. We make no attempt to reduce the resulting formulas. The image formula is defined first, because it is the simplest.

First, we construct the two-surface transfer equation using eq (3.20) twice and defining L2 = L+2. Thus:

$$Z(L2) = \int du_\ell \; dv_\ell \; Y1(L) \; Z(L) \; , \tag{3.45}$$

where

$$Y1(L) \equiv \int du_{\ell+1} \; dv_{\ell+1} \; Y(L) \; Y(L1) \; . \tag{3.46}$$

Integration of eq (3.46) generates the form:

$$Y1(L) = EXP\left(\begin{array}{l} K1 + u_\ell \, K2 + v_\ell \, K3 + u_\ell^2 \, K4 + v_\ell^2 \, K5 \\[2ex] + u_{\ell+2} \, K6 + v_{\ell+2} \, K7 + u_{\ell+2}^2 \, K8 + v_{\ell+2}^2 \, K9 \\[2ex] + u_\ell \, u_{\ell+2} \, K10 + v_\ell \, v_{\ell+2} \, K11 \end{array} \right) , \tag{3.47}$$

where the complex numbers K1 to K11 and B4 and B5 are defined:

K1 = D1 + F1 + LN[π/SQR(B4*B5)] - (E1 + F3) ↑ 2/(4*B4)
  -(E3 + F5) ↑ 2/(4*B5) ,

K2 = D3 - E9*(E1 + F3)/(2*B4) ,

K3 = D5 - E11*(E3 + F5)/(2*B5) ,

K4 = D7 - (E9 ↑ 2)/(4*B4) ,

K5 = D9 - (E11 ↑ 2)/(4*B5) ,

K6 = G1 - G9*(E1 + F3)/(2*B4) ,

K7 = G3 - G11*(E3 + F5)/(2*B5) ,

K8 = G5 - (G9 ↑ 2)/(4*B4) ,

K9 = G7 - (G11 ↑ 2)/(4*B5) ,

$$K10 = -E9*G9/(2*B4) ,$$

$$K11 = -E11*G11/(2*B5) ,$$

$$B4 = E5 + F7 , \text{ and}$$

$$B5 = E7 + F9 . \tag{3.48}$$

The above terms are defined by the following complex numbers that are correlated to the terms in Y(L) and Y(L1), respectively. Thus:

$$D1 = D(1,L) + iD(2,L) , \quad F1 = D(1,L1) + iD(2,L1) ,$$

$$D3 = D(3,L) + iD(4,L), \quad F3 = D(3,L1) + iD(4,L1) ,$$

$$D5 = D(5,L) + iD(6,L), \quad F5 = D(5,L1) + iD(6,L1) ,$$

$$D7 = D(7,L) + iD(8,L) , \quad F7 = D(7,L1) + iD(8,L1) ,$$

$$D9 = D(9,L) + iD(10,L) , \quad F9 = D(9,L1) + iD(10,L1) ,$$

$$E1 = E(1,L) + iE(2,L) , \quad G1 = E(1,L1) + iE(2,L1) ,$$

$$E3 = E(3,L) + iE(4,L) , \quad G3 = E(3,L1) + iE(4,L1) ,$$

$$E5 = E(5,L) + iE(6,L) , \quad G5 = E(5,L1) + iE(6,L1) ,$$

$$E7 = E(7,L) + iE(8,L), \quad G7 = E(7,L1) + iE(8,L1) ,$$

$$E9 = E(9,L) + iE(10,L) , \quad G9 = E(9,L1) + iE(10,L1) ,$$

$$E11 = E(11,L) + iE(12,L), \text{ and } G11 = E(11,L1) + iE(12,L1). \tag{3.49}$$

To get the image formula, we want a delta function for the u_ℓ and v_ℓ variables in Y1(L). To define the image plane for a single mirror from a known object plane, we first fix the ratio:

$$R = b_{\ell+1}/b_\ell .$$

This is adjusted subject to the derived constraints in eq (3.50) to generate the appropriate magnification of the desired image. To locate conveniently the object and the image plane, we fix the curvature of the mirror's y coordinate, $e_{\ell+1}$. Now we set the curvature $d_{\ell+1}$ and the image distance $b_{\ell+1}$ by requiring that the imaginary parts of B4 and B5 are zero. This implies:

$$E(6,L) + D(8,L1) = 0, \text{ and}$$

$$E(8,L) + D(10,L1) = 0. \tag{3.50}$$

If these are true, then K4 and K5 in eq (3.47) have been made as large as possible; we approach the delta function. To do better requires that the aperturing is insignificant so the real parts of B4 and B5 can be near zero. In this case, the integral in eq (3.45) can be approximated appropriately, and the image can look like the object. If the aperturing is significant, there is a convolution of the object function, Z(L), with a Gaussian-like intensity distribution, Y1(L). The resulting

image, Z(L2), is thus smeared and cannot be made sharp. The high-frequency features of Z(L) are filtered out by the convolution process.

In the reflection apparatus, the R is fixed by the required dimensions for imaging on the detector array. The curvature of the mirror is fixed by the required distances between mirrors to allow a clear field of view for the object and the image plane.

The Fourier transform in eq (3.45) has the position, $b_{\ell+1}$, and the curvature, $d_{\ell+1}$, such that the imaginary parts of K4 and K5 are zero in eq (3.47). Here we presume that the y curvature, $e_{\ell+1}$, is fixed by design constraints. The ideal transform has the real parts of K4 and K5 zero also. However, the usual aperturing by the mirror causes eq (3.45) to convolute the Fourier transforms of Z(L) and Y1(L). The transform of Y1(L) is almost a delta function if the aperturing is small enough; otherwise, it smears the Fourier transform of Z(L).

After identifying the Fourier tranform plane, we adjust the distance b_ℓ in front of the mirror to make the phase front in the Fourier plane as flat as possible. This happens when the imaginary parts of K9 and K8 are both zero. Usually, adjustment of one cannot make both zero simultaneously; therefore, we just make these two numbers as small as possible. The practical situation has their curvatures equal but of opposite signs.

This concludes the discussion of the practical formulas, and we proceed to subsection 3.5.

3.5 Application of the Formulas in the Apparatus under Design

As can be seen from the previous subsection, the mathematics for the reflection apparatus is complex algebraically. However, the discussions in the previous subsections have made clear the qualitative features of the apparatus so that it is unnecessary to know its quantitative details. In subsections 3.5.1 and 3.5.2 we use these previous discussions to note what is pertinent to each surface of the reflection apparatus. By confirming the presence of these features in the alignment of the apparatus, we can test its status on a surface-by-surface basis to confirm whether the apparatus is aligned and constructed properly. Because the computer code in sections 4, 5, and 6 uses Gaussian beams to propagate through the simulated apparatus, we discuss in subsection 3.5.1 how to align the apparatus when it has Gaussian beams. In subsection 3.5.2 we discuss how the results of subsection 3.5.1 are modified because the actual apparatus has circular sampling holes in the plate at the prefilter plane.

3.5.1 Assume a Gaussian Beam Undulating through the Apparatus

In section 2 we traced the actual apparatus in general terms. Here we get more technical about each surface, using the fictitious and simplifying condition that the Hartmann plate at surface 1 has holes which generate an array of beams with Gaussian profiles when irradiated by an arbitrary, unknown laser beam. Each surface of the apparatus is labeled in figure 3.1. To construct the apparatus requires understanding numerous technical details. In the paragraphs below we define these details so that each component has a proper position. The beams indicated below are those generated behind the prefilter by illumination with a cw laser of the desired wavelength. The discussion below requires numerous background points. In the following paragraphs we address them first, and then we indicate the adjustment sequences.

There are three stages in the adjustment process for each surface. The first stage uses the results of the theory and the computer simulations to fix the distances (b_ℓ) between surfaces. The second stage uses the expected results at a key surface

to make precision adjustments of optical components tied to that surface. The end result of this adjustment sequence is an apparatus assembled with minimum deviation from the expected. The third stage makes the apparatus a precision unit by calibrating it with the aid of the mathematical model defined in reference [1, pages 31-4].

We make here a collection of general conditions for alignment of the apparatus: (1) The precise positions for each surface are documented in sections 5 and 6 for an apparatus using Gaussian beams. In this subsection, we accept that these beams exist and that they can be used to adjust the optics. (2) A single laser beam going through the hole at the center of the Hartmann plate operationally defines the optical axis of the apparatus. (3) The first series of position adjustments can be easily set correctly within 1 mm. (4) If the room containing the apparatus is large enough, the corresponding angle adjustments can be adjusted to 0.1 mrad. (5) The initial placement of each optical component is added as the beams from the prefilter transverse the apparatus. (6) Because placement errors accumulate, the preliminary positioning and precision adjustments of each component may have to be performed together. (7) Because radiation of a new wavelength requires substantial shifts in position for all optical components, the apparatus must be recalibrated to optimize its use.

In addition to the list of general conditions defined above, we must prescribe the mirrors. Selecting a mirror depends on what can be purchased. Each may have either an elliptical or a spherical surface. In the simulation process in section 4 we ignore the deviations from the two-curvature parabolic symmetry and pretend that the real optics behave similarly to these parabolas. We presume in the alignment process defined below that the deviations from ideal symmetry cause small changes in the placement of each mirror. These changes are less than the travel range of the micropositioning equipment holding each optical component. In the assembly of a particular apparatus, we use the results from the computer code to identify sensitivities indicated by the deviations from ideal. The positioning devices are tied to a stable reference table so that they bracket the conditions that make the real apparatus behave as ideal as possible. In brief, each mirror position must be insensitive to distortions by curvature errors and surface defects in the mirrors. Of course, these effects are never zero; therefore, they affect the ultimate accuracy and dynamic range of the apparatus. To establish precision and dynamic range, we made simulations at two carrier wavelengths which contain the best optics using elliptical mirrors with two curvatures. For contrast, we simulate the two wavelengths using spherical mirrors with a single curvature. These simulations identify possible errors during the assembly and design of the apparatus.

We discuss beam properties and their ease of measurement before we define the adjustment process. We can measure the positions for the center of irradiance of each beam relative to the optical axis. In addition, we can measure the degree to which the irradiance of each beam deviates from a cylindrical symmetry. These measurements are the practical data available during adjustments of the mirrors and other parts of the apparatus. If two beams overlap at a particular surface, we can then scan the resulting irradiance and interference pattern to establish the relative curvature of the phase front for two beams assuming their separate irradiance patterns are sufficiently similar. Alignment with more than two beams could be used if the resulting complex irradiance patterns at each surface have the required intuitive character. It is much easier in both the computer simulations and in the actual apparatus to use only one- or perhaps two-beam structures to adjust all the mirrors to their required positions. Measurement for the center of irradiance is easily done with a beam-scanning technique. We measure the deviation from cylindrical symmetry by using a spinning slit in a mask before an appropriate detector. The slit is rectangular with 100 μm and 1 μm edges. These dimensions are arbitrary but consistent with the design conditions discussed in sections 4 and 5. To make the cylindrical check, the mask

spins parallel to the optical axis. The unit is moved perpendicular to the optical axis to establish three numbers, namely the x, y, and z coordinates of the maximum dc signal with a minimum time-varying signal [10].

By selecting individual beams near the optical axis and on the edge for the field of view in the apparatus, we develop at each surface the true structure for the image or Fourier transform relative to their ideal. The adjustment sequence in either the simulation or the real apparatus can use a minimum least squares fit relative to the ideal. The proper number of necessary test beams depends on the form of the final apparatus. In our test of a proposed apparatus, we use six beams. During construction of the final apparatus, I would expect a fairly complete map. Once that simulation has been done, I would expect the six beams used in this simulation to be adequate for final adjustments.

We now define the position adjustments for a mirror when it is used either for imaging or for making a Fourier transform.

When a fixed-curvature mirror creates an image, a critical positioning of this mirror can minimize the deviations from ideal for all beams at the image plane. This action can fix the position of the mirror. If we allow x-axis curvature to be adjusted in addition to the position adjustment for the image, then we can also get a different position for the mirror. It is also unique. This latter adjustment will reduce the size of the deviation for all beams from the ideal more than the case where the curvatures are fixed and the mirror is simply moved.

In like manner, when the mirror acts to generate the Fourier transform of a beam, its position coordinates can be fixed by some least square criteria. If possible, we adjust the curvature for the x axis of the mirror to improve the cylindrical symmetry for the Fourier transform of each beam.

These adjustments do not prescribe uniquely the Fourier transform position. To fix the position coordinate in front of the mirror that makes the Fouier transform requires a confirmation that the phase front of each beam at the Fourier plane is flat. Two tests of this flatness are possible for the real apparatus. One method uses two beams of equal irradiance to intersect in the Fourier plane and to show a modulation of dark and straight lines. The second method uses the six beams individually and locates where the beam size of each has a minimum for both the x and y coordinates. For these methods, we presume the beams have peak irradiance at the center of each beam. In contrast, the computer simulation allows us to adjust the phase front for a single beam directly because the mathematics contains those phase details.

One adjustment to these mirrors has been ignored in the computer simulations of this paper. All rigid bodies have five degrees of freedom which must be adjusted relative to another rigid body. Four degrees are fixed by the constraints on the optical axis and by the conditions for proper imaging or Fourier transforms. There remains the rotation of each mirror so that its two radii of curvature are consistent with the general x and y coordinates of the apparatus. If a mirror is cylindrically symmetric, this rotation has no effect. If there is any nonsymmetry, then the rotation affects the details of each laser beam as well as the location for the image or Fourier transform plane as defined by that mirror. Therefore, during the adjustment of these mirrors, it will be necessary to rotate each to test and confirm that the ideal and actual curvatures are as intended.

Given the above discussion, we define our alignment sequence as follows: (1) Set each mirror to an accuracy of 1 mm on the basis of the simulation results using the design parameters for each mirror. (2) Adjust each mirror in sequence using the six test beams and the spinning slit-detector unit to fine-tune the position of each mirror. These two procedures should get each mirror within 100 μm of the ideal position and within 1 mrad in the angle adjustments. The final adjustments would employ the output from the array of detectors and would move slightly each unit in the apparatus so that the measurements of the phase and irradiance are modified to get best accuracy.

This paper does not specify the final adjustments. They are unique to a given apparatus. For example, one mirror may be most sensitive in its final positioning because it has peculiar surface properties. Further, the position of the hologram at surface 7 will affect significantly the output for phase measurements. Both ambiguities mean the final adjustment must use a walk-in process where each available parameter is moved one at a time. We would expect the most sensitive parameters to be moved after the least sensitive ones are positioned for their best conditions. In these final adjustments, some minimum-maximum criteria must be uniformly applied. Examples of the criteria are: (1) a maximum dynamic range for each detector in the array; (2) a maximum range of allowed wavelengths for a given dynamic range; or (3) a minimum distortion by apparatus on the phase fronts of a plane wave.

All the general discussion on the alignment process is finally complete; therefore, we pass to the specific adjustment conditions for each mirror in figure 3.1.

The mirrors at surfaces 4, 8, and 10 each generate a periodic array of spots of minimum size, similar in size and relative position to those in the Hartmann plate at surfaces 5, 9, and 11, respectively. The scale size for these arrays of spots can be different for each laser wavelength. The adjustments for the ideal imaging of these spots will minimize barrel distortion in these image planes.

Mirrors 2 and 6 generate Fourier transforms of the original spot patterns at surfaces 3 and 7, respectively. Here we have one spot centered around the optical axis. The sequential illumination of each aperture generates the required test beams from the Hartmann plate. A stationary center of irradiance of the spot at the Fourier plane exists when these two mirrors are properly adjusted. To verify that the phase front of each spot in this Fourier plane is flat, we either inspect the resulting interference pattern produced by two beams simultaneously intersecting at the Fourier plane or check that the spot size in each transverse coordinate for a single beam is a minimum at the Fourier plane. In the computer simulation, the test is simple: we look at the phase front for each beam. In the actual apparatus, the test is more difficult: we must make a numerous measurements using the spinning slit-detector unit and a cw laser source of the desired wavelength. The signal out of the detector allows deduction of the optimum adjustments. This paper does not detail what should be done; reference [10] develops the necessary concepts.

3.5.2 What Happens When the Initial Beam Is a Spot of Uniform Irradiance

Because the actual apparatus cannot realize Gaussian apertures in the Hartmann plate, we note the change in the alignment process for real beams. All the discussion in subsection 3.5.1 applies except that the reader must know these beams are not simple structures. Nevertheless, the Airy patterns at the Fourier transform planes and spots at the imaging planes do not change the basic alignment procedures at either plane.

The signal waveform from the spinning slit-detector unit will change; therefore, this output must be properly understood to allow proper adjustment of the apparatus.

4. THE COMPUTER PROGRAM

Normally, computer programs are relegated to appendices. We include one because this program provides a detailed understanding of the simulations in sections 5 and 6. The summary of these simulations appears in section 7. In the next three subsections of section 4 we explain the structure of the computer program and define the input and the output variables so the program can be used. In subsection 4.1 we show the logic flow and define the input parameters. In subsection 4.2 we list the appropriate blocks either for function or for logical flow. The identification also ties the listing to those equations in section 3 and in particular to those in subsections 3.1, 3.2, and 3.3. In subsection 4.3, we describe the output from a sample run so that the data from such output can be understood.

4.1 The Logic Flow of the Computer Program

Figure 4.1 shows, in three pages, the structure for the possible flows in logic within the program BEAM. This figure has four columns of descriptions. The first column shows the entry statement number for a block of statements. The second column defines the function of the block and how the block is correlated to other blocks in the program. The third column gives various temporary jumps to subroutines and other such blocks. Finally, the fourth column defines the range of statments in the listing containing the function block. To understand completely the potential logic flows requires four items: the actual computer system; the definitions for the control parameters as shown in figure 4.3; the descriptions for the output statments on the operator console as shown in figure 4.2; and finally, a detailed listing of the program, BEAM, as shown in figure 4.4.

Because there are numerous possibilities for operation of this program, it is impossible to give a simple sequence showing this program. Nevertheless, the program can be executed after appropriate study of these four figures which collectively provide the needed explanations. The discussion in this subsection only indicates the basic possibilities. This program has a general design purpose; therefore, the decisions for a computing sequence are numerous.

BEAM traces a beam with a Gaussian profile from surface 1 to 11. Each trace corresponds uniquely to a chosen aperture in the prefilter. This trace remains a single beam until it reaches the hologram at surface 7. The tracing from surface 1 to 7 is called stage I. At surface 7, the operator selects one of the diffraction orders so a single beam trace can continue. This continued trace between surface 7 to 11 defines stage II in the program.

Stages I and II represent two logic flows in BEAM. First, program use centers on stage I for beam traces up to surface 7. Second, assuming fixed values from stage I results, the program now centers on stage II with a series of beam traces after surface 7.

There are numerous uses for the program such as determining the proper control parameters in a given apparatus before purchase of expensive equipment. Sections 5 and 6 show such examples. A second use of BEAM would test the sensitivity for adjustment of these parameters at all surfaces during a beam trace. These results permit choice of adjustment strategies and estimates for the allowed dynamic ranges of beam profile parameters.

The program, written in BASIC, uses the input and output codes appropriate to an Interdata computer system. It is necessary to use 14 significant figures to prevent serious round-off errors in the simulations. The program assumes there are six modules for real-time use--the CPU with 16- or 32-bit words, about 40 kilobytes of memory, a disk for file storage, a printer (PR), an operator terminal with cathode ray tube (CRT) for read out, a keyboard for input, and finally the appropriate software for the operating system.

During a beam trace, the operator would use the information in figure 4.2 to choose appropriate control parameters. No further discussion of this figure should be necessary.

Also during this same beam trace, the operator would use the explanations from figure 4.3. Here some comments should expedite its use. The number on the left is the statement number that put the quoted statement on the CRT. The following explanation defines what it means and what the operator should do, if anything. If questions remain, the operator must use figure 4.4 and puzzle out the answer. I have tried to construct a program that works correctly; however, the many options can cause inconsistencies in status. If the reader gets such a case, the best course is to start with RUN and reset the program.

There remains one logic flow that requires further discussion, namely how the least-squares-fit sequence works. To execute it properly, the operator repeats the beam trace one more time than the number of varied parameters. For example, an adjustment sequence at a given surface requires the four values defined in figure 4.3 to be zero for surface 3 and three adjustment parameters--b_1, b_2, and d_2. Each parameter changes one at a time to generate the necessary data. In this example, four beam traces result. The first trace uses the base parameters--b_1, b_2, and d_2. The second changes b_1 to b_1'. The third returns b_1' to b_1 and changes b_2 to b_2'. Finally, the last trace in this LSQ sequence returns b_2' to b_2 and changes d_2 to d_2'. Each change is about 1 percent or less of the original parameter. The LSQ part of the program then generates a new set of b_1, b_2, and d_2. These latter values should produce a better working apparatus. The LSQ process is converged when all differences between the old and new sets of parameters are less than 1 μm for a given LSQ. The simulations in sections 5 and 6 tabulate such results for the surface of interest and for the chosen beam.

Figure 4.2 refers to an equation defining the initial parameters of the traced beam as it exits from the prefilter in surface 1. We give that equation here.

MAIN PROGRAM LOGIC FLOW

Entry	Function	Jump to Outside Block	Range
RUN	To run program BEAM (Initializes program arrays) Flow to 36	---	10-34
36	Control data defined Flow to 38	840	36-36
38	Read and change control data Options: blocks--134 individual--162 set initial conditions and flow to 60	134 or 162 or 194	38-58
60	Propagates Gaussian from surface L = 1 to L = 7 Flow to 66	390	60-64
66	Set up LSQ fit controls Flow to 68	912	66-66
68	Decision to print Stage I data Options: IF YES, go to 566 If NO, continue Flow to 76	566	68-74
76	Decision to generate new Stage I data Options: YES go to 40 NO continue Calls 796 for S7 and T7 values Flow to 94	40 or 796	76-94
94	Selected exit beam from surface 7 (Propagates Gaussian beam from surface L = 7 to L = 11) Flow to 114	390 662	94-112
114	Decision to generate new beam from surface 7 Options: IF YES, go to 94 IF NO, continue Flow to 120	94	114-118
120	Decision to generate new beam from surface 1 Options: IF YES, go to 40 IF NO, continue	40	120-124
126	Preparing main program for exit Flow to 130 (STOP)	830	126-130

Figure 4.1. Logic flow of BEAM (page 1).

VARIOUS SUBFUNCTION LOGIC BLOCKS

Entry	Function	Jump to Outside Block	Range
840	Read control data from floppy disk (Subroutine) Options are: Do it or return		840-362
864	Print control data to floppy disk (Subroutine) Options: Do it or return	134	864-886
134	Print to CRT block of control data (Subroutine) Options are: Range of each block and number of such blocks		132-152
156	Prints to CRT one control value at a time (Subroutine) Options are: To select a value or to quit Flow to 162		
162	Decide to get new control data IF YES, go to 156 IF NO, continue Flow to 168	156	162-166
168	Display range of control data Options: Select new ranges or return		168-192
194	Set up initial data using control data for each surface (Subroutine)	390	194-384
390	Propagating the Gaussian beam from surface L to L + 1 (Subroutine)	514 (many times)	386-508
514	Computes form: AX*AY/Y*AZ Given input J1, J3, J5, J7 (Subroutine)		510-562
564	Decision tree 3 options: bulk print--612 individual print--612 skips everything--662	578 or 612 or 662	564-576
578	Print on printer (PR) initial data in proper form	624	578-610

Figure 4.1. Logic flow of BEAM (page 2).

ADDITIONAL SUBFUNCTION LOGIC BLOCKS

Entry	Function	Jump to Outside Block	Range
612	Print individual control values Options: Select value or flow to 624	---	612-622
624	Selects surfaces to be printed Flow to 648	---	624-646
648	Print initial data for surface L = 1 Options: Do it or skip it Flow to 662	---	648-660
662	Complicated sequence Options are: Print on CRT or PR and print out selected surfaces as queried, or print according to control data	888	662-790
796	Computes expected S7, T7 to compare with actual S7, T7 (Subroutine)	---	792-828
830	Starts exiting from program and commences the filing of data in storage (Subroutine)	864	830-838
840	Read in control data from floppy disk (Subroutine) Options: Do it or skip it	---	840-862
864	Print control data to floppy disk (Subroutine) Options: Do it or skip it	---	864-886
888	Store control data for least squares fit (LSQ) process (Subroutine) Options: Do it--returns Skip it--returns to 682 data for LSQ fit--goes to 966	682 or 966	888-964
966	LSQ fit analysis	12	966-1082

Figure 4.1. Logic flow of BEAM (page 3).

X(1) = λ in μm: wavelength of laser beam
X(2) = θ in rad: angle of reflection for all elements of apparatus
X(3) = LA: hole coordinate for real X (an integer) [see eq (4.1)]
X(4) = LB: hole corrdinate for real Y (an integer) [see eq (4.1)]
X(5) = S1 in mm: the X distance between holes in prefilter [see eq (4.1)]
X(6) = T1 in mm: the Y distance between holes in prefilter [see eq (4.1)]
X(7) = LC: hole coordinate for imaginary X (an integer) [see eq (4.1)]
X(8) = LD: hole coordinate for imaginary Y (an integer) [see eq (4.1)]
X(9) = S7 in 1/(mm): the spatial frequency for the X coordinate of the hologram [see eq (3.41)]
X(10) = T7 in 1/(mm): the spatial frequency for the Y coordinate of the hologram [see eq (3.41)]
X(11) = d_1 in m: curvature of X coordinate for surface 1 (positive)
X(12) = d_2 in m: curvature for surface 2 (negative)
X(13) = d_3 (positive)
X(14) = d_4 (positive)
X(15) = d_5 (positive)
X(16) = d_6 (negative) [see eqs (3.14)]
X(17) = d_7 (positive)
X(18) = d_8 (negative)
X(19) = d_9 (positive)
X(20) = d_{10} (positive) X(21) = $d_1$1 (positive)
X(21) = d_{11} (positive)
X(22) = e_1 in m: curvature of Y coordinate for surface 1 (positive)
X(23) = e_2 (negative)
X(24) = e_3 (positive)
X(25) = e_4 (positive)
X(26) = e_5 (positive)
X(27) = e_6 (negative) [see eqs (3.14)]
X(28) = e_7 (positive)
X(29) = e_8 (negative)
X(30) = e_9 (positive)
X(31) = e_{10} (positive)
X(32) = e_{11} (positive)
X(33) = p_1 in mm: aperture for surface 1 [see eq (3.13)]
X(34) = p_2
X(35) = p_3
X(36) = p_4
X(37) = p_5
X(38) = p_6
X(39) = p_7

Figure 4.2. Control parameters for BEAM (page 1).

$X(40) = p_8$
$X(41) = p_9$
$X(42) = p_{10}$
$X(43) = p_{11}$
$X(44) = b_1$ in m: distance for surface 1 and 2 [see figure 3.1)]
$X(45) = b_2$
$X(46) = b_3$
$X(47) = b_4$
$X(48) = b_5$
$X(49) = b_6$
$X(50) = b_7$
$X(51) = b_8$
$X(52) = b_9$
$X(53) = b_{10}$
X(54) = -30: this parameter has no meaning; it is present to satisfy array constraints
$X(55) = W_x$ in mm: the width of the X coordinate [see eq (4.1)]
$X(56) = W_y$ in mm: the width of the Y coordinate [see eq (4.1)]
$X(57) = R_x$ in m: the curvature of the beam in X [see eq (4.1)]
$X(58) = R_y$ in m: the curvature of the beam in Y [see eq (4.1)]
$X(59) = A$ in $(W/m^2)^{1/2}$: amplitude of beam [see eq (4.1)]
$X(60) = \Phi$ in rad: phase of beam [see eq (4.1)]

X(61):	print control for surface	1	(if 1 print; if 0 no print)
X(62)	"	2	"
X(63)	"	3	"
X(64)	"	4	"
X(65)	"	5	"
X(66)	"	6	"
X(67)	"	7	"
X(68)	"	8	"
X(69)	"	9	"
X(70)	"	10	"
X(71)	"	11	"

<u>Beam deflection control below.</u>
<u>These are changed during the computer runs at Stage II.</u>

$X(72) = m \equiv L1$: the order of X coordinate beam [see eq (3.43)]
$X(73) = n \equiv L2$: the order of Y coordinate beam [see eq (3.43)]
X(74) = real part of G(m,n) [see eq (3.44)]
X(75) = imaginary part of G(m,n) [see eq (3.44)
-- Remaining control variables are generated by operator during a simulation run.

Figure 4.2. Control parameters for BEAM (page 2).

40 "BLOCK DATA YES = 1 or NO = 0"
Here operator decides if a range of control data is to be typed by operator at teletype.
Use 1 if yes, 0 if no.

56 "ALL DATA STAGE I INITIALIZED"

58 "NOW GENERATE SURFACES: G(,L) WHERE L = 1 to 7"
Here program informs operator of the status of the program. Purpose is to detect program traps and give flow information to operator. Stage I generates results for surfaces 1 to 7.
No response needed.

68 "DEAL WITH STAGE I DATA FOR PRINT?, YES = 1, NO = 0"
Here operator decides if Stage I data should be printed at all. When using LSQ features of program and a surface adjustment has L less than 8, operator must say yes.
Use 1 if yes, 0 if no.

76 "NEW VALUE STAGE I YES = 1, NO = 0"
Here operator decides if new control values are needed to compute stage I results without going to stage II.
Use 1 if yes, 0 if no.

90 "BEGIN STAGE II"
Program informs operator it is in stage II, namely generating the details of surfaces 8 to 11.

94 "L1, L2, AND G(L1, L2) RE AND IMAG PAIR VALUES ARE"
L1 is order on surface 7 in X coordinate; L2 is order on surface 7 in Y coordinate. G(L1,L2) is the complex number in eq (3.44). Type L1, then L2, then real part of G(L1,L2), and finally imaginary part of G(L1,L2).

114 "NEW VALUES OF L1, L2, G(L1, L2) RE AND IMAG YES= 1, NO = 0"
Here operator decides if new stage II beam trace is wanted.
Use 1 if yes, 0 if no.

126 "EXITING FROM PROGRAM"
Status information on logic flow.
No response needed.

134 "BLOCK DATA GROUP GIVE LOW I2, HIGH I3 RANGE, FIRST"
To read from teletype the block of control data, operator must give inclusive range of that data.
Give the low and then the high.

140 "HERE I = ", I4, "X(I) = "
To aid in typing the block of control data, each subscript is noted. Type the appropriate X(I).

146 "A NEW INITIAL DATA BLOCK YES = 1, NO = 0"
Operator has chance to transmit new block of control data.
Use 1 if yes, 0 if no.

Figure 4.3. Statements at CRT generated by BEAM (page 1).

156 "INITIAL X(I) DATA, GIVE I FIRST, THEN X"
Operator can give a single control value.
First give subscript, then the value for the subscript.

162 "NEW X DATA YES = 1, NO = 0"
Operator has chance to transmit a single value of control data.
Use 1 if yes, 0 if no.

168 "DISPLAY RANGE OF X VALUES, I4 LOWER, I5 UPPER, I4 = I5 = 0 SKIPS"
Operator selects inclusive range of control values for display on CRT.
Select I4 first, then I5. If operator wishes to skip display type 0 for I4 and I5.

176 SHOWS I, X(I)
Operator can decide if control value is correct or not.
If correct, type 0; if not, type -1, and then type correct value.

186 "DONE WANT TO DISPLAY NEW X RANGE YES = 1, NO = 0"
Operator can choose to display new range of control data.
Use 1 if yes, 0 if no.

202 "GENERATING INITIAL DATA"
Program informs operator where it is.
No response needed.

566 "BULK INITIAL DATA PRT = 1, NO = 0, SKIP TO PRINT CONTROL = -1"
Operator has three options: first, generate the details of the initial control data on the printer; second, to select individual control values for print on CRT; finally, skip control data, print details, and continue automatic control of printing for each surface.
First option, use 1; second, use 0; third, use -1.

612 "DESIRED X(L) VALUE, L = "
Operator selects the control value to be printed on CRT.
Choose L.

618 "NEW X VALUE YES = 1, NO = 0"
Operator has option to print new control values.
Use 1 if yes, 0 if no.

624 "PRINT OUTPUT CONTROL"
Here the control values for printing data on each surface are shown.
No response needed here.

634 "A 1 MEANS PRINT, 0 MEANS NO PRINT IN THIS CONTROL"

636 "I = SURFACE TO BE CHANGED 0 MEANS NO CHANGE"
Operator decides which surfaces should print automatically to CRT or PR. If some surfaces to be printed show incorrect control, then that surface control must be changed.
Type surface number if change is desired. Then type new control value either at 0 or 1. Type 0 is no change is desired.

Figure 4.3. Statements at CRT generated by BEAM (page 2).

648 "INITIAL DATA L = 1 SURFACE PRINT YES = 1, NO = 0"
Operator has option to print on PR initial conditions of the beam at surface 1 beyond that already recorded in statements 578-608.
Use 1 if wanted, 0 if not.

662 "CONT = 1, SINGLE SURFACE = 0: PRINT ON 1 = CRT, 3 = PR"
Operator has option to use or not use the control data to select surfaces to be printed on either the PR or CRT.
If control is used, type 1; if not, type 0; to select output medium, type 1 or 3.

804 "SIMPLE THEORY EXPECT S7 = ", S7, "ACTUAL = ", X(9)

806 "CHANGE ACTUAL VALUE YES = 1, NO = 0"
Operator looks at expected S7 compared with the control S7.
If value to be changed, type 1; otherwise, type 0.

812 "S7 = ?"
Asks what should S7 be.
Type it in.

816 SIMPLE THEORY EXPECT T7 = ", T7, "Actual =", X(10)

818 "CHANGE ACTUAL VALUE YES = 1, NO = 0
Operator looks at expected T7 compared with the control T7.
If value to be changed type 1; otherwise, type 0.

824 "T7 = ?"
Asks what should T7 be.
Type it in.

830 "DONE WITH PROGRAM AND NOW EXITING"
Program telling operator where it is.
No response needed.

840 "READ IN FROM FILE X(1-75) DATA"

842 "YES = 1, NO = 0"
Operator has option to read control data from a disk.
Use 1 if yes, 0 if no.

864 "PRINT TO FILE X(1-75) DATA"

866 YES = 1, NO = 0"
Operator has option to print on disk the current control data for subsequent use in a new simulation session.
Type 1 if yes, 0 if no.

888 "STORE LSQFIT DATA, 1 = YES, 0 = NO"
Operator has option to store desired data from a selected surface to deduce the proper values of control parameters. Both control parameters and test values are saved in LSQ file.
If you want to save data, type 1; if not, type 0.

Figure 4.3. Statements at CRT generated by BEAM (page 3).

912 "RESET AND OPEN LSQ FILE 1 = YES, 0 = NO"
Operator has option to clear the LSQ file for a least squares fit sequence. If the sequence is to be started, type 1; otherwise, type 0.

924 "NUMBERS OF PARAMETERS = ?"
Operator supplies number of control parameters to be varied in the least square fit sequence.
Type a number less than four. Up to three can be varied.

928 "LOCATION OF PARAMETERS"

930 "FIRST L3 ="
Give subscript of X(L3), the first parameter of variation.

942 SECOND L4 ="
Give subscript of X(L4), the second parameter of variation.

952 "THIRD L5 ="
Give subscript of X(L5), the third parameter of variation.

974 "NUMBER OF VALUES TO BE DRIVEN TO REFERENCE"
A given surface has up to four values that are required to be fixed so a surface can have the desired form. The first value is X1, the center of irradiance in the X coordinate. The second value is Y1, the center of irradiance in the Y coordinate. The third value for all surfaces except 11 is proportional to the inverse of the curvature in the X coordiante. If this term and the following are zero, then plane waves are present. The fourth value for all surfaces except 11 is proportional to the inverse of the curvature in the Y coordinate. Surface 11 has its third value as the ratio of the beam width in the X and Y irradiances, namely, WX/WY. Surface 11's fourth value is proportional to the inverse of the curvature for the X coordinate. Normal least squares fit sequence uses the first three values for surface 11 and all four values for the remaining surfaces.

982 "REFERENCES VECTOR C(L2) ="

986 "I =", I, "C(I) = ?"
Here operator supplies the desired X1, Y1, inverse curvature in X, and inverse curvature in Y values, if not, surface 11; otherwise, the set is X1, Y1, WX/WY, etc. If less than four values are requested, then the desired terms are the same order up to the number of requested values. For example, two values would only give X1 and Y1, respectively. Note: the order and types of values are fixed. Only the number can be varied.

1070 "I, OLD, NEW, INCREMENT RESPECTIVELY"
Here the least squares fit sequence tabulates the subscript for the parameter, the extrapolated value of the parameter, and finally the change between the old and new state of each parameter. In an adjustment sequence, convergence of this LSQ process occurs when the increments are less than adjustment accuracy of the apparatus, namely about 1 μm.

Figure 4.3. Statement at CRT generated by BEAM.

```
10 DIM A$(60),B$(60)
12 DIM A(200),B(200),C(200),D(200),E(200),F(200),G(200),X(200)
14 DIM Y(200),S(20)
16 REM NOTE THE VERSION PRINT DATE
18 REM "BEAM" IS WHERE THIS PROGRAM IS STORED"
20 CLOSE 1
22 CLOSE 3
24 OPEN "PR:",3,1
26 OPEN "LO:",1,1
28 DIM A(4,11),B(5,11),C(10,11),D(10,10)
30 DIM E(12,10),F(10),X(75)
32 MAT C=(0)
34 B$="BEAM TRACE                  **********
36 GOSUB 840
38 REM MAIN PROGRAM FOR LOGIC FLOW.
40 PRINT "BLOCK DATA YES=1 OR NO=0"
42 INPUT I1
44 IF I1=0 GOTO 50
46 GOSUB 134
48 REM ABOVE HAS INPUT 1 DATA BLOCK FORM
50 GOSUB 162
52 REM ABOVE HAS INPUT   DATA ONE AT ATIME.
54 GOSUB 194
56 PRINT "ALL DATA STAGE I INITIALIZED"
58 PRINT "NOW GENERATE SURFACES: C(  ,L) WHERE L=1 TO 7"
60 FOR L=1 TO 6
62 GOSUB 390
64 NEXT L
66 GOSUB 912
68 PRINT "DEAL WITH STAGE I DATA FOR PRINT?, YES=1, NO=0"
70 INPUT I1
72 IF I1=0 GOTO 76
74 GOSUB 566
76 PRINT "NEW VALUES STAGE I YES=1, NO=0"
78 INPUT I1
80 IF I1=1 GOTO 40
82 P8=D(1,7)
84 T8=D(4,7)
86 P9=D(2,7)
88 T9=D(6,7)
90 PRINT "BEGIN STAGE II"
92 GOSUB 796
94 PRINT "L1,L2, AND G(L1,L2)RE AND IMAG PAIR VALUES ARE"
96 INPUT X(72),X(73),X(74),X(75)
98 D(4,7)=T8+X(72)*X(9)
100 D(1,7)=X(74)+P8
102 D(6,7)=T9+X(73)*X(10)
104 D(2,7)=X(75)+P9
106 FOR L=7 TO 10
108 GOSUB 390
110 NEXT L
112 GOSUB 662
114 PRINT "NEW VALUES OF L1,L2,G(L1,L2) RE AND IMAG YES=1,NO=0"
116 INPUT I1
118 IF I1=1 GOTO 94
120 PRINT "NEW INITIAL DATA YES=1, NO=0"
122 INPUT I1
124 IF I1=1 GOTO 40
126 PRINT "EXITING FROM PROGRAM"
128 GOSUB 830
130 STOP
132 REM THIS SUBROUTINE INPUTS THE INTITIAL DATA X(1) TO X(75)
134 PRINT "BLOCK DATA GROUP GIVE LOW I2,HIGH I3 RANGE FIRST"
136 INPUT I2,I3
138 FOR I4=I2 TO I3
140 PRINT "HERE I=",I4,"X(I)="
142 INPUT X(I4)
144 NEXT I4
146 PRINT "A NEW INITIAL DATA BLOCK YES=1, NO=0"
148 INPUT I5
150 IF I5=1 GOTO 134
152 RETURN
154 REM THIS SUBROUTINE INPUTS ONE INITIAL VALUE AT ATIME.
156 PRINT "INITIAL X(I) DATA, GIVE I FIRST, THEN X "
158 INPUT I2
160 INPUT X(I2)
162 PRINT "NEW X DATA YES=1, NO=0"
164 INPUT I5
166 IF I5=1 GOTO 156
168 PRINT "DISPLAY RANGE OF X VALUES, I4 LOWER, I5 UPPER, I4=I5=0 SKIPS"
170 INPUT I4,I5
172 IF I4=0 GOTO 192
174 FOR I=I4 TO I5
176 PRINT "I=",I,"X(I)=",X(I),"TYPE 0 TO CON, -1 TO GET NEW VALUE"
178 INPUT I8
180 IF I8=0 GOTO 184
182 INPUT X(I)
184 NEXT I
186 PRINT "DONE WANT TO DISPLAY NEW X RANGE YES=1, NO=0"
188 INPUT I8
190 IF I8=1 GOTO 168
192 RETURN
194 C1=COS(X(2))
```

Figure 4.4. List of computer program BEAM (page 1).

```
196 S1=SIN(X(2))
198 L7=1
200 L8=11
202 PRINT "GENERATING INITIAL DATA"
204 REM ALL DATA INITIALIZED HERE EXCEPT L1,L2.
206 REM ALSO INCLUDE G(L1,L2) IN EXCEPTION.
208 P1=3.14159
210 K=P1*2000/X(1)
212 FOR I=1 TO 11
214 I1=I+10
216 I2=I+21
218 I3=I+32
220 I4=I+43
222 A(1,I)=(K/X(I1))/2000
224 A(2,I)=(K/X(I2))/2000
226 A(3,I)=-1/X(I3)^2
228 A(4,I)=X(I4)*1000
230 NEXT I
232 REM ALL UNITS IN PROGRAM IN MM SCALE.
234 REM INITIAL PROFILE INPUT GENERATED HERE.
236 C(7,1)=-1/X(55)^2
238 C(9,1)=-1/X(56)^2
240 C(8,1)=K/X(57)/2000
242 C(10,1)=K/X(58)/2000
244 C(3,1)=-2*C(7,1)*X(3)*X(5)
246 C(5,1)=-2*C(9,1)*X(4)*X(6)
248 C(4,1)=-2*C(8,1)*X(7)*X(5)
250 C(6,1)=-2*C(10,1)*X(8)*X(6)
252 C(1,1)=LOG(X(59))+C(7,1)*(X(3)*X(5))^2+C(9,1)*(X(4)*X(6))^2
254 C(2,1)=X(60)+C(8,1)*(X(7)*X(5))^2+C(10,1)*(X(8)*X(6))^2
256 REM FIX THE B(1-5,L) VALUES FOR CONTROL
258 FOR I1=1 TO 11
260 FOR I2=1 TO 5
262 B(I2,I1)=1
264 NEXT I2
266 NEXT I1
268 B(1,2)=0
270 B(1,4)=0
272 B(1,6)=-1
274 B(1,8)=0
276 B(1,10)=0
278 B(2,1)=0
280 B(2,3)=0
282 B(2,5)=0
284 B(2,6)=-1
286 B(2,9)=0
288 B(3,2)=0
290 B(3,4)=0
292 B(3,10)=0
294 B(3,8)=0
296 B(4,1)=0
298 B(4,3)=0
300 B(4,5)=0
302 B(4,9)=0
304 B(1,3)=-1
306 B(1,9)=-1
308 B(2,2)=-1
310 B(2,8)=-1
312 FOR I1=2 TO 10
314 B(5,I1)=C1
316 NEXT I1
318 B(5,1)=-1
320 B(5,3)=-1
322 B(5,5)=-1
324 B(5,9)=-1
326 REM NOW WE FIX THE D AND E SET OF INITIAL DATA
328 FOR L=1 TO 10
330 T1=K/A(4,L)*.5
332 T2=B(5,L)*T1/P1
334 IF T2<0 GOTO 342
336 D(1,L)=LOG(T2)
338 D(2,L)=P1/2
340 GOTO 346
342 D(1,L)=LOG(-T2)
344 D(2,L)=-P1/2
346 L9=L+1
348 FOR I2=3 TO 10
350 D(I2,L)=0
352 E(I2,L)=0
354 NEXT I2
356 E(11,L)=0
358 E(1,L)=0
360 D(7,L)=A(3,L)
362 D(9,L)=A(3,L)
364 REM IMAGINARY SET BELOW ---REAL SET ABOVE
366 D(4,L)=S1*K*B(4,L)
368 E(2,L)=-S1*K*B(3,L)
370 D(8,L)=T1*B(5,L)^2-C1*B(2,L)*A(1,L)
372 E(6,L)=T1*B(5,L9)^2+C1*B(1,L)*A(1,L9)
374 D(10,L)=T1-C1*B(2,L)*A(2,L)
376 E(8,L)=T1+C1*B(1,L)*A(2,L9)
378 E(10,L)=-2*ABS(B(5,L)*B(5,L9))*T1
380 E(12,L)=-2*T1
```

Figure 4.4. List of computer program BEAM (page 2).

```
382 NEXT L
384 RETURN
386 REM SUBROUTINE NEED L, C(L), D(L), E(L) SET
388 REM GENERATE C(   ,L+1) FROM D(   ,L),E(   L), AND C(   ,L)
390 FOR I=1 TO 4
392 I1=6+I
394 F(I)=C(I1,L)+D(I1,L)
396 NEXT I
398 R1=F(1)*F(3)-F(2)*F(4)
400 R2=F(1)*F(4)+F(3)*F(2)
402 R3=SQR(R1^2+R2^2)
404 R4=R1/R3
406 R5=R2/R3
408 IF R4<0 GOTO 410 ELSE 416
410 R7=ATN(-R5/R4)
412 R6=P1-R7
414 GOTO 424
416 IF R4>0 GOTO 422
418 R6=(P1/2)*SGN(R5)
420 GOTO 424
422 R6=ATN(R5/R4)
424 R8=LOG(P1/SQR(R3))
426 R9=-R6/2
428 J1=3
430 J7=1
432 J3=3
434 J5=7
436 GOSUB 514
438 R8=R8+Q7
440 R9=R9+Q8
442 J1=5
444 J3=5
446 J5=9
448 GOSUB 514
450 L1=L+1
452 C(1,L1)=R8+Q7+C(1,L)+D(1,L)
454 C(2,L1)=R9+Q8+C(2,L)+D(2,L)
456 J7=2
458 J1=3
460 J3=9
462 J5=7
464 GOSUB 514
466 C(3,L1)=E(1,L)+Q7*2
468 C(4,L1)=E(2,L)+Q8*2
470 J1=5
472 J3=11
474 J5=9
476 GOSUB 514
478 C(5,L1)=E(3,L)+Q7*2
480 C(6,L1)=E(4,L)+Q8*2
482 J1=9
484 J7=3
486 J3=9
488 J5=7
490 GOSUB 514
492 C(7,L1)=E(5,L)+Q7
494 C(8,L1)=E(6,L)+Q8
496 J1=11
498 J3=11
500 J5=9
502 GOSUB 514
504 C(9,L1)=E(7,L)+Q7
506 C(10,L1)=E(8,L)+Q8
508 RETURN
510 REM SUBROUTINE FOR -AX*AY/(4*AZ)
512 REM NEED J1,J3,J5,J7
514 J2=J1+1
516 J4=J3+1
518 J6=J5+1
520 F(9)=C(J5,L)+D(J5,L)
522 F(10)=C(J6,L)+D(J6,L)
524 IF J7>1 GOTO 532
526 F(7)=C(J3,L)+D(J3,L)
528 F(8)=C(J4,L)+D(J4,L)
530 GOTO 536
532 F(7)=E(J3,L)
534 F(8)=E(J4,L)
536 IF J7>2 GOTO 544
538 F(5)=C(J1,L)+D(J1,L)
540 F(6)=C(J2,L)+D(J2,L)
542 GOTO 548
544 F(5)=E(J1,L)
546 F(6)=E(J2,L)
548 Q1=F(5)*F(7)-F(6)*F(8)
550 Q2=F(5)*F(8)+F(6)*F(7)
552 Q3=F(9)^2+F(10)^2
554 Q5=-F(9)/Q3
556 Q6=F(10)/Q3
558 Q7=(Q1*Q5-Q2*Q6)*.25
560 Q8=(Q1*Q6+Q5*Q2)*.25
562 RETURN
564 REM SELECTED INITIAL ,INTERMEDIATE, AND FINAL DATA TO BE PRINTED.
566 PRINT "BULK INITIAL DATA PRT=1, NO=0, SKIPTO PRINT CONTROL=-1"
```

Figure 4.4. List of computer program BEAM (page 3).

```
568 L7=1
570 INPUT I1
572 L8=7
574 IF I1=(-1) GOTO 662
576 IF I1=0 GOTO 612
578 PRINT ON (3)"VERSION 3/9/78"
580 PRINT ON (3) B$,GETDATE$(0),GETTIME$(0)
582 PRINT ON (3)"WAVLGN=";X(1),"MICROMETERS","ANG=";X(2);"RAD"
584 PRINT ON (3)"COS(ANG)=",C1
586 PRINT ON (3)"LA=";X(3),"LB=";X(4),"S1,T1(MM)=",X(5),X(6)
588 PRINT ON (3)"LC,LD=";X(7),X(8)
590 A$="XCUR(M)      YCUR(M)      APER(M)RADIUS    L TO L+1 DIS(M)"
592 PRINT ON (3)"<10>"
594 PRINT ON (3)"L=",A$
596 FOR I=1 TO I1
598 I3=I+10
600 I4=I+21
602 I5=I+32
604 I6=I+43
606 PRINT ON (3) I,X(I3),X(I4),X(I5),X(I6)
608 NEXT I
610 GOTO 624
612 PRINT "DESIRED X(L) VALUE, L="
614 INPUT I6
616 PRINT "X(L)=",X(I6)
618 PRINT "NEW X VALUE YES =1, NO=0"
620 INPUT I6
622 IF I6=1 GOTO 612
624 PRINT "PRINT OUTPUT CONTROL"
626 FOR I=1 TO I1
628 I6=60+I
630 PRINT "I=",I,X(I6)
632 NEXT I
634 PRINT " A 1 MEANS PRINT, 0 MEANS NO PRINT IN THIS CONTROL"
636 PRINT "I=SURFACE TO BE CHANGED, 0 MEANS NO CHANGE"
638 INPUT I7
640 IF I7=0 GOTO 648
642 I6=I7+60
644 INPUT X(I6)
646 GOTO 636
648 PRINT "INITIAL DATA L=1 SURFACE PRINT YES=1,NO=0"
650 INPUT I7
652 IF I7=0 GOTO 662
654 PRINT ON (3)"WX(MM)=";X(55),"WY(MM)=";X(56),"RX(M)=";X(57)
656 PRINT ON (3)"AMPL=";X(59),"PHASE(RAD)=";X(60),"RY(M)=";X(58)
658 PRINT ON (3)"########### END OF INITIAL DATA #############"
660 PRINT ON (3)"<10>"
662 PRINT "CONT=1,SINGLE SURFACE=0 : PRINT ON 1=CRT,3=PR"
664 INPUT J5,J6
666 IF J5=0 GOTO 682
668 FOR J5=L7 TO L8
670 I7=J5+60
672 GOSUB 702
674 NEXT J5
676 L7=8
678 L8=11
680 GOTO 698
682 PRINT "J5=0 SKIPS SURFACE"
684 PRINT "SURFACE TO BE PRINTED J5=, HERE J6=1 FOR CRT,3 FOR PR"
686 INPUT J5,J6
688 I7=J5+60
690 IF J5=0 GOTO 676
692 GOSUB 702
694 GOTO 888
696 GOTO 682
698 RETURN
700 REM OUTPUT PRINT CONTROL J5 SURFACE, J6 PRINT MEDIUM
702 IF X(I7)=0 GOTO 790
704 IF J5=11 GOTO 706 ELSE 722
706 PRINT ON (J6)"<10> ######ORDER OF BEAM REFRACTED BY HOLOGRAM <10>"
708 PRINT ON (J6)"L1,L2=",X(72),X(73),"RG(L1,L2)=";X(74);
710 PRINT ON (J6)"IMG(L1,L2)=";X(75),"S7,T7 (1/MM)=";X(9),X(10)
712 PRINT ON (J6)"C(1-10,11)"
714 FOR I=1 TO 10
716 PRINT ON (J6) C(I,11),
718 NEXT I
720 PRINT ON (J6)"#########################<10>"
722 X8=.1E-19
724 IF C(7,J5)<0 GOTO 730
726 PRINT "IMPROPER WX FOR L=",J5
728 GOTO 126
730 W1=SQR(-1/C(7,J5))
732 IF C(9,J5)<0 GOTO 740
734 PRINT "IMPROPER WY FOR L=",J5
736 PRINT "C(9,L)=",C(9,J5)
738 GOTO 126
740 W2=SQR(-1/C(9,J5))
742 T5=C(8,J5)
744 IF ABS(T5)>X8 GOTO 750
746 T5=T5+.1E-29*SGN(T5)
748 T5=X8*SGN(T5)*K*.5
750 R1=K/T5*.5
752 T6=C(10,J5)
```

Figure 4.4. List of computer program BEAM (page 4).

```
754 IF ABS(T6)>X8 GOTO 760
756 T6=T6+.1E-29*SGN(T6)
758 T6=X8*SGN(T6)*K*.5
760 R2=K/T6*.5
762 X1=C(3,J5)/C(7,J5)*(-.5)
764 X3=-C(4,J5)/T5*.5
766 Y1=C(5,J5)/C(9,J5)*(-.5)
768 Y3=-C(6,J5)/T6*.5
770 P3=C(2,J5)-C(8,J5)*X3^2-C(10,J5)*Y3^2
772 P0=C(1,J5)+(X1/W1)^2+(Y1/W2)^2
774 P2=EXP(P0)
776 Q9=P2*P2*PI*WI*W2*(.5)*ABS(B(5,J5))
778 PRINT ON (J6)"SURFACE PARAMETERS PRINTED NEXT HAS L=",J5
780 PRINT ON (J6)"ALL IN MM, WX,WY,RX,RY=",WI,W2,R1,R2
782 PRINT ON (J6)"RATIO WX/WY=,1/RX,1/RY PROP TO",W1/W2,C(8,J5),C(10,J5)
784 PRINT ON (J6)"ALL IN MM, X1,X3,Y1,Y3=",X1,X3,Y1,Y3
786 PRINT ON (J6)"AMPLITUDE=",P2,"PHASE(RAD)=",P3,"POWER=",Q9
788 PRINT ON (J6)"<10><10>"
790 RETURN
792 REM THIS SUBROUTINE COMPARES EXPECTED S7,T7 WITH ACTUAL S7,T7
794 REM USE (A*2*PI/LAMDA/F)*.5*(CI OR 1.0) TO GET S7,T7 RESPECTIVELY
796 T7=P1*4*X(25)/(X(1)*X(23)*X(27))
798 T7=T7*X(6)*.5*C1
800 S7=P1*4*X(14)/(X(1)*X(12)*X(16))
802 S7=S7*X(5)*.5
804 PRINT "SIMPLE THEORY EXPECT S7=",S7,"ACTUAL=",X(9)
806 PRINT "CHANGE ACTUAL VALUE YES=1, NO=0"
808 INPUT I1
810 IF I1=0 GOTO 816
812 PRINT "S7=?"
814 INPUT X(9)
816 PRINT "SIMPLE THEORY EXPECT T7=",T7,"ACTUAL=",X(10)
813 PRINT "CHANGE ACTUAL VALUE YES=1,NO=0"
820 INPUT I1
822 IF I1=0 GOTO 828
824 PRINT "T7=?"
826 INPUT X(10)
828 RETURN
830 PRINT "DONE WITH PROGRAM AND NOW EXITING"
832 GOSUB 864
834 CLOSE 1
836 CLOSE 3
838 RETURN
840 PRINT "READ IN FROM FILE X(1-75) DATA"
842 PRINT "YES=1, NO=0"
844 INPUT I1
846 IF I1=0 GOTO 862
848 CLOSE 2
850 OPEN "DATA",2,2
852 REW 2
854 FOR I8=1 TO 75
856 INFILE ON (2) X(I8)
858 NEXT I8
860 CLOSE 2
862 RETURN
864 PRINT "PRINT TO FILE X(1-75) DATA"
866 PRINT "YES=1, NO=0"
868 INPUT I1
870 IF I1=0 GOTO 886
872 CLOSE 2
874 OPEN "DATA",2,1
876 REW 2
878 FOR I8=1 TO 75
880 OUTFILE ON (2) X(I8)
882 NEXT I8
884 CLOSE 2
885 RETURN
888 PRINT "STORE LSQFIT DATA, 1=YES, 0 = NO"
890 INPUT I8
892 IF I8=0 GOTO 682
894 OUTFILE ON (4) X(L3),X(L4),X(L5),L6
896 IF J5=11 GOTO 904
898 OUTFILE ON (4) X1,Y1,C(8,J5),C(10,J5)
900 GOTO 906
902 PRINT "CASES LEFT L6=",L6
904 OUTFILE ON (4) X1,Y1,WI/W2,C(8,11)
906 PRINT "CASES LEFT L6=",L6
903 L6=L6-1
910 GOTO 960
912 PRINT "RESET AND OPEN LSQ FILE 1=YES, 0=NO"
914 INPUT I8
916 IF I8=0 GOTO 958
918 CLOSE 4
920 OPEN "ERIC:LSQ",4,1
922 REW 4
924 PRINT "NUMBERS OF PARAMETERS=?"
926 INPUT L6
928 PRINT "LOCATION OF PARAMETERS?"
930 PRINT "FIRST L3="
```

Figure 4.4. List of computer program BEAM (page 5).

```
932 INPUT L3
934 IF L6>1 GOTO 942
936 L4=1
938 L5=1
940 GOTO 956
942 PRINT "SECOND L4="
944 INPUT L4
946 IF L6>2 GOTO 952
948 L5=1
950 GOTO 956
952 PRINT "THIRD L5="
954 INPUT L5
956 OUTFILE ON (4) L6,L3,L4,L5
958 RETURN
960 IF L6>(-1) GOTO 698
962 GOTO 966
964 RETURN
966 CLOSE 4
968 OPEN "LSQ",4,2
970 REW 4
972 INFILE ON (4) L1,L3,L4,L5
974 PRINT "NUMBER OF VALUES TO BE DRIVEN TO REFERENCE"
976 INPUT L2
978 DIM E(L2),C(L2),D(L1),H(L1),B(L2,L1),F(L1,L1),G(L1,L1)
980 DIM A(4)
982 PRINT "REFERENCE VECTOR C(L2)="
984 FOR I=1 TO L2
986 PRINT "I=",I,"C(I)=?"
988 INPUT C(I)
990 NEXT I
992 INFILE ON (4) S(1),S(2),S(3),S(4)
994 INFILE ON (4) A(1),A(2),A(3),A(4)
996 FOR L8=1 TO L1
998 INFILE ON (4) Y(1),Y(2),Y(3),Y(4)
1000 A1=Y(L8)-S(L8)
1002 INFILE ON (4) S(5),S(6),S(7),S(8)
1004 FOR I=1 TO L2
1006 B(I,L8)=(S(I+4)-A(I))/A1
1008 NEXT I
1010 NEXT L8
1012 FOR I=1 TO L2
1014 E(I)=A(I)-C(I)
1016 NEXT I
1018 FOR I1=1 TO L1
1020 D(I1)=0
1022 FOR I2=1 TO L1
1024 F(I1,I2)=0
1026 FOR I3=1 TO L2
1028 IF I2>1 GOTO 1032
1030 D(I1)=D(I1)+B(I3,I1)*E(I3)
1032 F(I1,I2)=F(I1,I2)+B(I3,I1)*B(I3,I2)
1034 NEXT I3
1036 NEXT I2
1038 NEXT I1
1040 FOR I1=1 TO L1
1042 FOR I2=1 TO L1
1044 IF I2=I1 GOTO 1048
1046 F(I1,I2)=F(I1,I2)/F(I1,I1)
1048 NEXT I2
1050 D(I1)=D(I1)/F(I1,I1)
1052 F(I1,I1)=1
1054 NEXT I1
1056 MAT G=INV(F)
1058 FOR I1=1 TO L1
1060 H(I1)=0
1062 FOR I2=1 TO L1
1064 H(I1)=H(I1)-G(I1,I2)*D(I2)
1066 NEXT I2
1068 NEXT I1
1070 PRINT "I, OLD, NEW, INCREMENT RESPECTIVELY"
1072 FOR I1=1 TO L1
1074 PRINT "I=";I1,S(I1),S(I1)+H(I1),H(I1)
1076 NEXT I1
1078 CLOSE 4
1080 GOTO 12
1082 END
```

Figure 4.4. List of computer program BEAM (page 6).

```
VERSION 6/29/78
BEAM TRACE               **********           06/29/78        11:17:19
WAVLGN= 1.06     MICROMETERS      ANG= .14 RAD
COS(ANG)=        .990216
LA= 7            LB= 7            S1,T1(MM)=      5               5
LC,LD= 7         7
L=               XCUR(M)       YCUR(M)      APER(MM)RADIUS  L TO L+1 DIS(M)
 1                .1E21          .1E21           10000           1.0098859
 2               -2.0397183     -2               224             1.0098713
 3                .1E21          .1E21           400              .10098901
 4                .2039718       .2              50               .10098787
 5                .1E21          .1E21           400             1.0098759
 6               -2.0396975     -2               224             1.0107332
 7                .1E21          .1E21           20              1.0090289
 8               -2.0397384     -2               224             1.0098854
 9                .1E21          .1E21           400              .11108752
 10               .20397546      .2              50              1.1108761
 11               .1E21          .1E21           400            -30
WX(MM)= .5       WY(MM)= .5       RX(M)= .1E21
AMPL= 1          PHASE(RAD)= 0    RY(M)= .1E21
*********** END OF INITIAL DATA *************
SURFACE PARAMETERS PRINTED NEXT HAS L=        1
ALL IN MM, WX,WY,RX,RY=           .5            .5               .1E24          .1E24
RATIO WX/WY=,1/RX,1/RY PROP TO 1                .29637642E-19    .29637642E-19
ALL IN MM, X1,X3,Y1,Y3=           35            35               35             35
AMPLITUDE=       1                PHASE(RAD)=   .43140831E-31 POWER=            .39269875

SURFACE PARAMETERS PRINTED NEXT HAS L=        2
ALL IN MM, WX,WY,RX,RY=           .85358927     .84523775        6863.2254      6729.5864
RATIO WX/WY=,1/RX,1/RY PROP TO 1.0098807        .43183256        .44040807
ALL IN MM, X1,X3,Y1,Y3=           35.345824     1110.8293        35             151.61552
AMPLITUDE=       .59153504        PHASE(RAD)=  -538306.88        POWER=         .39267951

SURFACE PARAMETERS PRINTED NEXT HAS L=        3
ALL IN MM, WX,WY,RX,RY=           .68148381     .68148373        .14623131E11   -.49125667E10
RATIO WX/WY=,1/RX,1/RY PROP TO 1.0000001        .20267644E-6    -.60330258E-6
ALL IN MM, X1,X3,Y1,Y3=           .39192519E-6  .50679937E9      .10080396E-5   -.17025672E9
AMPLITUDE=       .69836857        PHASE(RAD)=  -.34568409E11     POWER=          .35579506
SURFACE PARAMETERS PRINTED NEXT HAS L=        4
ALL IN MM, WX,WY,RX,RY=           .69006626     .68331455       -208.21691      -204.16244
RATIO WX/WY=,1/RX,1/RY PROP TO 1.0098808       -14.234022       -14.516697
ALL IN MM, X1,X3,Y1,Y3=          -3.5345964    -36.162624       -3.5000142      -7.0378505
AMPLITUDE=       .6964964         PHASE(RAD)=   18613.48         POWER=          .35579403

SURFACE PARAMETERS PRINTED NEXT HAS L=        5
ALL IN MM, WX,WY,RX,RY=           .50004885E-1  .50004798E-1     80789106        40294169
RATIO WX/WY=,1/RX,1/RY PROP TO 1.0000017        .36685196E-4     .73553177E-4
ALL IN MM, X1,X3,Y1,Y3=          -3.4999781     501.11065       -3.4999791       243.24743
AMPLITUDE=       9.4229956        PHASE(RAD)=  -16.900377        POWER=          .34875593

SURFACE PARAMETERS PRINTED NEXT HAS L=        6
ALL IN MM, WX,WY,RX,RY=           6.8816677     6.8143492        2060.0948       2019.9598
RATIO WX/WY=,1/RX,1/RY PROP TO 1.0098789        1.4386543        1.4672392
ALL IN MM, X1,X3,Y1,Y3=          -3.5409303     280.40251       -3.5061631      -7.0003012
AMPLITUDE=       .69137E-1        PHASE(RAD)=  -113119.65        POWER=          .34864914

SURFACE PARAMETERS PRINTED NEXT HAS L=        7
ALL IN MM, WX,WY,RX,RY=           6.8782011     6.8110474       -.19980748E9     .20721711E9
RATIO WX/WY=,1/RX,1/RY PROP TO 1.0098595       -.14833099E-4     .143027E-4
ALL IN MM, X1,X3,Y1,Y3=          -.12029812E-4 -27196046         .12082362E-4   -718159.61
AMPLITUDE=       .69104703E-1     PHASE(RAD)=   .10963553E11     POWER=          .3479793I
SURFACE PARAMETERS PRINTED NEXT HAS L=        8
ALL IN MM, WX,WY,RX,RY=           6.504488      6.4476755       -2060.1489      -2020.0522
RATIO WX/WY=,1/RX,1/RY PROP TO 1.0088113       -1.4386165       -1.467172
ALL IN MM, X1,X3,Y1,Y3=           3.5316034    -280.40989        3.4970375       7.0004621
AMPLITUDE=       .6910239E-1      PHASE(RAD)=   113113.34        POWER=          .31149557

SURFACE PARAMETERS PRINTED NEXT HAS L=        9
ALL IN MM, WX,WY,RX,RY=           .5292771E-1   .5287127IE-1    -4032425.7      -2421566.2
RATIO WX/WY=,1/RX,1/RY PROP TO 1.0010675       -.73498294E-3    -.12239038E-2
ALL IN MM, X1,X3,Y1,Y3=           3.5000479     27.233733        3.4999786       17.494229
AMPLITUDE=       8.4104591        PHASE(RAD)=  -2.4272773        POWER=          .31092939

SURFACE PARAMETERS PRINTED NEXT HAS L=        10
ALL IN MM, WX,WY,RX,RY=           .71716338     .71089624        254.90627       249.93493
RATIO WX/WY=,1/RX,1/RY PROP TO 1.0088158        11.626878        11.858143
ALL IN MM, X1,X3,Y1,Y3=           3.5352909     43.479015        3.5006205       7.8310115
AMPLITUDE=       .62607663        PHASE(RAD)=  -22061.484        POWER=          .31083417


 ******ORDER OF BEAM REFRACTED BY HOLOGRAM
L1,L2=           0                0             RG(L1,L2)= 0  IMG(L1,L2)= 0     S7,T7 (1/MM)= 1.4530308 1.4673733
C(1-10,11)
-8753.6118       -3.7435917       -249.83561    -.52222223E-1  -250.36028       .13694027E-1  -3.56908 2.9339998
-3.5765753       2.9349362        ***************************
SURFACE PARAMETERS PRINTED NEXT HAS L=        11
ALL IN MM, WX,WY,RX,RY=           .52932434     .5287694         1010.1446       1009.8223
RATIO WX/WY=,1/RX,1/RY PROP TO 1.0010495        2.9339998        2.9349362
ALL IN MM, X1,X3,Y1,Y3=          -35.000001     .88994933E-2    -35.000001      -.23329344E-2
AMPLITUDE=       .83246726        PHASE(RAD)=  -3.74384          POWER=          .30467864
```

Figure 4.5. Sample print of BEAM (page 1).

```
SURFACE PARAMETERS PRINTED NEXT HAS L=        8
ALL IN MM, WX,WY,RX,RY=         6.504488      6.4476755     -2060.1489      -2020.0522
RATIO WX/WY=,1/RX,1/RY PROP TO 1.0088113     -1.4386165     -1.467172
ALL IN MM, X1,X3,Y1,Y3=         3.5316034     -280.40989      3.2472501       6.5004295
AMPLITUDE=       .6910239E-1    PHASE(RAD)=   113108.38      POWER=          .31149557

SURFACE PARAMETERS PRINTED NEXT HAS L=        9
ALL IN MM, WX,WY,RX,RY=         .5292771E-1   .52871271E-1  -4032425.7      -2421566.2
RATIO WX/WY=,1/RX,1/RY PROP TO 1.0010675     -.73498294E-3  -.12239038E-2
ALL IN MM, X1,X3,Y1,Y3=         3.5000479     27.233733      3.2499804       16.24279
AMPLITUDE=       8.4107413      PHASE(RAD)=  -2.4645316      POWER=          .31095025

SURFACE PARAMETERS PRINTED NEXT HAS L=        10
ALL IN MM, WX,WY,RX,RY=         .71716338     .71089624      254.90627       249.93493
RATIO WX/WY=,1/RX,1/RY PROP TO 1.0088158     11.626878      11.858143
ALL IN MM, X1,X3,Y1,Y3=         3.5352909     43.479015      3.2505763       7.271654
AMPLITUDE=       .62610424      PHASE(RAD)=  -22006.085      POWER=          .31086158


 ######ORDER OF BEAM REFRACTED BY HOLOGRAM
L1,L2=           0              -1            RG(L1,L2)= 0 IMG(L1,L2)= 0    S7,T7 (1/MM)= 1.4530308 1.4673733
C(1-10,11)                                                                                    -
-8150.0644      -3.7815591      -249.83561    -.52222223E-1  -232.47742      .12716337E-1  -3.56908 2.9339998
-3.5765753       2.9349362      ##########################
SURFACE PARAMETERS PRINTED NEXT HAS L=        11
ALL IN MM, WX,WY,RX,RY=         .52932434     .5287694       1010.1446       1009.8223
RATIO WX/WY=,1/RX,1/RY PROP TO 1.0010495     2.9339998      2.9349362
ALL IN MM, X1,X3,Y1,Y3=        -35.000001     .88994933E-2  -32.500003      -.21663736E-2
AMPLITUDE=       .83306618      PHASE(RAD)=  -3.7818052      POWER=          .3051172
```

Figure 4.5. Sample print of BEAM (page 2).

$$Z(1) = A*EXP\left\{ -[(u_1 - S1*LA)/WX]\uparrow 2 \\ -[(v_1 - T1*LB)/WY]\uparrow 2 \\ + ik[(u_1 - S1*LC)\uparrow 2/(2*RX)] \\ + ik[(v_1 - T1*LD)\uparrow 2/(2*RY)] \\ + i\phi \right\}. \qquad (4.1)$$

4.2 The Detailed Listing of the Computer Program

The logic flow gives the boundaries for each function in the program. In most cases, knowing these functions and using the list of the program gives sufficient information. In subsection 3.3 and in other parts of section 3, we define the mathematics. All that remains to be described about the program's logic flow is the fact that there is temporary storage of numbers which allows appropriate interface between function blocks. Examples are those statements at 100 to 104 and those at 456 and 462.

There are many system-sensitive statements in this listing such as the opening and closing of files. The program will have to be adjusted to reflect the system used so the program can function as intended.

For convenience in analysis, the program computes RX and RY and X3 and Y3. In some cases, RX and RY can be so large that the computation becomes meaningless; therefore, statements around 744 and 754 will cause the value of RX and RY to be set to a maximum. The prime result of this constraint is an absurd value for X3 and Y3. Since this condition occurs when the phase front is almost plane wave, X3 and Y3 are poorly defined anyway. If a different range is wanted, X8 in statement 722 can be changed to some other value.

4.3 Sample Output to Illustrate the Program

Figure 4.5 shows a print for two different beam traces (a zero and a -1 diffraction order) from surfaces 1 to 11 to illustrate what output can appear on the printer.

Given all previous discussions and definitions, most terms should be clear except the POWER term. This represents the total power in watts in the Gaussian beam incident on the designated surface. This term helps the user to select appropriate aperturing by each mirror so that there is no serious attenuation for off-axis beams, namely those with large LA, LB, LC, and LD.

Notice that this print has the same stage I results for these beam traces. In contrast, the stage II results are printed twice to reflect changes.

Also note that the control parameters for stage II are printed next to surface 11 print rather than at the beginning of stage II. This is done because many traces will print only the initial conditions and the surface 11 results. The intermediate data usually have no interest and are therefore suppressed. To reproduce results, control

data cannot be suppressed and are recorded in the output.

5. THE 10.6 μm WAVELENGTH

Here we select the control values for an apparatus that would be optimum for 10.6 μm wavelength. As already stated, some of these values must be arbitrary. Once they have been selected, then other values can optimize the desired output of the apparatus. In subsection 5.1 we select the arbitrary values, and in subsection 5.2 we define the criteria that optimize the remaining values.

We examine two configurations, namely a version that uses only off-the-shelf mirrors with spherical or single curvature and a more expensive version that uses custom-made mirrors with two (elliptical) curvatures.

In subsection 5.3 we develop the expected output when all mirrors have fixed spherical curvatures.

In subsections 5.4, 5.4.1, and 5.4.2, we deal with the elliptical optics. In subsection 5.4.1 we show what happens for changing wavelength, and in subsection 5.4.2 we show how the positions of the mirrors change the output.

Because 10.6 μm is not a convenient wavelength for alignment, we show in subsection 5.5 what to expect for selected beams at 0.6328 μm wavelength going through the apparatus using the elliptical optics.

This section is concluded in subsection 5.6 by a discussion of high irradiance effects on the surfaces of the mirrors and hologram. This consideration is important to establish the limits to the incident irradiance at the prefilter.

5.1 Selecting Some Initial Control Values

To design this reflection apparatus, we must select some arbitrary values. We discuss them in this subsection. We note at this point that there are numerous other choices, and some may prove to be better than those described here.

The first arbitrary value is the focal length for each focusing mirror. For an apparatus to be of a moderate size when using 10.6 μm wavelength, the unit should not be much larger than a meter. Therefore, we set the radius of curvature in the Y coordinate at 2 meters for all focusing mirrors. This curvature implies a focal length of 1 meter.

The second arbitrary parameter is the width of a beam. I selected 10 cm as a convenient size for the diameter of the beam because most reflection optics that are not custom made are restricted to 20 cm (8 inches) in diameter or less and because we need adequate clearance for each beam to account for diffraction effects created at the Hartmann plate.

The third parameter is the size of the sampling holes; they should be as small as possible. To drill a hole less than 1 mm in diameter requires extraordinary procedures; therefore, we set the sampling hole size to 1 mm.

The fourth parameter is the sampling frequency for the square array in the Hartmann plate. The key constraints here are the size of the detectors in the array at the cross-correlation plane and the size of each cross-correlation spot. Aperturing

and cross-correlation effects cause each spot to be 2 mm or less in diameter. For a 10 ns speed of response, each detector should be less than this diameter. Since the distance between detectors should allow clearance for adjustment, say 0.5 mm, to account for various astigmatic effects, we assume each detector in the array is separated by 2.5 mm to capture the center of these cross-correlation spots. Given this form, we infer the separation at the prefilter is 5 mm between centers of sampling holes.

In the test beam analysis, our nominal sampling values for (LA,LB) are: (10,0) for a deflection in the x axis; (0,10) for a deflection in the y axis; (7,7) for a deflection along the 45° diagonal; and (0,0) for the zero deflection or optical axis beam. These four principal values are arbitrarily chosen to define all simulation studies. Additional test beams may be used; however, each is keyed to one of the principal beams.

As a matter of convenience, the simulation studies in this paper set LC = LD = 7 for all runs because the initial curvatures imply a plane wave which means the positions of X3 and Y3 are irrelevant.

The plane surfaces, namely 1, 3, 5, 7, 9, and 11 all have a radius of curvature equal to 10^{20} m for both the X and Y coordinates.

The 1 mm sampling holes imply at a distance of 1 m an Airy disk with a 26 mm diameter. To avoid significant aperturing by a sample beam 5 mm from the optical axis, we increase the radius of our optics by two Airy diameters. This means 102 mm (4 inch) radius optics. To simulate the aperture properly for the Gaussian beams, we arbitrarily require that 80% of the Gaussian beam power pass when the beam radius is 100 mm. This implies:

$$\frac{P}{P_o} = \exp(-x^2/\sigma^2) \text{ or } (x^2/\sigma)^2 = 0.2 \; .$$

With x = 100, then σ = 225 mm.

We arbitrarily set those flat surface apertures at 400 mm which means no significant absorption takes place at these surfaces. Since surface 7 has an Airy disk of approximately 26 mm in diameter (the second ring is at 48 mm), we choose an aperture that will pass this basic beam with room to spare. A convenient size for the Gaussian beam and the design sample is 40 mm in diameter. This dimension will comfortably fit the 50 mm optical flats that can be plated with available equipment during metal evaporation. The remaining 10 mm can be used for fiducial marks which are needed during the multiple evaporation cycles on these flats. In the final construction of the apparatus, it may be necessary to use a larger diameter aperture such as 100 mm to avoid a significant distortion to the final spots in the cross-correlation plane.

The remaining aperture at surface 1 is arbitrarily set to 10 m which obviously is a meaningless number. It makes the aperturing by surface 1 unimportant. All aperturing by the prefilter shows in the initial beam parameters.

We fix the initial beam parameters by four assumptions: (1) We assume the curvatures exiting from each sampling hole are very large, say 10^{20} m. (2) We set the phase of a single beam to zero and its amplitude to 1. This implies no loss in generality, but a gain in convenience for comparison of various simulations. (3) We

assume circular sampling holes; hence, we set WY = WX to fix the y width of the Gaussian beam. (4) We select the nominal value for WX by the following ad hoc reasoning. At the Fourier plane, the true pattern produced by the sampling holes at the Hartmann plate is an Airy disk with a diameter of 26 mm. This disk contains 84 percent of the power in the beam. If we set the width of a Gaussian beam to this diameter, we would have a Gaussian beam with 86 percent of the power within this area. This beam size implies a Gaussian beam of 0.5 mm in diameter at the prefilter. Because we wish less variation in beam size, we double this value to equal the sample hole. In this case, the beam at surface 7 is 13 mm in diameter. We use WX = 0.5 mm for the simulations.

This choice for beam width affects critically the necessary size for the aperture at surface 7 that will minimize distortion in the cross-correlation plane. A builder of the apparatus should run additional simulations to test the effect of aperturing on the beam profile measurements. For now, we dispense with these detailed studies. Our goal in this paper is to identify what must be done. This paper does a first-order pass at the design so the preliminary costs for construction of the apparatus can be estimated as realistically as possible.

There remains one control parameter to be fixed within this subsection, namely the angle of reflection, θ, along the optical axis. Given the 204 mm optics and the 1 m distance between surfaces 1 and 2, we require this angle to exceed 0.102 radians. We clearly need significant clearance to allow proper baffling of stray beams in the apparatus and appropriate room for mechanical fixtures. A reasonable margin would make a 50 percent increase in angle. For example, when $\cos(\theta) = 0.99$, the angle is 0.14 rad. We choose this value for our simulations. In the final construction of the apparatus, the reader should expect this angle to change because some mechanical or optical part will bend some beam in the unit. A smaller angle implies less elliptical curvatures. Unfortunately, this reduction of the angle implies mirrors with much larger focal lengths and a correspondingly longer apparatus.

5.2 The Convergence Criteria for the Rest of the Control Values

There remain seventeen control values to be fixed in these simulations: the five x-curvature values for the mirrors; the ten position values for placement of these mirrors; and the hologram parameters S7 and T7. In this subsection we set them for our design. The selection process is slightly different for spherical mirrors than for elliptical mirrors. This procedure is not unique because there are arbitrary choices. The best method depends on the allowed parameters for adjustment.

Given the above, we fix these control values as follows: First, we guess initial values for each type of mirror. Second, some arbitrary formulas constrain others. Third, figures 5.1 and 5.2 show the required convergence conditions for other control values. Finally, the values of S7 and T7 are adjusted to get the desired diffraction of the incident beams at surface 7.

As already discussed, this optimization uses one beam, namely that with LA = LB = 7 for the simulation. Here we use a nominal focal length for our optics, namely f = 1 m, and use the angle for astigmatism effects as $\theta = 0.14$ rad. Three constants are useful for fixing initial data, namely $Cx \equiv (Cy)^2 = 1.019858981$, $Cy \equiv f/\cos\theta = 1.009880676$, and $M = \lambda/10.6$. Here λ is the wavelength of the laser beam in micrometers. Thus, M = 1 for $\lambda = 10.6$ µm and 0.1 for $\lambda = 1.06$ µm.

Given these constants, the initial values for the elliptical mirrors are:

$$X(12) = X(16) = X(18) = -2*Cx/f, \text{ and}$$

$$X(14) = X(20) = 2*M*Cx/f \ . \qquad (5.1)$$

The distance values are started at:

$$X(44) = X(45) = X(48) = X(49) = X(50) = X(51) = Cy \ ,$$

$$X(46) = X(47) = Cy*M \ ,$$

$$X(52) = Cy*M/(1+M) \ , \text{ and}$$

$$X(53) = X(52)/M \ . \qquad (5.2)$$

If the simulations uses spherical mirrors only, then exactly the same distance values are used, but the mirror curvatures are set to:

$$X(12) = X(16) = X(18) = -2*f \ , \text{ and}$$

$$X(14) = X(20) = 2*M*f \ . \qquad (5.3)$$

S7 and T7 use the formula in the program and their values are printed during a computer run. This fixes an initial guess for starting the simulation process.

Because the apparatus has discrete beams progressing through it and because the number of those beams are restricted during the adjustment sequence in the interest of keeping the process simple, we must constrain somewhat arbitrarily several distance values between the mirrors. These values are insensitive to the critical features of the beams; thus, the constraints remove simply unneeded degrees of freedom. If a different alignment or simulation technique is chosen which uses many beams in addition to the LA = LB = 7 case, then the adjustment sequence changes and these arbitrary constraints should be dropped for a different criteria such as a least squares fit technique. The constraints are:

$$X(46) = M*Cx/X(45) \ ,$$

$$X(50) = Cx/X(49), \text{ and}$$

$$X(52) \text{ remains constant.} \qquad (5.4)$$

Thus, two distances are constrained relative to other distances. These constraints arise by requiring the mirrors to be separated by their respective focal lengths with a modification due to the fact there is off-axis illumination. The choice for X(52) arises by using the image equation, again with the adjustment for the off-axis illumination.

In the case of elliptical mirrors there remain twelve control values to adjust for the desired beam behavior in the apparatus. These are shown in figure 5.1 along with the desired target values for the beam parameters at each surface. In this simulation, we track four terms, namely the center of the beam, X1 and Y1, and two terms proportional to inverse of the curvature, $\pi/(Rx*\lambda)$ and $(\pi/Ry*\lambda)$.

In the real apparatus, these curvature parameters are not accurately or easily measured; therefore, two beams can be used to create an interference pattern at each surface exposing the details of the phase front. We have not established which pair of beams is best for this adjustment; therefore, we only suggest that an appropriate beam pair may be either (LA,LB) = (7,7) and (-7,-7) or (7,7) and (0,0).

In considering other adjustment strategies, we suggest that the reader consider the changes in the X3 and Y3 values for each beam to help infer appropriate positions for the mirrors.

In the case of only spherical mirrors, there remain five control values to be adjusted. The mirror curvatures are fixed, and the distances X(45) and X(49) are set to the initial values as defined in eqs (5.1)-(5.3). The results in figure 5.2, similar to those in figure 5.1, show the desired converged values for the spherical mirrors. When a physical apparatus is adjusted, we have fixed-curvature mirrors; therefore, the strategy for its adjustment would follow the sequence defined for these spherical mirrors. The difference between the two types of mirrors shows how accurately the beams remain astigmatic at each surface. For the ideal situation with no astigmatism, surfaces 3, 5, 9, and 11 would each show a square array of spots when the Hartmann plate is illuminated by a uniform irradiance and flat, phase front beam.

To get accurate control values during these simulations, we use the LSQ part of the program. The simulation process adjusts the parameters of each surface as shown in figures 5.1 or 5.2. These parameters are adjusted completely to get as close as possible the desired final values for each surface before any adjustments are made at the next surface. This process causes the accumulative errors to transfer to the remaining surfaces. We do not prove that this sequence is best for adjusting an apparatus. We assume that it is best both for finding the ideal control parameters and for minimizing the astigmatism effects for the actual apparatus. As already stated, the preliminary adjustments in the physical apparatus would use these results.

Adjust Only	Surface	Final Values of: X1	Y1	$\pi/(RX*\lambda)$	$\pi/(Ry*\lambda)$
X(44), X(45), X(12)	3	0	0	0	0
X(47), X(14)	5	-35*M	-35*M	0	0
X(48), X(49), X(16)	7	0	0	0	0
X(51), X(18)	9	35*M	35*M	0	0
X(53), X(20)	11	-35	-35	**	**

** Means these values are not used for convergence.

Figure 5.1. Desired final values for beam parameters in elliptical case. Here we show the allowed control variables that are changed for each surface. The adjustment sequence is surface 3 first, then 5, etc.

Adjust Only	Surface	X1	Y1	$\pi/(RX*\lambda)$	$\pi/(Ry*\lambda)$
		Final Values of:			
X(44)	3	**	**	0	0
X(47)	5	-35*M	-35*M	**	**
X(48)	7	**	**	0	0
X(51)	9	35*M	35*M	**	**
X(53)	11	-35	-35	**	**

** Means these values are not used for convergence.

Figure 5.2. Desired final values for beam parameters in spherical case. Here we show the allowed control variables that are changed for each surface. The adjustment sequence is surface 3 first, then 5, etc.

As already stated the final adjustments would use the desired form of the spots at the cross-correlation plane as the reference base and then use all available adjustments in distances as well as angles between mirrors to fine tune the actions of the apparatus. If possible, the positions of detectors may also be adjusted during this adjustment sequence.

After the curvatures and distances are fixed by the computer runs, then the ideal hologram can be identified. Using LSQ and L1 = L2 = 1, we adjust S7 and T7 so the diffracted beams form spots for surface 11 at X1 = Y1 = -37.5 mm. Because the real apparatus has a hologram with fixed S7 and D7, the adjustment strategy changes. Here adjustments use the desired structure of all spots in the cross-correlation plane. This structure controls the final adjustment for the distances between mirrors, the various angle coordinates of the mirrors, and finally the spatial distribution of the array of detectors at the cross-correlation plane. The form of this final adjustment process critically depends on the allowed dynamical range for incident laser wavelengths at a given setup as well as on the allowed field of view for the incident beam at the Hartmann plate.

5.3 The Spherical Optics Data

We list here a summary of the data generated in the computer simulation runs using spherical optics. These data are shown in figures 5.3 to 5.8. This subsection briefly explains each figure and expands where necessary on the results to explain what each figure means.

Figure 5.3 contains a summary of the initial data for the simulation. These data and the convergence criteria of subsection 5.2 imply the final data shown in figure 5.4. To sense what these results imply, we print selected numbers in figures 5.5 through 5.8 for some surfaces and some beams. Figures 5.5 and 56 show results for the initial configuration case, and figures 5.7 and 5.8 show those same results after the mirrors have been adjusted according to the convergence criteria.

The principal conclusion drawn from these results is that beam profile work of high precision with spherical mirrors is not possible. To use these mirrors requires substantial reduction of the reflection angle with corresponding substantial increases in the distances between mirrors and in the curvatures of these mirrors. In addition, we need significant reduction of the field of view for the apparatus.

```
VERSION 6/29/78
BEAM TRACE                           *********          07/14/78        14:42:43
WAVLGN  10.6          MICROMETERS        ANG.  .14 RAD
COS(ANG)               .990216
LA 7                  LB 7               S1,T1(MM)        5               5
LC,LD  7               7

 L                     XCUR(M)          YCUR(M)     APER(MM)RADIUS    L TO L+1 DIS(M)
 1                      .1E21            .1E21           10000           1.0098807
 2                    -2                -2               224             1.0098807
 3                      .1E21            .1E21           400             1.0098807
 4                     2                 2               224             1.0098807
 5                      .1E21            .1E21           400             1.0098807
 6                    -2                -2               224             1.0098807
 7                      .1E21            .1E21           20              1.0098807
 8                    -2                -2               224             1.0098807
 9                      .1E21            .1E21           400             2.0197613
 10                    2                 2               224             2.0197613
 11                     .1E21            .1E21           400             -30
WX(MM)     .5          WY(MM)     .5     RX(M)   .1E21
AMPL    1              PHASE(RAD)    0   RY(M)   .1E21
                     END OF INITIAL DATA

                      S7, T7 (1/MMD) = 1.4530308     1.4673733
```

Figure 5.3. Initial guess of control data for spherical mirrors.

```
VERSION 6/29/78
BEAM TRACE                           *********          07/17/78        09:29:17
WAVLGN  10.6          MICROMETERS        ANG.  .14 RAD
COS(ANG)               .990216
LA 7                  LB 7               S1,T1(MM)        5               5
LC,LD  7               7

 L                     XCUR(M)          YCUR(M)     APER(MM)RADIUS    L TO L+1 DIS(M)
 1                      .1E21            .1E21           10000           .9997152
 2                    -2                -2               224             1.0098807
 3                      .1E21            .1E21           400             1.0098807
 4                     2                 2               224             .98995757
 5                      .1E21            .1E21           400             1.0100388
 6                    -2                -2               224             1.0098807
 7                      .1E21            .1E21           20              1.0098807
 8                    -2                -2               224             .98169863
 9                      .1E21            .1E21           400             2.0197613
 10                    2                 2               224             2.0027554
 11                     .1E21            .1E21           400             -30
WX(MM)     .5          WY(MM)     .5     RX(M)   .1E21
AMPL    1              PHASE(RAD)    0   RY(M)   .1E21
                     END OF INITIAL DATA

                      S7, T7 (1/MM) = 1.4530308     1.4673733
```

Figure 5.4. Final values of control data for spherical mirrors.

Beam Surface	LA = 0 X1(mm)	LB = 0 Y1(mm)	$\pi/(RX * \lambda)[(mm)^{-2}]$	$\pi/(RY * \lambda)[(mm)^{-2}]$
1	0.000	0.000	.296E-20	.296E-20
3	-.344E-18	-.353E-18	-.591E-2	.292E-5
5	-.115E-19	.208E-25	-1.64	.319E-5
7	.339E-18	.352E-18	-.174E-1	.291E-5
			L1 = 0	L2 = 0
9	-.214E-19	-.401E-24	1.78	.553E-4
11	.493E-19	-.314E-23	1.66	.293
			L1 = 1	L2 = 0
9	2.450	-.401E-24	1.78	.553E-4
11	-2.543	-.314E-23	1.66	.293
			L1 = 0	L1 = 1
9	-.214E-19	2.450	1.78	.553E-4
11	.493E-19	-2.450	1.66	.293

Figure 5.5. Beam trace at selected surfaces with control data from figure 5.3.

Beam Surface	LA = 7 X1(mm)	LB = 7 Y1(mm)	$\pi/(RX * \lambda)[(mm)^{-2}]$	$\pi/(RY * \lambda)[(mm)^{-2}]$
1	35.000	35.000	.296E-20	.296E-20
3	-.727	-.324E-1	-.591E-2	.292E-5
5	-34.972	-35.000	1.64	.320E-5
7	2.137	.323E-1	-.174E-1	.292E-5
			L1 = 0	L2 = 0
9	-34.906	34.999	1.78	.541E-4
11	-36.075	-34.999	1.66	.293
			L1 = 1	L2 = 0
9	37.356	34.999	1.78	.541E-4
11	-38.619	-34.999	1.66	.293
			L1 = 0	L2 = 1
9	34.906	37.499	1.78	.541E-4
11	-36.075	-37.499	1.66	.293

Figure 5.6. Beam trace at selected surfaces with control data from figure 5.3.

Beam Surface	LA = 0 X1(mm)	LB = 0 Y1(mm)	$\pi/(RX * \lambda)[(mm)^{-2}]$	$\pi/(RY * \lambda)[(mm)^{-2}]$
1	0	0	.296E-20	.296E-20
3	-.344E-18	-.353E-18	-.284E-2	.296E-2
5	.116E-20	-.105E-19	.471	-1.39
7	.339E-18	.352E-18	-.852E-2	.870E-2
			L1 = 0	L2 = 0
9	-.390E-20	.182E-19	.816	-1.68
11	.259E-19	-.231E-19	1.99	-1.53
			L1 = 1	L2 = 0
9	-.390E-20	2.500	.816	-1.68
11	.259E-19	-2.458	1.99	-1.53
			L1 = 0	L2 = 1
9	2.452	.182E-19	.816	-1.68
11	-2.504	-.231E-19	1.99	-1.53

Figure 5.7. Beam trace at selected surfaces with control data from figure 5.4.

Beam Surface	LA = 7 X1(mm)	LB = 7 Y1(mm)	$\pi/(RX * \lambda)[(mm)^{-2}]$	$\pi/(RY * \lambda)[(mm)^{-2}]$
1	35.000	35.000	.296E-20	.296E-20
3	-.727	-.320E-1	-.283E-2	.296E-2
5	-35.000	-35.000	.477	-1.39
7	2.136	.304E-1	-.852E-2	.870E-2
			L1 = 0	L2 = 0
9	35.000	34.999	.816	-1.68
11	-35.623	-34.413	1.99	-1.53
			L1 = 1	L2 = 0
9	37.452	34.999	.816	-1.68
11	-38.126	-34.413	1.99	-1.53
			L1 = 0	L2 = 1
9	35.000	37.499	.816	-1.68
11	-35.623	-36.871	1.99	-1.53

Figure 5.8. Beam trace at selected surfaces with control data from figure 5.4.

5.4 The Elliptical Optics Data

Here the mirrors with elliptical surfaces are used in the computer simulation runs. Figure 5.9 shows the initial data for the simulation, and figure 5.10 shows the final results for best fit mirrors for the 10.6 μm wavelength. These data were derived by using the initial conditions of figure 5.9 and the criteria of subsection 5.2. Figures 5.11 through 5.15 show selected data for some beams and surfaces.

The conclusions drawn from these figures are:

1. The change in curvature for best elliptical mirrors is less than 0.002% from the nominal identical mirrors shown in figure 5.9. Clearly, this result is beyond fabrication accuracies; therefore, identical mirrors can be used.

2. It is possible to have a significant field of view and plane phase fronts at surfaces 1, 3, 5, 7, and 9 of the apparatus.

3. The power and phase distribution at surface 11 as shown in figure 5.15 shows significant changes over the field of view. These changes are small for each beam pair; therefore, the device can measure the beam profile at 10.6 μm under proper calibration.

```
VERSION 6/29/78
BEAM TRACE                              *********           07/17/78        10:26:11
WAVLGN  10.6          MICROMETERS          ANG.   .14 RAD
COS(ANG)                .990216
LA    7               LB    7              S1,T1(MM)       5                5
LC,LD  7               7

L                     XCUR(M)          YCUR(M)      APER(MM)RADIUS     L TO L+1 DIS(M)
 1                      .1E21             .1E21          10000              1.0098807
 2                    -2.039718         -2                224               1.0098807
 3                      .1E21             .1E21           400               1.0098807
 4                     2.039718          2                224               1.0098807
 5                      .1E21             .1E21           400               1.0098891
 6                    -2.039718         -2                224               1.0098807
 7                      .1E21             .1E21           20                1.0098807
 8                    -2.039718         -2                224               1.0098807
 9                      .1E21             .1E21           400               2.0197613
 10                    2.039718          2                224               2.0197613
 11                     .1E21             .1E21           400              -30
WX(MM)     .5          WY(MM)      .5     RX(M)    .1E21
AMPL    1              PHASE(RAD)    0    RY(M)    .1E21
                     END OF INITIAL DATA

                        S7, T7 (1/MM)= 1.4530264      1.4673833
```

Figure 5.9. Initial guess of control data on elliptical mirrors.

```
VERSION 6/29/78
BEAM TRACE                                 *********          08/04/78          15:03:36
WAVLGN= 10.6              MICROMETERS          ANG=   .14 RAD
COS(ANG)=                   .990216
LA=  7                    LB=  7               S1,T1(MM)=       5                 5
LC,LD=  7                  7


L=                        XCUR(M)           YCUR(M)      APER(MM)RADIUS     L TO L+1 DIS(M)
 1                          .1E21              .1E21           10000             1.009895
 2                        -2.0397555        -2                 224               1.0089468
 3                          .1E21              .1E21           400               1.0108155
 4                         2.0397242         2                 224               1.0098771
 5                          .1E21              .1E21           400               1.0098841
 6                        -2.0397115        -2                 224               1.0089475
 7                          .1E21              .1E21           20                1.0108147
 8                        -2.0397422        -2                 224               1.0098816
 9                          .1E21              .1E21           400               2.0197614
 10                        2.0397172         2                 224               2.0197912
 11                         .1E21              .1E21           400              -30
WX(MM)=   .5                WY(MM)=   .5       RX(M)=   .1E21
AMPL=  1                    PHASE(RAD)=  0     RY(M)=   .1E21
                          END OF INITIAL DATA

                          S7, T7 (1/MM)= 1.4530308      1.4673733
```

Figure 5.10. Final values of control data on elliptical mirrors.

Beam Surface	LA = 0 X1(mm)	LB = 0 Y1(mm)	$\pi/(RX * \lambda)[(mm)^{-2}]$	$\pi/(RY * \lambda)[(mm)^{-2}]$
1	0.000	0.000	.296E-20	.296E-20
3	-.351E-18	-.353E-18	.298E-5	.292E-5
5	-.188E-20	.208E-25	.115E-5	.319E-5
7	.346E-18	.352E-18	.292E-5	.291E-5
			L1 = 0	L2 = 0
9	.206E-20	-.401E-24	.538E-4	.553E-4
11	.102E-20	-.314E-23	.293	.293
			L1 = 1	L2 = 0
9	2.500	-.401E-24	.538E-4	.553E-4
11	-2.500	-.314E-23	.293	.293
			L1 = 0	L1 = 1
9	.206E-20	2.500	.538E-4	.535E-4
11	.102E-20	-2.500	.293	.293

Figure 5.11. Beam trace at selected surfaces with control data from figure 5.9.

Beam Surface	LA = 7 X1	LB = 7 Y1	π/(RX * λ)[(mm)$^{-2}$]	π/(RY * λ)[(mm)$^{-2}$]
1	35.000	35.000	.296E-20	.296E-20
3	-.330E-1	-.324E-1	.298E-5	.292E-5
5	-35.000	-35.000	.115E-5	.319E-5
7	.333E-1	.323E-1	.292E-5	.291E-5
			L1 = 0	L2 = 0
9	34.999	34.999	.538E-4	.553E-4
11	-34.999	-34.999	.293	.293
			L1 = 1	L2 = 0
9	37.499	34.999	.538E-4	.553E-4
11	-37.499	-34.999	.293	.293
			L1 = 0	L2 = 1
9	34.999	37.499	.538E-4	.553E-4
11	-34.999	-37.499	.293	.293

Figure 5.12. Beam trace at selected surfaces with control data from figure 5.9.

Beam Surface	LA = 0 X1	LB = 0 Y1	π/(RX * λ)[(mm)$^{-2}$]	π/(RY * λ)[(mm)$^{-2}$]
1	0.000	0.000	.296E-20	.296E-20
3	-.351B-18	-.353E-18	.273E-5	-.270E-5
5	-.188B-20	.376E-23	-.581E-3	+.578E-3
7	.346E-18	.352E-18	.269E-5	-.266E-5
			L1 = 0	L2 = 0
9	.207E-20	-.491E-23	-.653E-3	.647E-3
11	.103E-20	.107E-22	.293	.294
			L1 = 1	L2 = 0
9	2.500	-0.491E-23	-.653B-3	.647E-3
11	-2.500	.107E-22	.293	.294
			L1 = 0	L2 = 1
9	.207E-20	2.500	-.653E-3	.647E-3
11	.103E-20	-2.500	.293	.294

Figure 5.13. Beam Trace at Selected Surfaces with Control Data from Figure 5.10

Beam Surface	LA = 7 X1	LB = 7 Y1	$\pi/(RX * \lambda)[(mm)^{-2}]$	$\pi/(RY * \lambda)[(mm)^{-2}]$
1	35.000	35.000	.296E-20	.296E-20
3	.639E-6	-.137E-6	.273E-5	-.270E-5
5	-34.999	-35.000	-.581E-3	.578E-3
7	-.147E-5	-.149E-5	.269E-5	-.266E-5
			L1 = 0	L2 = 0
9	34.999	34.999	-.653E-3	.647E-3
11	-35.000	-35.000	.293	.294
			L1 = 1	L2 = 0
9	37.499	34.999	-.653E-3	.637E-3
11	-37.500	-35.000	.293	.294
			L1 = 0	L2 = 1
9	34.999	37.499	-.653E-3	.647E-3
11	-35.000	-37.500	.293	.294

Figure 5.14. Beam trace at selected surfaces with control data from figure 5.10.

Beam Parameters LA	LB	L1	L2	Position X1(mm)	Y1(mm)	Width Wx(mm)	Wy(mm)	Power(watts)	Phase(Rad)
10	0	0	0	-50.000	.107E-22	.531	.530	0.197	-1.294
[10	0	-1	0	-47.500	.107E-22	.531	.530	0.202	-1.407]
[9	0	1	0	-47.500	.107E-22	.531	.530	0.215	-1.538]
9	0	0	0	-45.000	.107E-22	.531	.530	0.220	-1.645
0	10	0	0	.102E-20	-50.000	.531	.530	0.199	1.787
[0	10	0	-1	.103E-20	-47.500	.531	.530	0.204	1.372]
[0	9	0	-1	.103E-20	-47.500	.531	.530	0.217	1.243]
0	9	0	0	.103E-20	-45.000	.531	.530	0.222	0.850
1	0	0	0	-5.000	.107E-22	.531	.530	0.347	-3.123
[1	0	-1	0	-2.500	.107E-22	.531	.530	0.348	-3.132]
[0	0	1	0	-2.500	.107E-22	.531	.530	0.349	-3.139]
0	0	0	0	.103E-20	.107E-22	.531	.530	0.349	-3.142
[0	0	0	1	.103E-20	-2.500	.531	.530	0.349	-3.131]
[0	1	0	-1	.103E-20	-2.500	.531	.530	0.348	-3.124]
0	1	0	0	.103E-20	-5.000	.531	.530	0.348	-3.093
7	6	0	0	-35.000	-30.000	.531	.530	0.216	-0.462
[7	6	0	1	-35.000	-32.500	.531	.530	0.213	-0.196]
[7	7	0	-1	-35.000	-32.500	.531	.530	0.204	-0.108]
7	7	0	0	-35.000	-35.000	.531	.530	0.201	0.179
[7	7	-1	0	-32.500	-35.000	.531	.530	0.204	0.100]
[6	7	1	0	-32.500	-35.000	.531	.530	0.213	.011]
6	7	0	0	-30.000	-35.000	.531	.530	0.216	-.062

"[...]" means overlapping beams.

Figure 5.15. Here is spot position, beam width, power, and phase at surface 11 with base control data given in figure 5.10.

5.4.1 Effects of Wavelength Change to the Base Field at Surface 11

In the design of an apparatus, it seems reasonable to change various parameters to test how they influence the final output at the detectors in surface 11. Figures 5.16 to 5.21 contain examples of such changes. In this subsection we discuss what happens when there is a change in wavelength λ in these figures. Basically, this change of 10% implies a shift of position for the defracted beams (L1 or L2 not zero) by 0.2359 mm. Since the beam width at surface 11 is 0.53 mm, this shift causes significant change in functional form. This form change affects significantly the accuracy for determining the relative phase at the neighboring sampling holes of the Hartmann plate.

This sensitivity to the change in the wavelength of the laser radiation is a principal limit to this holographic technique. To increase the dynamic range for allowed changes in wavelength requires: (1) substantial adjustments to the mirror curvatures to reduce the path differences for the diffracted beams; (2) some means to apply the correct equivalent of eq (5.4.5) shown in reference [1] to the measured output of the detectors at surface 11; or (3) sufficient aperturing of the beams striking the hologram at surface 7 to generate at surface 11 beams with widths near 1 mm.

BEAM LA = 0 LB = 0 L1 = 0 L2 = 0

Variable of Change	Position of Spot X1(mm)	Y1(mm)
Base Case	.1029E-20	.1069E-22
$\Delta\lambda$ = 1 μm	.1219E-20	.1091E-22
Δb_1 = -1 mm	.7301E-21	-.3008E-21
Δb_2 = -1 mm	.1030E-20	.1048E-22
Δb_3 = 1 mm	.1027E-20	.1090E-22
Δb_4 = -1 mm	.7301E-21	-.3008E-21
Δb_5 = -1 mm	.7301E-21	-.3008E-21
Δb_6 = -1 mm	.1030E-20	.1049E-22
Δb_7 = 1 mm	.1027E-22	.1070E-22
Δb_8 = -1 mm	.7301E-21	-.3008E-21
Δb_9 = -1 mm	.7301E-21	-.3008E-21
Δb_{10} = -1 mm	.7286E-21	-.3008E-21

Figure 5.16. Spot position change at surface 11 due to one control parameter change. Base control data given in figure 5.10.

BEAM LA = 0 LB = 0 L1 = 1 L2 = 0

Variable of Change	Position of Spot X1(mm)	Y1(mm)
Base Case	-2.5001	.1069E-22
$\Delta\lambda$ = -1 μm	-2.2642	.1091E-22
Δb_1 = -1 mm	-2.5001	-.3008E-21
Δb_2 = -1 mm	-2.5001	.1048E-22
Δb_3 = 1 mm	-2.5001	.1090E-22
Δb_4 = -1 mm	-2.5001	-.3008E-21
Δb_5 = -1 mm	-2.5001	-.3008E-21
Δb_6 = -1 mm	-2.5001	.1049E-22
Δb_7 = 1 mm	-2.5001	.1070E-22
Δb_8 = -1 mm	-2.5001	-.3008E-21
Δb_9 = -1 mm	-2.5001	-.3008E-21
Δb_{10} = -1 mm	-2.4976	-.3008E-21

Figure 5.17. Spot position change at surface 11 due to one control parameter change. Base control data given in figure 5.10.

BEAM LA = 0 LB = 0 L1 = 1 L2 = 1

Variable of Change	Position of Spot X1(mm)	Y1(mm)
Base Case	.1029E-20	-2.5000
$\Delta\lambda$ = -1 μm	.1219E-20	-2.2642
Δb_1 = -1 mm	.7301E-21	-2.5000
Δb_2 = -1 mm	.1030E-20	-2.5000
Δb_3 = 1 mm	.1027E-20	-2.5000
Δb_4 = -1 mm	.7301E-21	-2.5000
Δb_5 = -1 mm	.7301E-21	-2.5000
Δb_6 = -1 mm	.1030E-20	-2.5000
Δb_7 = 1 mm	.1027E-20	-2.5000
Δb_8 = -1 mm	.7301E-21	-2.5000
Δb_9 = -1 mm	.7301E-21	-2.5000
Δb_{10} = -1 mm	.7286E-21	-2.4976

Figure 5.18. Spot position change at surface 11 due to one control parameter change. Base control data given in figure 5.10.

BEAM LA = 7 LB = 7 L1 = 0 L2 = 0

Variable of Change	Position of Spot X1(mm)	Y1(mm)
Base Case	-35.0000	-35.0000
$\Delta\lambda$ = -1 μm	-35.0000	-35.0000
Δb_1 = -1 mm	-35.0001	-35.0000
Δb_2 = -1 mm	-35.0000	-35.0000
Δb_3 = 1 mm	-35.0000	-35.0000
Δb_4 = -1 mm	-35.0001	-35.0001
Δb_5 = -1 mm	-35.0001	-35.0001
Δb_6 = -1 mm	-35.0000	-35.0000
Δb_7 = 1 mm	-35.0000	-35.0000
Δb_8 = -1 mm	-35.0001	-35.0001
Δb_9 = -1 mm	-35.0001	-35.0001
Δb_{10} = -1 mm	-34.9654	-34.9654

Figure 5.19. Spot position change at surface 11 due to one control parameter change. Base control data given in figure 5.10.

BEAM LA = 7 LB = 7 L1 = -1 L2 = 0

Variable of Change	Position of Spot X1(mm)	Y1(mm)
Base Case	-32.4999	-35.0000
$\Delta\lambda$ = -1 μm	-32.7358	-35.0000
b_1 = -1 mm	-32.5000	-35.0001
Δb_2 = -1 mm	-32.4999	-35.0000
Δb_3 = 1 mm	-32.4999	-35.0000
Δb_4 = -1 mm	-32.5000	-35.0001
Δb_5 = -1 mm	-32.5000	-35.0001
Δb_6 = -1 mm	-32.4999	-35.0000
Δb_7 = 1 mm	-32.4999	-35.0000
Δb_8 = -1 mm	-32.5000	-35.0001
Δb_9 = -1 mm	-32.5000	-35.0001
Δb_{10} = -1 mm	-32.4678	-34.9654

Figure 5.20. Spot position change at surface 11 due to one control parameter change. Base control data given in figure 5.10.

BEAM LA = 7 LB = 7 L1 = 0 L2 = -1

Variable of Change	Position of Spot X1(mm)	Y1(mm)
Base Case	-35.0000	-32.5000
$\Delta\lambda$ = -1 μm	-35.0000	-32.7358
Δb_1 = -1 mm	-35.0001	-32.5000
Δb_2 = -1 mm	-35.0000	-32.5000
Δb_3 = 1 mm	-35.0000	-32.5000
Δb_4 = -1 mm	-35.0001	-32.5000
Δb_5 = -1 mm	-35.0001	-32.5000
Δb_6 = -1 mm	-35.0000	-32.5000
Δb_7 = 1 mm	-35.0000	-32.5000
Δb_8 = -1 mm	-35.0001	-32.5000
Δb_9 = -1 mm	-35.0001	-32.5000
Δb_{10} = -1 mm	-34.9654	-32.4679

Figure 5.21. Spot position change at surface 11 due to one control parameter change. Base control data given in figure 5.10.

5.4.2 Effects of 1 mm Changes in Positions to Base Field at Surface 11

Figures 5.16 to 5.21 show, in addition to the wavelength effects, the influence of a 1 mm shift of each mirror on the output of the detectors at surface 11. In all cases except changes in the imaging mirror at surface 10, these movements are completely negligible. Moving the imaging mirror causes primarily the obvious change in magnification of the pattern at surface 9 to the pattern at surface 11. Clearly this adjustment requires sensitive movement of the mirror.

These results imply that the final imaging mirror can cause adjustment problems. Using fine adjustment of the detector array to find the best position of surface 11 improves the situation.

5.5 Alignment of Apparatus Using 0.6328 μm

Figures 5.22 and 5.23 show the position of two beams at selected surfaces of the apparatus. These beams permit accurate placement within 100 μm of the mirrors, the hologram, and the detector array. This final adjustment of the apparatus will require using a cw laser beam with 10.6 μm wavelength for maximum precision and dynamic range of the apparatus.

Beam	LA = 7	LB = 7		
Surface	X1(mm)	Y1(mm)	$\pi/(RX * \lambda)[(mm)^{-2}]$	$\pi/(RY * \lambda)[(mm)^{-2}]$
1	35.000	35.000	.496E-19	.496E-19
3	.329E-1	.323E-1	-.693E-2	.689E-2
5	-34.999	-35.000	.657E-4	.300E-4
7	-.332E-1	-.322E-1	-.678E-2	-.687E-2
			L1 = 0	L2 = 0
9	34.999	34.999	.862E-4	.361E-4
11	-35.000	-35.000		
			L1= -1	L2 = 0
9	34.850	34.999	.862E-4	.361E-4
11	-34.851	-35.000	4.916	4.916
			L1 = 0	L2= -1
9	34.999	34.850	.862E-4	.361E-4
11	-35.000	-34.851	4.916	4.916

Figure 5.22. Beam trace at selected surfaces with control data from figure 5.10, λ = 0.6328 μm.

Beam	LA = 0	LB = 0		
Surface	X1(mm)	Y1(mm)	$\pi/(RX * \lambda)[(mm)^{-2}]$	$\pi/(RY * \lambda)[(mm)^{-2}]$
1	0.000	0.000	.496E-19	.496E-19
3	-.141E-18	-.353E-18	-.693E-2	-.689E-2
5	.432E-19	.376E-23	.657E-4	.300E-4
7	.588E-20	.353E-18	-.678E-2	-.687E-2
			L1 = 0	L2 = 0
9	.350E-20	-.508E-23	.862E-4	.361E-4
11	.310E-21	.120E-22	4.916	4.916
			L1 = 1	L2 = 0
9	.149	-.508E-23	.862E-4	.361E-4
11	-.149	.120E-22	4.916	4.916
			L1 = 0	L2 = 1
9	.350E-20	.149	.862E-4	.361E-4
11	.310E-21	-.149	4.916	4.916

Figure 5.23. Beam trace at selected surfaces with control data from figure 5.10, λ = 0.6328 μm.

5.6 High Irradiance Constraints in the Design for the 10.6 μm Wavelength

Reference [1] established that the peak irradiance allowed at the Hartmann plate is 200 W/cm^2. The surface hologram fixes this limit because the coherence effects in the Fourier plane at surface 7 can increase the peak irradiance by a factor of N^2, where N is the number of sampling holes. This sampling process also reduces the peak irradiance by the factor $[\pi a^2/(4\lambda f)]^2$, where a is the diameter of the sampling holes, f is the effective distance to the Fourier plane from the Hartmann plate, and λ is the wavelength of the radiation. For the current design, this factor becomes 5.5×10^{-3}. Given that N = 300, we find the peak irradiance at the hologram is 99 kW/cm^2 which approaches the cw limit for mirrors with copper substrates.

This 200 W/cm^2 at the Hartmann plate implies a 15 kW beam, which is a low range in high-power laser beams. This constraint implies the beam profile apparatus must use

a beam splitter or grating in front of it to look at 20 kW and higher-power beams. This apparatus captures from the splitter one of the lower peak irradiance beams that can satisfy this 200 W/cm^2 limit. In the conclusion (section 10), I mention a way to increase the allowed flux significantly. Consequently, we must test if this lower-power beam copies the primary beam.

There are at least three test strategies depending on the primary beam.

First, if the original high-power beam has known range of irradiances and its highest value does not exceed the damage threshold of the beam splitter or grating, then the one-time test using a laser beam of much smaller cross section but with peak irradiance equal to the peak of original laser beam can be used. Here we would determine the splitting ratio as a function of position and verify that this peak irradiance does not change the splitting ratio [11,12] from the value measured at much lower irradiances.

Second, if the potential peak irradiance has significant power compared with the power in the rest of the beam, then a pair of calorimeters can check for potential power dependence in the splitter ratio.

Finally, if the primary beam has unknown peak irradiances, then real-time measurements are needed. Pulse systems or situations that require control or extreme precision are examples for real-time measurements. Two methods to obtain these measurements are: (1) an ideal technique that is very expensive, uses two beam profile apparatuses to sample simultaneously several of the lower-power diffraction orders and compares their beam profiles in real time. This process tests for significant distortion by the grating or splitter; (2) scattered radiation from the splitter or grating can show changes in the splitter ratio. Implementation of this second technique depends on the expected scattering. Again, ratio measurements of several beams are necessary for both methods.

In conclusion, measuring high-power laser beams requires boostrap techniques that extrapolate the results from direct measurements in low-power beams. Appropriate tests must be made to confirm that the extrapolation process is valid.

6. THE 1.06 µm WAVELENGTH

Here we change the scale of two mirrors in the apparatus to make it work accurately for 1.06 µm. We reduce their curvatures by approximately 10 for surfaces 4 and 10. This section is briefer than section 5 because most concepts and criteria for adjustment of the control variables are defined in section 5 and its subsections. In section 6 and its subsections we report only changed values because we wish to use the same apparatus as much as possible for a range of wavelengths. In this way, the unit can justify its cost. If a unit with multiple ranges of wavelength is not needed, then three mirrors could be eliminated if the resulting physical size of the apparatus proves to be convenient.

Because the design of the apparatus is directed first toward the 10.6 µm and second toward the 1.06 µm, the choice of arbitrary values is controlled by the decisions in subsections 5.1 and 5.2. In subsection 6.1 we note the new changes in some values and in subsection 6.2 we define the new adjustment criteria given these changes.

We again examine the spherical and elliptical cases. In subsection 6.3 we document the data for spherical mirrors, and in the remaining subsections we document the data for the elliptical mirrors in direct correspondence to that done for 10.6 µm.

In subsection 6.4 we generate the base data for the apparatus using elliptical mirrors. Here we accept that all mirrors can change their x curvatures. These results measure how far the ideal apparatus deviates from the practical that is optimized for 10.6 μm.

In subsection 6.4.1 we show what happens when the wavelength is changed to 0.96 μm, and in subsection 6.4.2 we show how the base data change when each distance variable is moved by 1 mm.

Because 1.06 μm is inconvenient for initial alignment, in subsection 6.5 we trace 0.6328 μm beams through the apparatus containing the elliptical mirrors.

This section is concluded with subsection 6.6 in which the allowed peak irradiance on the hologram is identified.

6.1 Selecting Some Initial Control Values

Subsection 5.1 contains all the selected arbitrary control values for the apparatus. In this subsection we only comment on one situation that becomes different. The Hartmann plate has 1 mm holes for sampling the laser beam. These sampled beams become Airy disks with 2.6 mm diameters. This significant reduction in beam size implies reduction in the absorption rate of the laser beam as it progresses through the apparatus to one tenth of the 10.6 μm absorption rate.

6.2 The Convergence Criteria for the Rest of the Control Values

The discussion in subsection 5.2 defines the remaining control values for all wavelengths. It is only necessary to adjust M in each formula.

There remains one discrepancy implied by the discussion in subsection 6 compared to the data contained in later subsections. Here adjustments for the spherical and the elliptical mirror cases allow all relevant curvatures and distances to change as if the previous constraints generated for the 10.6 μm were not present. It becomes obvious from data in these later subsections that this discrepancy makes no difference. Nevertheless, I suggest the builder of the final apparatus use the computer program with the true constraints to achieve a proper adjustment of the apparatus. Because the possibilities for all types of design are very large, this paper does not try to document a final design.

6.3 The Spherical Optics Data

The discussion of subsection 5.3 applies here. The figures relevant to this subsection are 6.1 to 6.5. Again, the simulations show spherical symmetries preclude high precision measurements of beam profile unless significant changes in the design take place.

```
VERSION 6/29/78
BEAM TRACE                           *********            08/08/78        08:39:43
WAVLGN= 1.06         MICROMETERS          ANG.  .14 RAD
COS(ANG)=             .990216
LA = 7               LB = 7               S1,T1(MM) =     5                5
LC,LD = 7             7

L=                   XCUR(M)           YCUR(M)     APER(MM)RADIUS    L TO L+1 DIS(M)
 1                     .1E21             .1E21          10000          1.0098807
 2                   -2                -2                224           1.0098807
 3                     .1E21             .1E21           400           .10098807
 4                     .2                .2              224           .10098807
 5                     .1E21             .1E21           400           1.0098807
 6                   -2                -2                224           1.0098807
 7                     .1E21             .1E21           20            1.0098807
 8                   -2                -2                224           1.0098807
 9                     .1E21             .1E21           400           .11108688
 10                    .2                .2              224           1.1108688
 11                    .1E21             .1E21           400          -30
WX(MM) =  .5          WY(MM) =   .5      RX(M) = .1E21
AMPL = 1              PHASE(RAD) =  0    RY(M) = .1E21
                        END OF INITIAL DATA

                        S7, T7 (1/MM)= 1.4818821     1.4673833
```

Figure 6.1. Initial guess of control data for spherical mirrors.

```
VERSION 6/29/78
BEAM TRACE                           *********            08/08/78        09:32:32
WAVLGN = 1.06          MICROMETERS         ANG = .14 RAD
COS(ANG) =              .990216
LA =  7                LB = 7              S1,T1(MM) =     5                5
LC,LD = 7               7

L=                     XCUR(M)           YCUR(M)     APER(MM)RADIUS  L TO L+1 DIS(M)S
 1                       .1E21             .1E21          10000        1.0053952
 2                     -2                -2                224         1.0098807
 3                       .1E21             .1E21           400         .10098807
 4                       .2                .2              224         .99019205E-1
 5                       .1E21             .1E21           400         1.0008226
 6                     -2                -2                224         1.0098807
 7                       .1E21             .1E21           20          1.0098807
 8                     -2                -2                224         .97981908
 9                       .1E21             .1E21           400         .11108688
 10                      .2                .2              224         1.1022951
 11                      .1E21             .1E21           400        -30
WX(MM) =  .5            WY(MM) =   .5      RX(M) = .1E21
AMPL = 1                PHASE(RAD) =  0    RY(M) = .1E21
                        END OF INITIAL DATA

                        S7, T7 (1/MM)= 1.453029      1.4673735
```

Figure 6.2. Final values of control data for spherical mirrors.

Beam Surface	LA = 0 X1(mm)	LB = 0 Y1(mm)	$\pi/(RX * \lambda)[(mm)^{-2}]$	$\pi/(RY * \lambda)[(mm)^{-2}]$
1	0.0000	0.000	.296E-19	.296E-19
3	-.223E-18	-.353E-18	-.261E-1	.292E-4
5	.313E-20	.149E-24	102.33	-.476E-2
7	.210E-17	.353E-17	-.644E-1	.480E-6
			L1 = 0	L2 = 0
9	-.779E-19	-.680E-25	68.851	-.126E-2
11	.849E-18	.679E-24	3.555	2.935
			L1 = 1	L2 = 0
9	.250	-.680E-25	68.851	-.126E-2
11	-2.554	.679E-24	3.555	2.935
			L1 = 0	L2 = 1
9	-.779E-19	.250	68.851	-.126E-2
11	.849E-18	-2.500	3.555	2.935

Figure 6.3. Beam trace at selected surfaces with control data from figure 6.1

Beam Surface	LA = 7 X1(mm)	LB = 7 Y1(mm)	$\pi/(RX * \lambda)[(mm)^{-2}]$	$\pi/(RY * \lambda)[(mm)^{-2}]$
1	35.000	35.000	.296E-19	.296E-19
3	-.695	-.325E-3	-.261E-1	.292E-4
5	-3.485	-3.500	102.33	-.476E-2
7	7.787	.616E-2	-.644E-1	.480E-6
			L1 = 0	L2 = 0
9	3.212	3.500	68.851	-.126E-2
11	-32.648	-35.000	3.555	2.935
			L1 = 1	L2 = 0
9	3.462	3.5000	68.851	-.126E-2
11	-35.201	-35.000	3.555	2.935
			L1 = 0	L2 = 1
9	3.212	3.750	68.851	-.126E-2
11	-32.648	-37.500	3.555	2.935

Figure 6.4. Beam trace at selected surfaces with control data from figure 6.1.

Beam Surface	LA = 0 X1(mm)	LB = 0 Y1(mm)	$\pi/(RX * \lambda)[(mm)^{-2}]$	$\pi/(RY * \lambda)[(mm)^{-2}]$
1	0.000	0.000	.296E-19	.296E-19
3	-.222E-18	-.353E-18	-.126E-1	.131E-1
5	.111E-20	.705E-17	1.519	-101.235
7	.210E-17	.353E-17	-.315E-1	.322E-1
			L1 = 0	L2 = 0
9	-.320E-20	.129E-18	10.372	-69.244
11	.596E-19	-.128E-17	3.930	2.257
			L1 = 1	L2 = 0
9	.245	.129E-18	10.372	-69.244
11	-2.484	-.128E-17	3.930	2.257
			L1 = 0	L2 = 1
9	-.320E-21	.250	10.372	-69.244
11	.596E-19	-2.479	3.930	2.257

Figure 6.5. Beam trace at selected surfaces with control data from figure 6.2

Beam Surface	LA = 7 X1(mm)	LB = 7 Y1(mm)	$\pi/(RX * \lambda)[(mm)^{-2}]$	$\pi/(RY * \lambda)[(mm)^{-2}]$
1	35.000	35.000	.296E-19	.296E-19
3	-.695	-.323E-3	-.126E-1	.131E-1
5	-3.500	-3.500	1.519	-101.235
7	7.787	.616E-2	-.315E-1	.322E-1
			L1 = 0	L2 = 0
9	3.500	3.500	10.372	-69.244
11	-35.298	-34.704	3.930	2.257
			L1 = 1	L2 = 0
9	3.745	3.500	10.372	-69.244
11	-37.782	-34.704	3.930	2.257
			L1 = 0	L2 = 1
9	3.500	3.750	10.372	-69.244
11	-35.298	-37.182	3.930	2.257

Figure 6.6. Beam trace at selected surfaces with control data from figure 6.2

6.4 The Elliptical Optics Data

Parallel to the discussion of subsection 5.4, this subsection generates comparable simulations for elliptical mirrors. Figures 6.7 through 6.13 apply here. Most conclusions are identical to those in subsection 5.4. We now conclude that the apparatus can work for both wavelengths. Only the mirrors at surfaces 4 and 10 need to be changed from those used by the 10.6 μm configuration. Because the focal lengths of these mirrors change various parts of the apparatus by a factor ten, it is very easy to accommodate the change in wavelength.

```
VERSION 6/29/78
BEAM TRACE                                  *********          08/08/78         08:25:53
WAVLGN = 1.06           MICROMETERS        ANG = .14 RAD
COS(ANG) =                .990216
LA =  7                 LB = 7             S1,T1(MM) =      5                5
LC,LD = 7                7

L=                      XCUR(M)           YCUR(M)       APER(MM)RADIUS    L TO L+1 DIS(M)
 1                        .1E21              .1E21             10000           1.0098807
 2                      -2.0397178         -2                  224             1.0098807
 3                        .1E21              .1E21             400             .10098807
 4                        .20397178          .2                224             .10098807
 5                        .1E21              .1E21             400             1.0098807
 6                      -2.0397179         -2                  224             1.0098807
 7                        .1E21              .1E21             20              1.0098807
 8                      -2.0397178         -2                  224             1.0098807
 9                        .1E21              .1E21             400             .11108688
 10                       .20397178          .2                224             1.1108688
 11                       .1E21              .1E21             400             -30
WX(MM) =   .5             WY(MM) =    .5      RX(M) = .1E21
AMPL = 1                  PHASE(RAD) =  0     RY(M) = .1E21
                        END OF INITIAL DATA

                        S7, T7 (1/MM)= 1.4530265      1.4673833
```

Figure 6.7. Initial guess of control data on elliptical mirrors.

```
VERSION 6/29/78
BEAM TRACE                                  *********          07/17/78         11:17:50
WAVLGN = 1.06           MICROMETERS        ANG = .14 RAD
COS(ANG) =                .990216
LA = 7                  LB = 7             S1,T1(MM) =      5                5
LC,LD = 7                7

L=                      XCUR(M)           YCUR(M)       APER(MM)RADIUS    L TO L+1 DIS(M)
 1                        .1E21              .1E21             10000           1.0098859
 2                      -2.0397183         -2                  224             1.0098713
 3                        .1E21              .1E21             400             .10098901
 4                        .2039718           .2                224             .10098787
 5                        .1E21              .1E21             400             1.0098862
 6                      -2.0397399         -2                  224             1.0089452
 7                        .1E21              .1E21             20              1.0090289
 8                      -2.039696          -2                  224             1.0098752
 9                        .1E21              .1E21             400             .11108687
 10                       .20396776          .2                224             1.110874
 11                       .1E21              .1E21             400             -30
WX(MM) =   .5             WY(MM) =    .5      RX(M) = .1E21
AMPL = 1                  PHASE(RAD) =  0     RY(M) = .1E21
                        END OF INITIAL DATA

                        S7, T7 (1/MM)= 1.453029       1.4673735
```

Figure 6.8. Final values of control data on ellipitical mirrors.

Beam Surface	LA = 7 X1(mm)	LB = 7 Y1(mm)	$\pi/(RX * \lambda)[(mm)^{-2}]$	$\pi/(RY * \lambda)[(mm)^{-2}]$
1	35.000	35.000	.296E-19	.296E-19
3	-.334E-3	-.325E-3	.297E-4	.292E-4
5	-3.500	-3.500	-.441E-2	-.476E-2
7	.637E-2	.616E-2	.344E-6	.480E-6
			L1 = 0	L2 = 0
9	3.500	3.500	.420E-2	-.126E-2
11	-35.000	-35.000	2.93	2.935
			L1 = 1	L2 = 0
9	3.750	3.500	.420E-2	-.126E-2
11	-37.500	-35.000	2.93	2.935
			L1 = 0	L2 = 1
9	3.500	3.750	.420E-2	-.126E-2
11	-35.000	-37.500	2.93	2.935

Figure 6.9. Beam trace at selected surfaces with control data from figure 6.7.

Beam Surface	LA = 0 X1(mm)	LB = 0 Y1(mm)	$\pi/(RX * \lambda)[(mm)^{-2}]$	$\pi/(RY * \lambda)[(mm)^{-2}]$
1	0.000	0.000	.296E-19	.296E-19
3	-.230E-18	-.353E-18	.297E-4	.292E-4
5	-.116E-20	-.149E-24	-.441E-2	-.476E-2
7	.218E-17	.353E-17	.344E-6	.480E-6
			L1 = 0	L2 = 0
9	.130E-21	-.680E-25	.420E-2	-.126E-2
11	.118E-19	.679E-24	2.93	2.935
			L1 = 1	L2 = 0
9	.250	-.680E-25	.420E-2	-.126E-2
11	-2.500	.679E-24	2.93	2.935
			L1 = 0	L2 = 1
9	.130E-21	.250	+.420E-2	-.126E-2
11	.118E-19	-2.500	2.93	2.935

Figure 6.10. Beam trace at selected surfaces with control data from figure 6.7.

Beam Surface	LA = 0 X1(mm)	LB = 0 Y1(mm)	$\pi/(RX * \lambda)[(mm)^{-2}]$	$\pi/(RY * \lambda)[(mm)^{-2}]$
1	0.000	0.000	.296E-19	.296E-19
3	-.230E-18	-.353E-18	.203E-6	-.603E-6
5	-.116E-20	-.667E-24	-.105E-1	-.103E-1
7	.218E-17	.353E-17	.159E-4	-.154E-4
			L1 = 0	L2 = 0
9	.130E-21	.431E-24	-.717E-3	-.103E-2
11	.118E-19	-.299E-23	2.936	2.935
			L1 = 1	L2 = 0
9	.250	.431E-24	-.717E-3	-.103E-2
11	-2.500	-.299E-23	2.936	2.935
			L1 = 0	L2 = 1
9	.130E-21	.250	-.717E-3	-.103E-2
11	.118E-19	-2.500	2.936	2.935

Figure 6.11. Beam trace at selected surfaces with control data from figure 6.8.

Beam Surface	LA = 7 X1(mm)	LB = 7 Y1(mm)	$\pi/(RX * \lambda)[(mm)^{-2}]$	$\pi/(RY * \lambda)[(mm)^{-2}]$
1	35.000	35.000	.296E-19	.296E-19
3	.392E-6	.101E-5	.203E-6	-.603E-6
5	-3.500	-3.500	-.105E-1	-.103E-1
7	.128E-4	-.130E-4	.159E-4	-.154E-4
			L1 = 0	L2 = 0
9	3.500	3.500	-.717E-3	-.103E-2
11	-35.000	-35.000	2.936	2.935
			L1 = 1	L2 = 0
9	3.750	3.500	-.717E-3	-.103E-2
11	-37.500	-35.000	2.936	2.935
			L1 = 0	L2 = 1
9	3.500	3.750	-.717E-3	-.103E-2
11	-35.000	-37.500	2.936	2.935

Figure 6.12. Beam trace at selected surfaces with control data from figure 6.8.

	Beam Parameters Phase(Rad)				Position		Width		Power(watts)		
	LA	LB	L1	L2	X1(mm)	Y1(mm)	Wx(mm)	Wy(mm)			
	10	0	0	0	-50.000	-.299E-23	.529	.529	0.315	-0.562	
[	10	0	-1	0	-47.500	-.299E-23	.529	.529	0.316	-0.800	]
[	9	0	1	0	-47.500	-.299E-23	.529	.529	0.322	-0.825	]
	9	0	0	0	-45.000	-.299E-23	.529	.529	0.322	-1.052	
	0	10	0	0	.118E-19	-50.000	.529	.529	0.316	-3.170	
[	0	10	0	-1	.118E-19	-47.500	.529	.529	0.316	-3.154	]
[	0	9	0	1	.118E-19	-47.500	.529	.529	0.322	-3.179	]
	0	9	0	0	.118E-19	-45.000	.529	.529	0.322	-3.164	
	1	0	0	0	-5.000	-.299E-23	.529	.529	0.351	-3.116	
[	1	0	-1	0	-2.500	-.299E-23	.529	.529	0.351	-3.134	]
[	0	0	1	0	-2.500	-.299E-23	.529	.529	0.351	-3.136	]
	0	0	0	0	.118E-19	-.299E-23	.529	.529	0.351	-3.142	
[	0	0	0	1	.118E-19	-2.500	.529	.529	0.351	-3.142	]
[	0	1	0	-1	.118E-19	-2.500	.529	.529	0.351	-3.141	]
	0	1	0	0	.118E-19	-5.000	.529	.529	0.351	-3.142	
	7	6	0	0	-35.000	-30.000	.529	.529	0.321	-1.888	
[	7	6	0	1	-35.000	-32.500	.529	.529	0.321	-1.897	]
[	7	7	0	-1	-35.000	-32.500	.529	.529	0.317	-1.881	]
	7	7	0	0	-35.000	-35.000	.529	.529	0.316	-1.891	
[	7	7	-1	0	-32.500	-35.000	.529	.529	0.317	-2.057	]
[	6	7	1	0	-32.500	-35.000	.529	.529	0.321	-2.074	]
	6	7	0	0	-30.000	-35.000	.529	.529	0.321	-2.227	

"[...]" means overlapping beams.

Figure 6.13. Here is spot position, beam width, power, and phase at surface 11 with base control data given in figure 6.8.

6.4.1 Effects of Wavelength Change to the Base Field at Surface 11

The 10 percent change in the wavelength at 1.06 μm implies exactly the same shift as a 10 percent change in the wavelength at 10.6 μm. This fact is shown by the data in figures 6.14 to 6.19. The conclusions of this subsection are those of subsection 5.4.1.

BEAM LA = 0 LB = 0 L1 = 0 L2 = 0

Variable of Change	Position of Spot X1(mm)	Y1(mm)
Base Case	.1182E-19	-.2994E-23
$\Delta\lambda$ = -0.1 μm	.1292E-19	-.3146E-23
Δb_1 = -1 mm	.1162E-19	-.3161E-23
Δb_2 = -1 mm	.1193E-19	-.2288E-22
Δb_3 = 1 mm	.1171E-19	.1689E-22
Δb_4 = 1 mm	.3070E-19	.3130E-19
Δb_5 = -1 mm	-.7054E-20	-.3131E-19
Δb_6 = -1 mm	.1182E-19	-.3191E-23
Δb_7 = -1 mm	.1182E-19	-.2995E-23
Δb_8 = -1 mm	-.7055E-20	-.3131E-19
Δb_9 = -1 mm	-.7055E-20	-.3131E-19
Δb_{10} = 1 mm	.1202E-19	.3101E-21

Figure 6.14. Spot position change at surface 11 due to one control parameter change. Base control data given in figure 6.8.

BEAM LA = 0 LB = 0 L1 = 1 L2 = 0

Variable of Change	Position of Spot X1(mm)	Position of Spot Y1(mm)
Base Case	-2.5000	-.2994E-23
$\Delta\lambda$ = -0.1 μm	-2.2642	-.3146E.23
Δb_1 = -1 mm	-2.5000	-.3161E-21
Δb_2 = -1 mm	-2.5000	-.2288E-22
Δb_3 = 1 mm	-2.5000	.1689E-22
Δb_4 = 1 mm	-2.5000	.3130E-19
Δb_5 = -1 mm	-2.5000	-.3131E-19
Δb_6 = -1 mm	-2.5000	-.3191E-23
Δb_7 = -1 mm	-2.5000	-.2995E-23
Δb_8 = -1 mm	-2.5000	-.3131E-19
Δb_9 = -1 mm	-2.5000	-.3131E-19
Δb_{10} = 1 mm	-2.5025	.3101E-21

Figure 6.15. Spot position change at surface 11 due to one control parameter change. Base control data given in figure 6.8.

BEAM LA = 0 LB = 0 L1 = 0 L2 = 1

Variable of Change	Position of Spot X1(mm)	Y1(mm)
Base Case	.1182E-19	-2.5000
$\Delta\lambda$ = -0.1 μm	.1292E-19	-2.2641
Δb_1 = -1 mm	.1162E-19	-2.5000
Δb_2 = -1 mm	.1193E-19	-2.5000
Δb_3 = 1 mm	.1171E-19	-2.5000
Δb_4 = 1 mm	.3070E-19	-2.5000
Δb_5 = -1 mm	-.7054E-20	-2.5000
Δb_6 = -1 mm	.1182E-19	-2.5000
Δb_7 = -1 mm	.1182E-19	-2.5000
Δb_8 = -1 mm	-.7055E-20	-2.5000
Δb_9 = -1 mm	-.7055E-20	-2.5000
Δb_{10} = 1 mm	.1202E-19	-2.5025

Figure 6.16. Spot position change at surface 11 due to one control parameter change. Base control data given in figure 6.8.

BEAM LA = 7 LB = 7 L1 = 0 L2 = 0

Variable of Change	Position of Spot X1(mm)	Y1(mm)
Base Case	-35.0000	-35.0000
$\Delta\lambda$ = -0.1 μm	-35.0000	-35.0000
Δb_1 = -1 mm	-35.0000	-35.0000
Δb_2 = -1 mm	-35.0000	-35.0000
Δb_3 = 1 mm	-35.0000	-35.0000
Δb_4 = 1 mm	-35.0000	-35.0000
Δb_5 = -1 mm	-35.0000	-35.0000
Δb_6 = -1 mm	-35.0000	-35.0000
Δb_7 = -1 mm	-35.0000	-35.0000
Δb_8 = -1 mm	-34.9999	-34.9999
Δb_9 = -1 mm	-34.9999	-34.9999
Δb_{10} = 1 mm	-35.03476	-35.0347

Figure 6.17. Spot position change at surface 11 due to one control parameter change. Base control data given in figure 6.8.

BEAM LA = 7 LB = 7 L1 = -1 L2 = 0

Variable of Change	Position of Spot X1(mm)	Y1(mm)
Base Case	-32.5000	-35.0000
$\Delta\lambda$ = -0.1 μm	-32.7258	-35.0000
Δb_1 = -1 mm	-32.5000	-35.0000
Δb_2 = -1 mm	-32.5000	-35.0000
Δb_3 = 1 mm	-32.4999	-35.0000
Δb_4 = 1 mm	-32.4999	-35.0000
Δb_5 = -1 mm	-32.5000	-35.0000
Δb_6 = -1 mm	-32.5000	-35.0000
Δb_7 = -1 mm	-32.5000	-35.0000
Δb_8 = -1 mm	-32.4999	-34.9999
Δb_9 = -1 mm	-32.4999	-34.9999
Δb_{10} = 1 mm	-32.5321	-35.0347

Figure 6.18. Spot position change at surface 11 due to one control parameter change. Base control data given in figure 6.8.

BEAM LA = 7 LB = 7 L1 = 0 L2 = -1

Variable of Change	Position of Spot X1(mm)	Y1(mm)
Base Case	-35.0000	-32.5000
$\Delta\lambda$ = -0.1 μm	-35.0000	-32.7359
Δb_1 = -1 mm	-35.0000	-32.5000
Δb_2 = -1 mm	-35.0000	-32.5000
Δb_3 = 1 mm	-35.0000	-32.5000
Δb_4 = 1 mm	-35.0000	-32.5000
Δb_5 = -1 mm	-35.0000	-32.5000
Δb_6 = -1 mm	-35.0000	-32.5000
Δb_7 = -1 mm	-35.0000	-32.5000
Δb_8 = -1 mm	-34.9999	-32.5000
Δb_9 = -1 mm	-34.9999	-32.5000
Δb_{10} = 1 mm	-35.0347	-32.5322

Figure 6.19. Spot position change at surface 11 due to one control parameter change. Base control data given in figure 6.8.

6.4.2 Effects of 1 mm Changes in Positions to Base Field at Surface 11

Again, figures 6.14 to 6.19 show the effects due to 1 mm shifts. The conclusions are identical to those of subsection 5.4.2.

6.5 Alignment of Apparatus Using 0.6328 μm

Figures 6.20 and 6.21 show the alignment results for the 1.06 μm configuration. These results parallel those of subsection 5.5.

Beam Surface	LA = 7 X1(mm)	LB = 7 Y1(mm)	$\pi/(RX * \lambda)[(mm)^{-2}]$	$\pi/(RY * \lambda)[(mm)^{-2}]$
1	35.000	35.000	.496E-19	.496E-19
3	.213E-3	.210E-3	-.448E-4	-.454E-4
5	-3.500	-3.500	-.359E-2	-.350E-2
7	-.406E-2	-.397E-1	.258E-4	-.266E-4
			L1 = 0	L2 = 0
9	3.500	3.500	.689E-2	.665E-2
11	-35.000	-35.000	4.917	4.916
			L1= -1	L2 = 0
9	3.351	3.500	.689E-2	.665E-2
11	-33.508	-35.000	4.917	4.917
			L1 = 0	L2= -1
9	3.500	3.351	.689E-2	.665E-2
11	-35.000	-33.508	4.917	4.916

Figure 6.20. Beam trace at selected surfaces with control data from figure 6.8, λ = 0.6328 μm.

Beam Surface	LA = 0 X1(mm)	LB = 0 Y1(mm)	$\pi/(RX * \lambda)[(mm)^{-2}]$	$\pi/(RY * \lambda)[(mm)^{-2}]$
1	0.000	0.000	.496E-19	.496E-19
3	-.141E-18	-.353E-18	-.448E-4	-.454E-4
5	-.178E-20	-.667E-24	-.359E-2	-.350E-2
7	.119E-17	.353E-17	.258E-4	-.266E-4
			L1 = 0	L2 = 0
9	.185E-21	.499E-24	.689E-2	.665E-2
11	.166E-19	-.357E-23	4.917	4.916
			L1= 1	L2 = 0
9	.149	.499E-24	19.132	19.513
11	-1.492	-.357E.23	4.917	4.916
			L1 = 0	L2= 1
9	.185E-21	.149	.689E-2	.665E-2
11	.166E-19	-1.492	4.916	4.916

Figure 6.21. Beam trace at selected surfaces with control data from figure 6.8.

6.6 High Irradiance Constraints in the Design for 1.06 μm Wavelength

The discussion in subsection 5.6 applies to this configuration. The only changes are the wavelength and the effective focal length. Their product does not change; therefore, the allowed irradiance at the Hartmann plate is unchanged. It is still 200 W/cm^2, and the potential peak irradiance on the hologram is still 99 kW/cm^2.

7. PUTTING THE RESULTS OF PREVIOUS AND NEW SIMULATIONS TOGETHER TO UNDERSTAND THE APPARATUS

This section fixes some additional conditions for proper use of the apparatus in three separate discussions. The first lists the key features deduced from sections 5 and 6. The second discussion examines how a phase curvature in a hole at the Hartmann plate affects the measured output at a detector. These new simulations as summarized

in figure 7.1 help define the allowed special frequencies for beam profiles. Finally, the section examines phase sensitivity.

7.1 Key Features of Sections 5 and 6

The key features deduced from the simulations of sections 5 and 6 are:

1. The peak irradiance allowed for the apparatus is 200 W/cm^2 regardless of wavelength if the hologram is on a metal substrate.

2. Appropriate change in two mirrors allows beam profile measurements at any wavelength between 1.06 and 10.6 μm.

3. To make precision measurements for details in beam profile, the wavelength from a laser source must be within 1 percent of the wavelength used to set up the apparatus.

4. Given the nominal dimensions and angles in these simulations, the apparatus can be packaged in a volume 2x2x0.5 m^3 if the hologram at surface 7 reflects the beam.

5. The power and phase distortions by the apparatus for each beam tracing through the apparatus are less than 5 percent in power and less than 0.2 rad in phase between interfering beam pairs. These simulations shown in figures 5.15 and 6.13 do not reflect defraction details as shown by nonzero G(m,n) at the hologram. Direct measurements will be necessary to fix the correct values for G(m,n). For our purposes, these details do not change the basic results from these simulations. They mainly reduce the power received at the detector for each beam pair by one order of magnitude (see section 8 and subsection 3.3 for further details.

6. The power variation is less than 50 percent from the sampled beam at the center of the Hartmann plate compared with those sampled beams on the edge of the plate. This variation is sensitive to the apertures of each mirror and the hologram. If this variation is a problem, then some mirrors will need larger diameters than those chosen in the simulation. Of course, the cost of the apparatus increases significantly.

7.2 Results of New Simulations

In all the previous simulations, the phase front at each sampling hole is presumed to be a plane wave normal to the Hartmann plate. We can change this constraint so that each hole has some curvature of the phase front at the hole and can be structured so that the direction of this front is no longer normal to the plate. To accomplish these changes, we would adjust LC and LD to allow nonnormal phase fronts in the x and y directions, respectively. For our purposes, it is unnecessary to make variations for both directions because the differences between the two directions are not significant at this time. For more precise simulations, details in direction could become important. Similar notions apply to the two curvatures, RX and RY, at each sampling hole. Therefore, we only vary the LC and RX in the simulations shown in figure 7.1.

$\lambda(\mu m)$	Power(Watts)	RX(m)	Φ (rad)[++]	α (LC * c/RX)[+]
1.06	0.316	1E20	-1.891	0
1.06	0.205	1E3	2937.204	1E-3
1.06	0.316	1E3	25.5328	1E-4
1.06	0.198	1E6	2,963,737.5	1E-3
1.06	0.315	1E6	29,633.5	1E-4
10.6	0.201	1E20	0.179	0
10.6	0.201	1E6	296,374.02	1E-3
10.6	0.201	1E6	2963.707	1E-4
10.6	0.201	1E3	293.986	1E-3
10.6	0.201	1E3	2.911	1E-4

\+ Here c = 5 mm.

++ Crude model has $\Phi \cong \Phi_0 + RX * \alpha^2 * \pi * D/\lambda$ and implies

$D \sim 1E3$ if $\alpha \leq 1E-4$ for 1.06 μm
$\alpha \leq 1E-3$ for 10.6 μm

Conclusion!!!

If $RX * \alpha^2 * D/\lambda << 1$, then
power and phase are unambiguous measurements for either wavelength.

If LC $\lesssim$ 10, then we require
RX > 2.5 E6 m for 1.01 μm, and
> 2.5 E5 m for 10.6 μm for unambiguous measurements.

Figure 7.1. Summary of simulation changing the parameters RX and LC for beams LA = LB = 7 and L1 = L2 = LD = 0.

The simulations in figure 7.1 make it clear that there are limits to the allowed curvature at each sampling hole and that there are severe limits to the angle as defined by α relative to the surface normal of the Hartmann plate. In brief, this angle must be less than 1 mrad for 10.6 μm and 100 mrad for 1.06 μm if we are to have insignificant power attenuation of the sampled beams. Further, to avoid ambiguity in the phase measurements, the curvature must be greater than 2.5 E +6 m for 1.06 μm and 2.5 E +5 m for 10.6 μm. Here we presume that LC cannot exceed 10. This latter result implies very stringent constraints to the apparent curvature at each sampling hole and to the degree the phase front deviates from the Hartmann plate normal. To relax these conditions requires significant change in the focal lengths of the mirrors and the allowed beam size. For the simulations in this paper, we presume that the local curvature at each hole is a plane wave with a phase front parallel to the Hartmann plate.

7.3 Phase Changes by Noise, Amplitude, Beam Direction, and Various Adjustments in Wavelength and Mirror Positions

We have examined many properties and variables of the reflection apparatus. We now look at the allowed variation in power and the phase between neighboring beams from the prefilter so there are unambiguous and reasonable accuracy measurements of phase at each sampled point. To be sure you know the phase at each point uniquely requires the direction variation over the entire beam profile of 10 cm diameter has the total phase

variation, $\Delta\Phi$, less than 2π from one edge of the beam to the other edge along any diameter through the beam center. This constraint implies a strong constraint to the average beam direction, α_A.

Thus with:

$$\Delta\Phi = k\,\alpha_A\,\Delta X,$$

where

$$\Delta X = 100 \text{ mm, and } \Delta\Phi \leq 2\pi \text{ , then}$$

$$\alpha_A \leq 10 \ \mu\text{rad for } 1.06 \ \mu\text{m and}$$

$$\leq 100 \ \mu\text{rad for } 10.6 \ \mu\text{m}.$$

If this average beam direction varies beyond this range given above, there can be $(2n + 1)\pi$ ambiguities in the phase front. If the beam phase front is sufficiently understood from previous information, then moderate changes in phase beyond this 2π restriction across the front can be inferred. In this case, the allowed range of α_A may increase by a factor of 10 to equal the constraint on beam direction, α, at each hole.

So far, the allowed variation in amplitude to get accurate phase measurements between neighboring sampling holes has not been fixed. Briefly, each pair of sampling holes in the prefilter generates three beams at surface 11, two with amplitude-only information labeled as I_1 and I_3 and a third labeled as I_2. The latter has relative phase information. If we pretend for this discussion that all calibration effects by each detector cancel and set the relative phase between the two beams equal to 0, the cos Q is given as:

$$\cos Q = (I_2 - I_1 - I_3)/2\sqrt{I_1 I_3} \ . \qquad (7.1)$$

The errors in measuring the relative phase, namely DQ, are primarily due to electronic noise in the three detectors of interest at surface 11. We simulate that noise by:

$$(DI_1)^2 = (gI_1)^2 \ ,$$

$$(DI_2)^2 = (gI_2)^2 \ , \text{ and}$$

$$(DI_3)^2 = (gI_3)^2 \ . \qquad (7.2)$$

Here we model the dominant noise as due to the amplication process in each detector; therefore, the noise is proportional to the appropriate input signal. If the final apparatus has different noise sources, this discussion must be changed accordingly. These results define the procedure.

In our analysis, we presume that the noises are independent between each detector; therefore, the standard deviation of $(DQ)^2$ is given as:

$$8(DQ)^2 \sin^2 Q = g^2[3(I_2)^2 + (I_1 - I_3)^2]/I_1 I_3. \tag{7.3}$$

If we accept for this discussion that I_2 is constrained by eq (7.1), that I_1 is more intense than I_3, and that $I_3 = u\ I_1$, where $u \leq 1$, eq (7.3) becomes:

$$8(DQ)^2 \sin^2 Q = g^2[3(1 + u + 2\sqrt{u} \cos Q)^2 + (1 - u)^2]/u. \tag{7.4}$$

There are three situations of primary interest in this equation, namely $Q = 0$, $\pi/2$, and π.

If $Q = \pi/2$, then:

$$(DQ)^2 = g^2[3(1 + u)^2 + (1 - u)^2/8u. \tag{7.5}$$

Here minimum error has $u = 1$. When $u \to 0$, the error increases without bound. Since the error is bounded to be less than π, this means the phase becomes undefined once u is small enough. How small depends on the noise value indicated by g.

If Q is near π or 0, the error is unbounded; therefore, the discussion must change. Here we set $DQ = \pi$ and estimate how close we can get $Q = 0$ or π for a given u. Here we let Q approach 0, then:

$$Q^2 = g^2[3(1 + u\ 2\ u)^2 + (1 - u)^2]/(8\pi^2\ u). \tag{7.6}$$

Here the smallest Q happens when $u = 1$, and the value of Q increases without bound when u approaches zero.

When Q is near π, it is possible for it to become arbitrarily close to π when u becomes close to 1. In this case we set $DQ = \pi$ and equate $Q = \pi - e$ where:

$$e^2 = g^2[3(1 + u - 2\ u)^2 + (1 - u)^2/(8\pi^2 u). \tag{7.7}$$

Note that $e = 0$ when $u = 1$. Again, as u goes to zero, the phase Q becomes undefined.

In summary, we have seen that the errors in measurement are complex functions of the actual beam profile. Therefore, a simple picture of the error profile for the phase front is not possible without significant constraints in the allowed beam profile. The results of sections 5 and 6 along with this section should permit the inference of beam profiles that allow precision measurements of phase. When the measurements require less precision, then the constraints on the profile can be reduced. One final question remains. How do the phase and power for the selected test beams change when the wavelengths and positions of the mirrors change. Figures 7.2 and 7.3 show the phase shifts caused by these changes. These results show that there is significant sensitivity to some position changes. This can allow fine positioning adjustments of the apparatus. The power variation for each beam is completely negligible under these conditions and therefore is not tabulated.

We make a brief overview based on these simulations. They show that there can be accurate phase and amplitude measurements provided: (1) there is less than 1 percent change in wavelength relative to the setup wavelength; (2) there are significant restrictions on the local beam curvatures, the average beam direction, and the bounds for the variation of the phase front; (3) there is a range of wavelengths that can be used if certain mirrors are changed; and finally, as is always the case, there is an ultimate accuracy of this system for measurements which are controlled by the noise in the detectors.

Beam							
	LA =	0	0	0	7	7	7
	LB =	0	0	0	7	7	7
	L1 =	0	1	0	0	-1	0
	L2 =	0	0	1	0	0	-1
Base		-3.142	-3.139	-3.131	.179	.100	-.108
$\Delta\lambda$		-3.142	-3.139	-3.133	-.034	-.100	-.279
$v\Delta b_1$		-3.130	-3.438	-3.429	-121.338	-113.028	-113.271
Δb_2		-3.142	-3.137	-3.130	.188	.116	-.093
Δb_3		-3.142	-3.140	-3.133	.170	.085	-.124
Δb_4		-3.130	-3.438	-3.429	-121.340	-113.030	-113.273
Δb_5		-3.130	-3.438	-3.429	-121.340	-113.030	-113.273
Δb_6		-3.142	-3.137	-3.130	.187	.116	-.0930
Δb_7		-3.142	-3.139	-3.131	.179	.100	-.108
Δb_8		-3.130	-3.438	-3.429	-121.338	-113.028	-113.272
Δb_9		-3.130	-3.438	-3.429	-121.338	-113.028	-113.272
Δb_{10}		-3.130	-3.438	-3.429	-121.490	-113.169	-113.413

Figure 7.2. The phase at surface 11 for test beams when the wavelength and mirror positions are changed (the 10.6 μm case).

Beam							
	LA =	0	0	0	7	7	7
	LB =	0	0	0	7	7	7
	L1 =	0	1	0	0	-1	0
	L2 =	0	0	1	0	0	-1
Base		-3.142	-3.136	-3.142	-1.891	-2.057	-1.881
$\Delta\lambda$		-3.142	-3.137	-3.142	-1.968	-2.110	-1.959
Δb_1		-3.141	-3.161	-3.168	-12.462	-11.901	-11.721
Δb_2		-3.142	-3.121	-3.128	-1.810	-1.912	-1.737
Δb_3		-3.142	-3.150	-3.157	-1.972	-2.201	-2.024
Δb_4		-3.262	-.942	-.938	906.900	844.270	844.171
Δb_5		-3.022	-6.111	-6.134	-1218.431	-1135.024	-1134.391
Δb_6		-3.142	-3.135	-3.142	-1.890	-2.055	-1.879
Δb_7		-3.142	-3.136	-3.142	-1.891	-2.057	-1.881
Δb_8		-3.022	-6.111	-6.134	-1218.464	-1135.052	-1134.423
Δb_9		-3.022	-6.111	-6.134	-1218.464	-1135.052	-1134.423
Δb_{10}		-3.143	-3.110	-3.116	8.638	7.749	7.921

Figure 7.3. The phase at surface 1 for test beams when the wavelength and mirror positions are changed (the 1.06 μm case).

8. DEVELOPMENT OF THE SURFACE HOLOGRAM

Subsection 3.3 defines the basic action of the surface hologram in eq (3.39). Section 8 and its subsections step from this basic formula toward the realization of such holograms. I define "surface hologram" at surface 7 functionally. Some readers may consider this hologram to be a filter, a Kinoform, or a complex grating [13,14,15]. Surface 7 must have a reflection surface with features shown in eq (3.44). This structure must generate the desired nine beams from each incident beam out of the prefilter. In addition, because this surface hologram is nonideal, it generates unwanted background radiation which must not cause significant overlap with desired beams. This latter fact influences the allowed form for this surface hologram. In subsection 3.3, we indicated one way to realize the ideal nine-beam output with minimum extraneous background radiation. In this section, we examine two approaches that realize the desired nine beams. Each has background radiation whose effects on the final cross-correlation pattern at surface 11 must be known. This section examines these two methods and develops their limits. The two methods are: (1) the binary type of hologram (see references [13,14,15]) with both reflecting and transmitting beams; and (2) a bumpy and essentially 100% reflecting binary type of hologram on a metal substrate [14].

In subsection 8.1 we discuss why the two methods are examined and develop the simplifications for modeling these two methods. In subsection 8.2 we apply these results to fit the constraints of the reflection apparatus, and we define the necessary work. In subsection 8.3 we list some computer codes that generate the masks needed for each surface hologram. Finally, in subsection 8.4 we indicate a suggested construction sequence for each method using the tools of the previous analysis and appropriate

facilities for thin-film deposition.

Subsection 9.5 contains the conclusions about the surface hologram drawn from the analysis in section 8, from various inquiries of commercial and technical sources, and from some preliminary work at NBS.

8.1 The Concept: Ideal and Practical

There are numerous ways to make holograms. Some transmission and reflection holograms are shown in reference [1] and in selected pages of [6,13,14, and 15]. By proper scaling as shown in reference [1], it is possible to get the desired hologram where a single beam illuminates it and nine similar beams exit from it either as a reflection or transmission process. These volume holograms can absorb significant laser energy; therefore, the substrate which holds the holographic materical can be heated differentially. For laser pulses of high power or energy, this implies serious errors in the measurement of the phase front. We avoid this problem by using holograms which have insignificant heating of the substrate. The bumpy and binary surface holograms can be constructed to have this condition.

The bumpy surface hologram has a substrate which is a good heat conductor, such as copper. This bumpy surface causes phase modulation of each incident beam. The modulation generates nine similar beams with almost 100 percent reflection as well as some extraneous radiation. We examine how this hologram could be realized in subsequent subsections. Reference [14] shows one example for such a 100% reflection hologram. That paper as well as subsection 3.3 shows that the depth of modulation is strongly wavelength dependent. We discuss the consequence of this dependence as we analyze the bumpy surface hologram. For example, the dependence makes each bumpy surface hologram useful only for a narrow range of wavelengths.

The second method or binary type for generating the desired nine-beam pattern uses a substrate that can transmit the laser beam with high power or energy through the substrate with little absorption. For example, 10.6 μm radiation could use a beam splitter wedge of ZnSe, NaCl, or KCl. Here the transmission hologram would be constructed by etching through a film of gold a complex but periodic pattern of nonoverlapping transmission ports on the exit surface of this wedge. These ports sample the incident beams from the prefilter and radiate a pattern in the transmitted direction that can look like nine beams of each original incident beam plus some background radiation of high spatial frequency. The reflected laser power returns to some energy dump for absorption. Because the wedge has low absorption, there is little distortion in this hologram; therefore, the reflection apparatus can operate accurately. (If antireflection types of coatings can be used, it may be possible to reverse the roles of the reflected and transmitted beams. We ignore that possibility here.)

If the use of the apparatus for beam profile measurements implies no distortion by the hologram, then we can use a film of some appropriate plastic on a flat mirror surface for this hologram. This film could create a reflection phase hologram. The plastic could record the needed pattern on a film of variable thickness. Because we expect to use the apparatus for high-power beams, we do not consider a plastic film; rather, we examine the two metal film techniques. When the apparatus has been constructed, then the plastic film approach should be considered. It may prove better than the techniques using metal films.

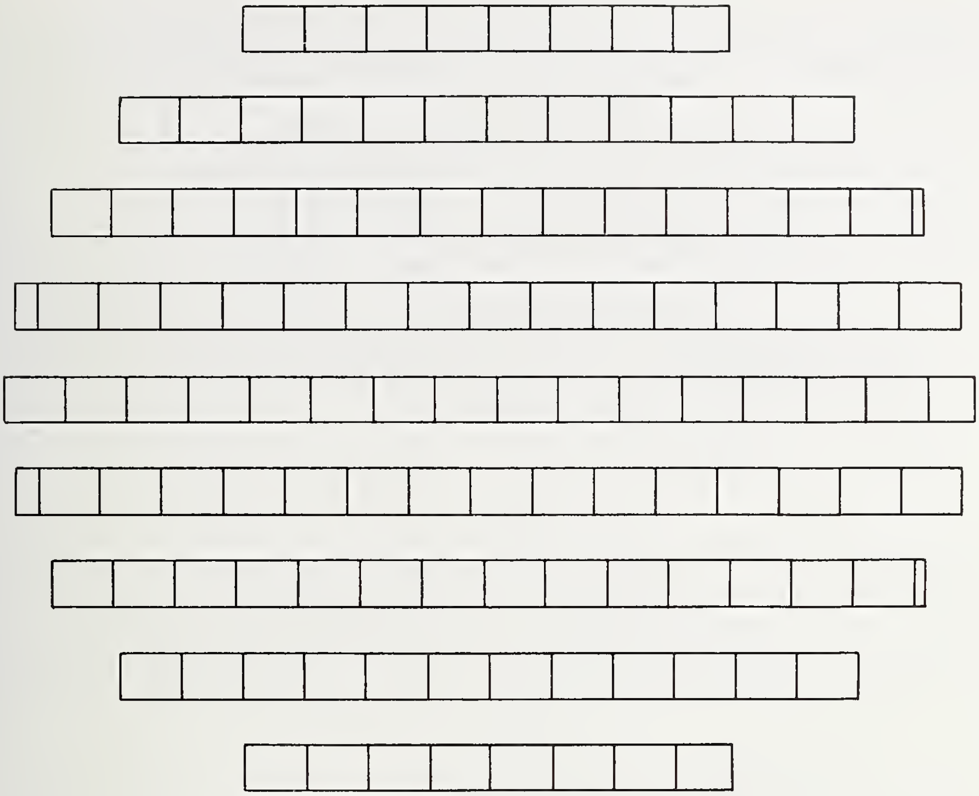

Figure 8.2 The Example of the Mask Output

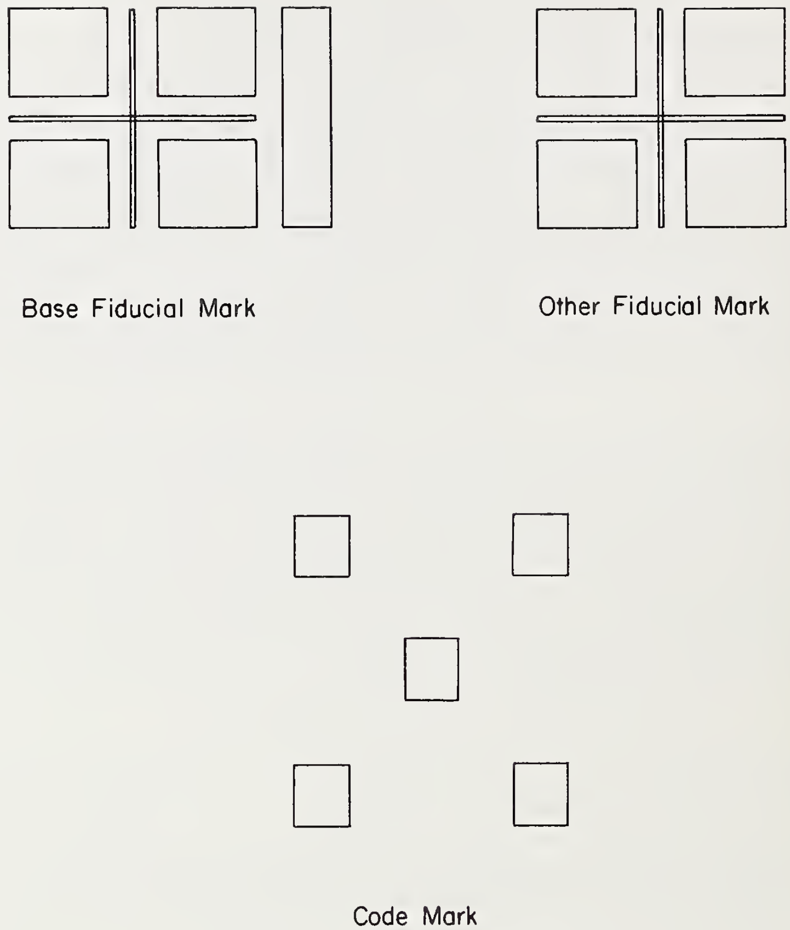

Figure 8.3 The Expansion of the Fiducial Marks and Code Mark To See Details

To make the analysis of the metal films as simple as possible, we eliminate details that can be considered extraneous.

Under reasonable conditions, we can reduce the two-dimensional features of the surface hologram to a one-dimensional discussion. We do this by observing that the surface hologram is defined by the function F(u,v) in eq (3.39). This function can be separated into:

$$F(u,v) = F(u)\ G(v), \tag{8.1}$$

where F(u) and G(v) are similar functions. If there were no off-axis illumination, these functions could be identical. Equations (3.40) and (3.41) show how the F(u) and G(v) can be different. First, the S7 and T7 need not be the same because there is off-axis illumination in the x plane. Second, there can be a weak dependence on the angle of illumination as shown by the C1 in eq (3.40). The simulations from sections 5 and 6 established that S7 = C1*T7 to high accuracy. This means that we can analyze the function F(u) only and accept that the only essential change to get G(v) for experimental realization of F(u,v) has G(v) = F(v/C1). The remaining C1 term in eq (3.40) is buried in the form of F(u).

Note that eq (3.40) implies F(u) has unit amplitude. This arises during the derivation of eq (3.39) where the surface reflection at surface 7 was allowed only a phase shift. Letting F(u) cause amplitude as well as phase modulation does not affect the form of eq (3.35). This flexibility in F(u) means holograms can cause either pure phase modulation, pure amplitude modulation, or mixed phase and amplitude modulation. The coefficients, G(m,n), in eq (3.44) are limited by the possible fabrication methods.

We simplify our discussion by studying F(u) only and ignoring the G(v). This means the two-dimensional array of detectors at surface 11 has collapsed into a one-dimensional array of detectors where there are alternate spots with a single-beam contribution and others with a two-beam contribution. Instead of nine beams, three beams now exit from surface 7. These propagate in the directions ℓ_a*S7 where the incident beam is designated with a $-\ell_a$ and the three exiting beams are labeled as $\ell_a + 1$, $\ell_a - 1$, and ℓ_a. The last beam is the direct reflected beam, and the former pair are the defracted beams.

To further simplify this analysis and to eventually make maximum economic use of equipment and techniques available from integrated circuit technology, we presume that the F(u) can be completely defined by a periodic function. Thus, F(u + D*n) = F(u), where n is an arbitrary integer and D is the fundamental spatial period of the pattern. Here D = 1/f and f = S7/2 . Here f is the fundamental spatial frequency for the hologram. We can represent F(u) and its Fourier transform as:

$$F(u) = \sum_{j=-\infty}^{\infty} A_j \exp(i\ j\ u\ 2\pi f)\ , \tag{8.2}$$

and

$$A_j = f \int_0^D du\ F(u)\ \exp(-i\ j\ 2\pi f u). \tag{8.3}$$

To realize the desired form of A_j, we must look at possible realistic forms for F(u) that can be made by lift-off techniques and other such processes from the integrated circuit technology. The ideal hologram for our case would have A_j nonzero, for j = 0, ± 1 and the remaining A_j zero. If we accept that this ideal cannot be made, we must relax this requirement and use the structure of the apparatus to help achieve the desired pattern at surface 11 even though the hologram does not behave as wished.

The discussion in subsection 3.3 shows that we can approach the ideal provided we allow small but nonzero values for A_j with $|j| \geq 2$. This case is one example of the bumpy surface. Subsection 8.2 contains a discussion of how to realize this hologram. Additional complex patterns using the bumpy surface concept are discussed in this paper after we explain the binary hologram.

If $A_j \neq 0$ for $|j| \leq 22$ in addition to the $j = \pm 1, 0$, then the radiation from the terms with $|j| \geq 22$ will miss the detector array; hence, we will operationally have the ideal hologram plus a significant loss of laser power. Reference [14] shows one example that could use this approach. Here there is almost 100 percent reflection of the incident beam. We skip this example until we have examined in some detail the binary transmission case. Once it is understood, then the binary reflection example for a bumpy surface can be properly discussed.

We represent the transmission structure of the binary type by a grid of segments (see reference [16]). Each has a transmission hole. Thus:

$$F(u) = \sum_{m=0}^{M-1} \{\theta\,[u - u_1(m)] - \theta[u - u_2(m)]\} \ . \qquad (8.4)$$

Here:

$$\begin{aligned} \theta(u) &= 1 \text{ if } u > 0, \\ &= 0 \text{ if } u < 0, \text{ and} \\ &= 1/2 \text{ if } u = 0. \end{aligned}$$

Also:

$$u_1(m) = [m + \alpha(m)]g, \text{ and}$$

$$u_2(m) = u_1(m) + g\beta \ .$$

Here each segment size is g = D/M. The width of each hole in the segment, $g\beta$, is constrained by $0 \leq \alpha \leq 1$. Finally, the position of each hole as indicated by $g\alpha(m)$ is constrained by:

$$0 \leq \alpha(m) \leq (1 - \beta).$$

If we define

$$B_j = [\exp(-i\ 2\pi\beta j/M) - 1]/(-2\pi i j),$$

and

$$C_m = \exp\ \{-i[2\pi(m + \alpha(m))/M]\}\ ,$$

the Fourier coefficients are:

$$A_j = B_j \sum_{m=0}^{M-1} (C_m)^j \ . \tag{8.5}$$

We discuss this equation system briefly. Note that real F(u) implies $A_j^* = A_{-j}$. Also note that $A_0 = \beta$. To satisfy the conditions of the previous paragraphs, we must adjust 2N-1 coefficients. This implies that M is equal to or greater than 2N-1, so we have sufficient $\alpha(m)$ for adjustment. These $\alpha(m)$ and β must be found by an appropriate computer program so that we have required spectra.

Our spectra have $|A_j| \leq 0.001$ for all $2 \leq |j| \leq 21$, and a maximum

$$|A_1|/\beta \text{ and } \beta\ . \tag{8.6}$$

For example $\beta = 1$ causes $A_1 = 0$, so the β must be a value between zero and 1.

For brevity, we make no attempt to find the correct set of $\alpha(m)$ and β. That exercise is reserved for the persons who construct the final apparatus.

To illustrate the expected form of the results, we look at a simple case where $\beta = 1/2$ and where $\alpha(m) = h[1-\sin(2\pi m/M)]$. Equation (8.5) can be expanded in terms of Bessel functions to give the results:

$$A_j = MB_j \sum_{m=-\infty}^{\infty} J_{j+mM}\ (2\ hj/M)\ \exp(-ij\ 2\pi h/M). \tag{8.7}$$

To have $|J_2(4\pi h/M)| \leq 0.001$ requires $h \leq M(0.1)/4\pi$. The constraint on $\alpha(m)$ requires $h \leq 0.5$. For example, we could choose M = 42 to illustrate a possible condition on h, namely h = 0.33. This case implies $J_1(0.05) = 0.025$ which is a very small amount of defracted beam. In this case:

$$A_0 = 0.5, \text{ and} \tag{8.8}$$

$$A_1 = 0.0125.$$

I recommend that the reader try new $\alpha(m)$ to see what spectra are possible. For example, two sine waves with phase factors give three parameters of adjustment that can be used to eliminate exactly the A_2 term and allow the strength for these modulations to be increased beyond the value allowed for a single sine wave. This discussion should have explained $\alpha(m)$; therefore, we now pass to the reflection hologram.

To construct the 100 percent reflection (binary type) case, we must make two adjustments.

First we modify the F(u) representing the surface to a sum of two terms. Namely, we add a second surface term to F(u) which is the complement of F(u) for transmission (see reference [13]). This complement is multiplied by a phase shift given as:

$$Q \equiv \exp(-i2ks).$$

Here s represents the displacement of the complement surface relative to the original surface.

Second, to make the surface a reflection hologram, we cover this two-level structure with a metal film. Our reflection hologram now has the following functional form for F(u), namely:

$$F(u)_r = F(u)_t + [1 - F(u)_t]*Q. \tag{8.9}$$

The $F(u)_t$ is the transmission function used in eq (8.8). The Fourier coefficients for the reflection system can be given in terms of those for the transmission system as:

$$A_j^r = (1 - Q)*A_j^t + Q*\delta_{j0} . \tag{8.10}$$

We note two cases of interest:

1. First, set s = 0, which is a flat mirror. Here we have pure reflection and no diffraction, namely $A_0 = 1$ and $A_j = 0$ where $j \neq 0$.

2. Second, set $s = \pm\lambda/4$; thus, $Q = -1$ and $A_j^r = 2A_j^t\ \delta_{jo}$. Note that $A_0^r = 2\beta - 1$.

A computer program is necessary to maximize the A_0^r and (A_1^r/A_0^r) values and to minimize the remaining A_j^r values. The optimum for the transmission case will be different from the reflection case. For example, $\beta = 1/2$ implies no A_0^r term.

We now have three realizations of surface holograms: a simple bumpy surface and two binary types with either transmission or reflection conditions. At this point, a few comments on the construction of a more complex bumpy surface hologram remain.

The binary type of hologram causes large amounts of laser power to be diffracted into the $|j| > 2$ modes. The ideal situation would be to construct an F(u) with surface variations so that the A_0, A_1, and A_{-1} are maximum and so that the remaining terms are minimized appropriately. This situation implies the following formulation. To prevent surface heating and to maximize the available power, we write the surface variation as a pure phase function. Thus:

$$F(u) = \exp i\ \phi(u), \tag{8.11}$$

where $\phi(u)$ is represented as a linear spline with appropriate support constants. The integral equations,

$$A_j = f\int_0^D du\, \exp\{i[\phi(u) - j\, 2\pi fu]\}\ . \tag{8.12}$$

are nonlinear functions of the support constants. We must adjust each support constant so that the diffraction spectra are as ideal as possible. If we can realize this hologram in both the computer model and in the technical details of thin-film operations, we would have the best hologram for two reasons: the laser power is not diffracted needlessly, and the surface structure has no sharp edges which would increase the chance for field breakdown at high irradiances. One suggestion by Dr. A. J. DeMaria, United Technologies Research Center, was to use ion beams to charge the reflectivity of the minor surfaces as a function of position. If a facility has this capability, then this may be a good way to get reflection holograms with the necessary smoothness. To realize this hologram requires significant development which has not been done; therefore, we settle for the simpler but less efficient bumpy surface hologram. The technical approach for it is detailed in subsections 8.2, 8.3, and 8.4. The technical realization of the binary types of holograms is already adequately discussed in references [13,16]. However, there remains some development work for these types, namely: (1) the computer codes to optimize the $\alpha(m)$ and β; (2) the computer codes to generate the masks for the pattern; and finally, (3) some measurements to document the influence of surface defects on the actual output at each appropriate wavelength.

8.2 The Parameters for the Surface Hologram

The remaining subsections for section 8 become more criptic. We indicate key details for construction of the surface hologram implied by eq (3.41) but do not step through each development sequence. This surface hologram can be constructed using this information as well as available thin-film technology and computer simulation techniques.

Equation (3.41) shows a sine wave for the $\phi(u)$. Thus:

$$F(u) = \exp[i\ \phi(u)]\ , \tag{8.13}$$

and

$$\phi(u) = -2k*C1*S*\sin(u*S7)\ . \tag{8.14}$$

How do we construct such a $\phi(u)$? To do this we need to understand the necessary mathematical representations and to give the parameters appropriate to the reflection apparatus under design in this paper. This subsection gives that information. In subsection 8.3 we list the computer codes used to generate the necessary bar-pattern masks, and finally, in subsection 8.4 we list a suggested construction procedure for the $\phi(u)$.

Here we generate a bumpy surface by starting with a flat substrate of copper. The ideal final surface should look like a sum of two sine waves--one for the x direction and one for the y.

To create the bumpy surface, we apply a series of uniform films of copper to the substrate. Each film is placed over a bar pattern of organic material. Each film has a different thickness. Because the film of copper sticks well to the substrate and because the organic materical can be dissolved, well-defined ribbons of copper can be added to the substrate. This deposition process is binary because each application adds a single uniform thickness of metal film at a time.

To represent a sine wave surface using these ribbons requires many applications and widths of ribbons. The precise number of films depends on the wavelength of the incident radiation and on how small those unwanted Fourier coefficients in eq (8.3) need be.

The mathematical representation of this operation shows the sine wave as expanded into a series of square waves of different heights and frequencies. Thus:

$$\sin p = (\pi/4) \left\{ \begin{array}{l} S(p) + S(3p + \pi/3)/3 + S(5p + \pi/5)/5 \\ + S(7p + \pi/7)/7 + S(11p + \pi/11)/11 \\ + \text{neglected terms} \end{array} \right\},$$

where

$$\begin{aligned} S(p) &= 1 \text{ if } 0 < p < \pi , \\ &= -1 \text{ if } \pi < p < 2\pi, \text{ and} \\ &= 0 \text{ if } p = 0 \text{ or } \pi. \end{aligned}$$

We control the sign of a square wave, $S(p)$, by shifting it by one-half cycle, $S(p + \pi) = -S(p)$.

We now specify parameters for the reflection apparatus. For the 10.6 µm wavelength, we set s = 0.084 µm. This implies the amplitude of each square wave as:

0.0660 µm	for the fundamental frequency, f,
0.0220 µm	for the third harmonic,
0.0132 µm	for the fifth harmonic,
0.0094 µm	for the seventh harmonic, and
0.0060 µm	for the eleventh harmonic.

Each amplitude is doubled to give the thickness of the film because we need peak-to-peak variation. The half period or bar width of the fundamental square wave is 2.162 mm for the x direction and 2.141 mm for the y direction. The substrate area for these sine waves is a circle 40 mm in diameter.

If we note that the diameter of an atom is about 0.1 nm, we see that the eleven-order frequency has about 60 atomic distances for its thickness. This fact indicates that we can build a high quality sine wave for 10.6 µm. Our technical constraint for this wavelength comes from the practical number of film deposition cycles.

If we shift the wavelength to 1.06 µm, then the cut-off frequency for construction of the sine wave at this wavelength is fixed by the requirement that the final film should have at least 10 to 100 layers of atoms to get a well-defined, "uniform" film. It is unclear if we can approach the sine wave with adequate accuracy for this and the visible wavelengths.

8.3 The Computer Codes

Figures 8.1 and 8.3 show the computer codes and an example of a computer run. Since the program is fairly straightforward, we do not discuss the codes in figure 8.1 in any detail. Briefly, the control data at statement 30 are read in for each mask as defined by the comment cards just below PROGRAM. These codes generate a file, TAPE11, which contains a series of commands to be used by another code [17] to generate the mask shown in figure 8.2

```
      PROGRAM ERIC (INPUT, OUTPUT, TAPES=INPUT, TAPE6=OUTPUT, TAPE 11)
C     D(1)=WIDTH OF DARK BAR IN MM.
C     D(2)=SHIFT OF DARK BAR IN MM.
C     D(3)=RADIUS OF CENTRAL MASK CUT OFF IN MM.
C     D(4)=RADIUS OF CROSS MARKS CENTER POSITION IN MM.
C     D(5)=X POSITION OF CODE STRUCTURE IN MM.
C     D(6)=Y POSITION OF CODE STRUCTURE IN MM.
C     D(7)=CODEΔ
C     D(8)=FRACTION OF PI, ANGLE RELATIVE TO X AXIS.
      DIMENSION D(8), ID(6)
5     J=5
      PRINT 6
6     FORMAT("NUMBER OF MASKS")
C
      REWIND 11
8     READ(J,*)I
      I=I+1
1Ø    I=I-1
2Ø    IF(I .LE. Ø) STOP
28    PRINT 29
29     FORMAT("NEW DATA 8 VALUES, FREE FORM USE COMMAS")
3Ø    READ(J,*)D
31    FORMAT("DATA RECEIVED")
      PRINT 31
      WRITE(11,32)D(7)
32    FORMAT("START,",F1Ø.5,".")
      D(8)=D(8)*3.141592654
      DO 4Ø I1=1,6
      ID(I1)=D(I1)*1ØØØØ/25.4+.5
4Ø    CONTINUE
5Ø    FORMAT("BOX",4(","I5)".")
      PRINT 45,D,ID
45     FORMAT("DATA=",/4F1Ø.5/4F1Ø.5617)
      I4=D(7)
      IDY=(ID(1)/2)*2
      IØ=ID(2)
      I1=ID(3)/(2*IDY)
      IY=IØ-2*(I1+1)*IDY
      F1=ID(3)
95    FØ=IY
1ØØ   X=1.-(FØ/F1)**2
      IF(X)15Ø,16Ø,16Ø
16Ø   X1=SQRT(X)
      IX=-ID(3)*X1
      IDX=-IX*2
      WRITE(11,5Ø)IX,IY,IDX,IDY
15Ø   IY=IY+IDY*2
      IF(IY-ID(3))95,95,2ØØ
2ØØ    IDX=5Ø
```

Figure 8.1. The computer listing for the mask generation--
bumpy surface case (page 1).

```
      HERE WE CODE THE MASK
      IDY=5Ø
      IXØ=ID(5)
      IYØ=ID(6)
      I1=1ØØ
      I2=1ØØ
      DO 24Ø I5=1,3
      IX=IXØ+(I5-1)*I1
      DO 23Ø I6=1,3
      IY=IYØ+(I6-1)*I2
      DA=CODE(I5,I6,I4)
      IF(DA)23Ø,23Ø,22Ø
22Ø   WRITE(11,5Ø)IX,IY,IDX,IDY
23Ø   CONTINUE
24Ø   CONTINUE
      TH=D(8)
      DTH=1.57Ø796327
      DO 3ØØ IA=1,4
      C1=COS(TH)
      S1=SIN(TH)
      IAY=ID(4)*S1+.5
      IAX=ID(4)*C1+.5
      CALL CROSS (IAX,IAY)
      TH=TH+DTH
      IF(IA-2)29Ø,3ØØ,3ØØ
29Ø   IX=IAX+12Ø
292   IY=IAY-1ØØ
294   IDX=4Ø
296   IDY=2ØØ
298   WRITE(11,5Ø)IX,IY,IDX,IDY
3ØØ   CONTINUE
      WRITE(11,329)
329   FORMAT("END.")
      ENDFILE 11
      GO TO 1Ø
      END
      SUBROUTINE CROSS(I,J)
1Ø    FORMAT("BOX",4(","I5),".")
      DIMENSION ILL1(6),!L2(6),IL3(6),IL4(6)
      DATA(IL1=-1ØØ,-1ØØ,-1ØØ,-2,2Ø,2Ø)
      DATA(IL2=-2,2Ø,-1ØØ,-1ØØ,-1ØØ,2Ø)
      DATA(IL3=2ØØ,8Ø,8Ø,4,8Ø,8Ø)
      DATA(IL4=4,8Ø,8Ø,2ØØ,8Ø,8Ø)
      DO 3Ø I1=1,6
      IX=IL1(I1)+I
      IY=IL2(I1)+J
      IDX=IL3(I1)
      IDY=IL4(I1)
      WRITE(11,1Ø)IX,IY,IDX,IDY
3Ø    CONTINUE
```

Figure 8.1. The computer listing for the mask generation --bumpy surface case (page 2.)

```
40        RETURN
50        END
          FUNCTION CODE(I,J,L)
          INTEGER I1
           DIMENSION I1(9)
          DATA(I1=1,Ø,1,Ø,1,Ø,1,Ø,1)
          K=3*(I-1)+J
          IF(I1(K))1,1,3Ø
1         IF(I-2)2,5,3
2        IF(L .LE. 8)22,3Ø
3        L1=L-(L/2)*2
4        ID(L1 .LE. Ø)3Ø,22
5        IF(J-2)8,5Ø,6
6        L1=(L-1)/4
         L2=L1-(L1/2)*2
         IF(L2)5Ø,22,3Ø
8        L1=(L-1)/4
         L2=L-L1*4
          IF(L2-2)22,22,3Ø
22        CODE=Ø
25        GO TO 4Ø
3Ø        CODE=1
4Ø        RETURN
5Ø          PRINT 6Ø
7Ø         STOP
6Ø        FORMAT("ERROR IN CODE SUBROUTINE")
8Ø        END
```

Figure 8.1. The computer listing for the mask generation --bumpy surface case (page 3).

Figure 8.2 has three features: (1) a series of rectangular boxes that correspond to the dark areas of a bar mask; (2) one basic fiducial mark for the angular position of a mask and three additional fiducial marks, all of which allow each mask to overlay properly the previous mask patterns; and (3) a code structure for 16 possible unique labels of these masks.

For convenience, figure 8.3 shows magnified versions of the fiducial marks. This sample case used the following values:

D(1) = 2.162 mm bar width	D(4) = 24 mm cross marks	D(7) = 1 Code No.
D(2) = 0 mm phase shift	D(5) = 24 mm x position	D(8) = 0 fraction of π
D(3) = 20 mm radius	D(6) = 24 mm y position	

8.4 The Proposed Construction Sequence

At least 4 masks are necessary for construction of the sin(S7*u) function with the correct amplitudes for 10.6 μm wavelength. In addition, at least 4 masks are necessary for the construction of the sin(T7*v) function again with appropriate amplitudes.

The sequence becomes:

1. Start with flat-copper substrate.

2. Follow this basic sequence for each addition of metal film:

   a. Use photoresist
   b. Use appropriate mask to expose photoresist
   c. Remove exposed photoresist
   d. Deposit appropriate thickness of build-up material such as copper
   e. Remove unexposed photoresist to lift off areas of metal.

   There remain ribbons of copper of desired thickness and width.

3. The ideal construction sequence is to repeat the above process eight times--once for each mask. The suggested order is:

   First, the S7 frequency,
   Second, the T7 frequency,
   Third, the 3*S7 frequency,
   Fourth, the 3*T7 frequency,
   Fifth, the 5*S7 frequency,
   Sixth, the 5*T7 frequency,
   Etc.

Once the bumpy surface has been built up to the desired accuracy, then the entire surface has a gold film added to maximize the reflectivity at 10.6 μm.

9. THE EQUIPMENT NECESSARY FOR CONSTRUCTION OF THE REFLECTION APPARATUS

In previous sections we described a complex theoretical analysis of the reflection apparatus. The discussions were directed toward an ideal model. In this section we begin the task of identifying necessary hardware. Because we did not actually build the device, the resulting lists and cost estimates are tentative and may even be speculative. When actually building the device, the designer should note the suggestions here and generate more complete lists, specifications, and strategies for construction of the various parts. For example, the optics part and the detector package are likely to be separate proposals because the detector package has too many unknowns that need to be defined. Because we expect the constructed device not to match the nominal design specifications in this paper, this section can serve only to suggest what must be considered and what may be possible. The discussion in these subsections does not exhaust the construction details. Only key components with their approximate costs are discussed, and many mechanical and electronic specifications are ignored. We have chosen a flexible design which is naturally very expensive. To reduce the costs of the device, significant simplifications in the system must be made. Each simplification may reduce the capability of the final unit.

Despite the above discussion, this paper makes a substantial first step in the design of a reflection system with potential for high accuracy.

The subsections are grouped according to a particular class of items. The choice of mirrors along with their costs is discussed in subsection 9.1. We need translation and rotation mounts to hold the mirrors, the prefilter, and the hologram as well as the array of detectors. This discussion is summarized in subsection 9.2. The most expensive part of the reflection apparatus is the array of detectors; in subsection 9.3 we discuss some possibilities. The prefilter is defined in subsection 9.4. Remaining disucssions beyond that in section 8 about the hologram are contained within subsection 9.5. Here we estimate costs from a commercial source. To make the apparatus insensitive to temperature changes as well as to vibration, we need to design the support of the various components to respond to or to reduce the effects of environmental changes. In subsection 9.6 we discuss what could be done. Finally, because it is not possible to just buy parts and then assemble the apparatus, we discuss the needed machine shop work.

9.1 Mirrors

Five mirrors, 200 mm in diameter, are needed for the reflection apparatus under design. These mirrors define the base apparatus at 10.6 μm wavelength. The nominal focal lengths of these mirrors are 1.000 m for the y axis and 1.020 m for the x axis.

When we change the wavelength to something like 1.06 μm, we must substitute two mirrors. For 1.06 μm these mirrors are 50 mm in diameter and have nominal focal lengths of 0.1000 m for the y axis and 0.1020 m for the x axis.

The above mirrors require a certain level of optical quality. There are three measures of this quality, namely the surface roughness, the optical figure, and the scratch and dig values. We ignore scratch and dig issues for these mirrors. The apparatus is too complex to estimate these effects in advance.

If we allow the shortest wavelength to be 1.06 μm and if we require that the reflections off each mirror distort the phase and amplitude less than 0.5 percent, then the surface roughness should be less than 5 nm rms for each mirror [18,19]. It is not clear at this time that we need this level of accuracy. The basic instrument would have problems induced by surface roughness if the background radiation from each mirror reaches the detectors and if each pair of beams forming the interference spots comes from significantly different scattering conditions. The quality of mirrors for the apparatus does not need to be as good as that for laser cavities or for beam forming and turning apparatuses. Probably more critical for this apparatus is the accuracy of the surface to the desired curvatures. The prime negative effect of surface roughness will be to induce unwanted signals at the spots in surface 11. These unwanted signals will cause a decrease in the signal to noise at each spot. It is difficult to estimate how this effect influences the accuracy of measurements.

Technically, the surfaces of these mirrors in this mathematical model are the product of two parabolas of different curvatures for each axis. For convenience, I have labeled the surfaces as "elliptical to reflect shape of the contours." The actual mirror surface would be almost parabolas with less than $\lambda/10$ deviation from the ideal. Since λ ranges from 1.06 to 10.6 μm, the allowed deviation for the apparatus under design is 0.1 μm. This appears to be within the capabilities of industry.

There are three types of mirrors that can be used in this device. The first type is a solid copper mirror which has been constructed by machining and polishing a copper blank. The second type uses electroforming to generate the mirror. This structure is either copper or nickel sheet with a copper or gold film as the mirror surface. The third type has a copper or gold film on a glass or plastic substrate. Because the capabilities of production in the industry are changing rapidly, each type should be investigated at the time of purchase of the mirrors. To specify these mirrors, the

surface qualities already mentioned should be fixed. In addition, the potential distortion in the mirrors by the heat from the laser beams must be considered. To have high precision measurements of the phase front, the errors in the value of the curvatures for these mirrors must be kept to less than 10 λ. How much less, must be tested with the simulation programs by varying each curvature. That simulation has not been done. The procedure is similar to the other simulations already performed and must be done before the mirrors are ordered. Remember, surface 11 output is the key control for all sensitivity tests.

If solid copper mirrors [20] are used because there can be significant thermal loading by the laser beams, we estimate the cost to be $6,000 for each 200 mm mirror [19]. They each weigh 10 kg. The solid copper, mirrors of 50 mm in diameter would cost about $1000 each and would each weigh 0.5 kg.

If we can use metal mirrors made of 6 mm thick copper plate by an electroforming technique, both the cost and weight of these mirrors are reduced substantially. We estimate [21,22] the cost of the two mandrels to be about $6000 each. After they have been made, the cost for construction of each mirror would be about $200. Some polishing may be necessary. The mirror surfaces made by this method may be distorted by the high-power loading. If appropriate water cooling can be done, then this distortion should not be a problem. My understanding [22] is that the surface figure of these electroformed mirrors can be adequate for this apparatus, namely λ/10.

I have no comments on the glass substrate.

In summary, the range of costs are $32,000 for solid mirrors and $14,400 for electroformed mirrors.

9.2 Translation Mounts

We have five degrees of freedom to position each mirror, the prefilter, the hologram, and the array of detectors. Thus, we use three translation mounts, namely one for x, y, and z motion, as well as two rotation mounts. When we use the 200 mm diameter solid copper mirrors, these mounts have to take significant weight. For units that have approximately 50 mm and 50 kg load capacity, the approximate price of each unit is $500 [23]. If the range is reduced and the loading is made smaller, then the cost is closer to $100. The two-angle rotation and mirror holder can cost about $500 for the 200 mm diameter mirror and about $100 for the 50 mm diameter mirror. In summary, we need about $2000 for the heavy-duty positioning system and about $400 for the light-duty system. I have not included cost of nuts and bolts or the possibilities of high precision types of mounts.

We require seven heavy-duty systems for the five mirrors, the prefilter, and the array. In addition, we use three light-duty systems for the two substitution mirrors and the hologram. The net cost is $15,200. If we use only light-duty systems, then the cost is $4000.

9.3 Detectors--Types and Construction of the Receiver Array

In this subsection we indicate one method for recording the information presented at surface 11. The correct method to use depends on the desired time response for measurement of the beam profile and on the available technology. The design goal of this reflection apparatus is to have a system capable of measuring at the 20 ns resolution so that the beam profile of laser pulses of 20 to 1000 ns in duration can be measured in real time. To make this design goal as realistic as possible in terms

of available capability, we will presume that the measurement process by a method would accomplish the following:

1. Each of the beams at surface 11 should be sampled in an analog manner using a time period of 20 ns. The time interval between these samplings would be variable from 20 ns to 1 ms. The maximum number of these samples that would be recorded for a data reduction cycle is 10.

2. To be sure that the measurement of beam profile is a faithful snapshot at selected time points, these samples are synchronized.

3. To get maximum accuracy from the reflection apparatus, each analog sample will be digitized for subsequent processing by a computer. This computer may be electronic or optical [24,25].

4. The minimum number of spots that must be measured at surface 11 are: (1) those with one beam contributing from the prefilter; and (2) those with two beams contributing from the prefilter. This implies about 600 spots for this apparatus.

For best accuracy, redundancy, and real-time control of the errors in the beam profile of the incident laser beam, it is also necessary to measure the power in those beams at surface 11 that are formed by four beams from the prefilter. If there are 300 holes in the prefilter, then there are approximately 600 beams that would be measured if the error signal beams are not used. If they are used, then there are approximately 1200 such beams.

In summary, for a single data reduction cycle we need to store the digitized value of the energy in each of the 1200 beams during the ten sampling periods. If we can construct such a unit, then the reflection apparatus can be of high value for beam profile control of the inital laser source as well as of high value as a primary method for absolute measurement of laser profile. The latter capability will be of use for checking less costly units such as the Hartmann plate unit.

From the above discussion, we will presume that a single cycle of data processing responds to the 12,000 words of data before a new block of data is needed. If the cycle cannot respond that fast, then the measurements must stop until the next data cycle can be processed properly. This rate of processing limits the throughput rate of the apparatus.

We now define one system. Remember that it has not been built and therefore some development may be needed.

The system would use individual pyroelectric detectors with diameters of 0.5 mm to convert the laser energy to an electron current. These currents would each flow in an appropriately impedance-matched coaxial delay line. Ten spatially separated sample and hold circuit units are attached to each delay line. The final readout sequence has a serial interrogation of these 12,000 sample and hold units for a sequential A/D conversion and storage in a computer memory. This system can be called a brute force technique. We estimate that it would cost $100,000 to buy the hardware. There are no new technologies needed to construct this device; just manpower and money. I have no cost estimate for the manpower.

9.4 Prefilter Construction

In this subsection we describe one possible prefilter design. There are obviously others. We selected the easiest, and hopefully the least expensive, version to construct. Its influence on the final accuracy is unknown but is presumed to imply a calibration correction near 1 to 5 percent.

Here we start with a square plate of copper showing volume of 12 by 12 by 0.6 cm^3. A square array of identical holes spaced 5 mm apart are drilled in this plate. This array is contained in a circle 10 cm in diameter. This implies approximately 300 holes.

There are three basic points about this prefilter that must be considered in the design. First, the plate of copper will be heated from the incident laser beam. This will induce stresses in the prefilter and thereby cause errors in the measurement of the beam profile. Second, the reflecting surface of the prefilter must have low absorption for all wavelengths of interest and must be structured so that the reflected laser beam does not return to the source. The former is necessary to minimize the impact of absorption on the prefilter as well as on the beam profile measurements. The latter is necessary to avoid feedback in the laser. Third, the structure of these holes must use the diffraction process properly so that there is accurate detection of the phase and amplitude at the center of each hole.

Surrounding the prefilter by a water-cooled mount and using various periodic beam blocking techniques such as a chopper will reduce the heating to a single correction. To account for the heating requires calibration of the apparatus. The measured beam profile is then used to correct for these heating effects and is thereby in turn modified to infer the corrected beam profile.

The reflecting surface is polished so that the reflectivity is better than 98 percent for the wavelength range of 1.06 to 10.6 μm. The holes are drilled at an angle of 0.5 degrees off normal so that the reflecting surface prevents the reflected beam from returning to the laser. Copper has less than 2 percent absorption for these wavelengths. To do better would require plating the reflection surface of the prefilter with other metals and/or various layers of dielectric coatings. This action is most useful when a particular wavelength is under study. For the beam profile apparatus with multiple wavelengths, we cannot use the dielectric coatings; rather, we could reduce the total power loading of the laser beam by some beam splitters. For the allowed irradiance of 200 W/cm^2, we find that a 1 percent absorption level implies about a 200 W load for a cw beam of 10 cm in diameter. This is easily handled by water cooling a mounting plate holding the prefilter. Pulsed lasers have different limits which need to be carefully considered. For example, we need to define the class of pulse shapes that will strike the device so we can determine the likelihood of surface damage at each optical component.

To keep the calibration process simple, the structure of each hole should be alike. This means the diameter of the hole should expand rapidly in a cone structure so that the surface of the hole has little effect on the diffracted beam within the hole. Reference [27] gives a criteria for the rate of expansion of this hole. Ideally, the holes should not shadow the exiting laser beam. Of course, that is only possible if the depth of the hole is zero. We can use a finite thickness by requiring that the influence from the surface of the hole on the diffraction pattern be less than 10 percent. Because the variation between each hole is the important cause of errors and because it is very likely that each hole can be made alike within a 10 percent accuracy, we can expect these differences to imply around 1 percent changes in the phases. These changes are reasonable for correction by calibration. The ideal hole is

an expanding cone with an angle of 5^{o} or more. This means a 1 mm diameter initial hole at the reflection surface would expand to a 2 mm diameter hole on the exit side for a distance of 6 mm. Construction of such a cone would be costly, so the simplest approach is to drill a 2 mm diameter hole for the 5 mm depth on the exit side and finish the hole with a 1 mm diameter hole in the reflection surface. This last hole would then be reamed for the 5^{o} cone. This configuration should easily satisfy the constraint for calibrations to eliminate 1 percent differences between holes.

Constructing such a prefilter is estimated to cost about $4000 for a solid plate unit. For the electroforming approach, we estimate the cost to be about $10,000 for the mandrel with about $500 cost per copy. The electroform units could be constructed so that they are water-cooled throughout the prefilter.

9.5 The Hologram

Most discussion on the holograms was completed in section 8. Here we make tentative conclusions on construction costs.

Using our preliminary construction attempts of the bumpy surface holograms, we conclude that they can be built [22]. The exact number of cycles for applying thin films is still an unknown. Our present information shows that at least four can be applied. This is insufficient for a high accuracy hologram. We need at least 6 cycles for each sine wave. The two sine wave systems described in section 8 would need 12 such cycles. We conclude that a sine wave hologram cannot be constructed properly at this time. Rather, the binary surface hologram should be constructed for the reflection apparatus. This method requires only two thin-film applications on the polished mirror substrate. Although the discussion of section 8 shows that the binary methods have significant loss in efficiency, this is unimportant for measurement of high-power laser beams.

Using present metal turning and polishing capabilities [18,19], we can develop an optical quality flat of stainless steel with a surface roughness of 50 nm rms. By using chromium as the evaporation metal for creating either the binary or some complex bumpy surface, we can create a mandrel which allows electroforming of the copper hologram with appropriate bumpy surfaces. This electroforming process permits mass production of the holograms. Using the estimates for the mirrors in subsection 9.1, this mandrel would cost $4000 and the copies would cost $200 each [22]. Custom construction of a single binary surface hologram on a polished mirror substrate is estimated to cost $500 once the binary masks have been developed. The cost of development of the binary mask is a manpower issue. It is estimated to cost $4000 using the codes shown in section 8.

9.6 Support Equipment

This category refers to two types of equipment, namely that used to insure the structural integrity of the apparatus and that used in feedback loops to adjust dynamically the positions of parts.

The former represents the support plate of honeycomb material and the rigid box to hold all the mirrors, mounts, etc. This equipment should fix the distances between mirrors as well as other parts even if the apparatus is moved, the temperature of the apparatus changes, or the apparatus is stressed. Moving parts can change the calibration of the unit. If recalibration is possible between moves, then the rigidity can be reduced. We suggest that this is the appropriate design mode for the reflection apparatus. The rigidity needed for the other approach would add much weight to the unit which would affect the unit's mobility.

Dynamic tuning of the apparatus would dampen the effects of temperature changes and vibration but would retain calibration. This can be done with numerous solid-state lasers and detector arrays to measure relative movements of parts. By appropriate adjustments of the mirrors with stepping motors and a computer system to define the appropriate adjustments, it will be possible to keep the apparatus calibrated for a selected changes in temperature, vibration, and other such strains.

It is difficult to estimate the cost of this support equipment. An estimate is $5000 for the nondynamic part and $150,000 for the design, development, and implementation of the dynamic part. Most likely, the apparatus would be built without dynamic feedback. Then when the need for more accuracy and flexibility increased, the feedback system would be added.

Copies of the dynamic support are estimated to cost $15,000. This will be mainly for parts and assembly.

9.7 Necessary Machine Shop Work

We include this subsection because first-time assembly of an apparatus requires custom work. It is impossible to specify this work before purchased parts are received. As a rough rule of thumb, we would expect a 20 percent cost for such custom machining added to the cost of the basic parts. Thus, if the parts cost $100,000, we would expect an additional $20,000 cost for the fitting process. This estimate does not include unique or complicated elements such as the electronics. These costs require different estimates as already indicated in subsection 9.3.

10. CONCLUSIONS

Costs:

1. Using heavy-duty equipment, solid mirror, and other cost estimates, we estimate the cost for construction of the reflection apparatus without the electronics to be $200,000 (see figure 10.1 for a summary).

2. If electroforming is used wherever possible, the comparable apparatus without the electronics would cost $150,000. I assume this unit would be built after the heavy-duty unit so most learning would be made there.

3. Once the mandrels have been made, then the cost of the additional copies would be about $40,000. This number is probably even less firm than the previous estimates. We need data that are not available at this time to establish a better number.

4. The final completion of this apparatus requires substantial research and development of the detector and electronics package. Cost estimates at this time are guesses.

Error Estimates:

1. The first source of error arises from the quality of the prefilter. I estimate this prefilter will create errors around 1 percent. This can be reduced by calibration and by not overheating the surface of the prefilter.

2. The second source of error in the apparatus is the effects from the failure of the optics to have the ideal surfaces. Calibration can reduce these errors.

3. A third source of error can come from the scattering off the mirrors and the hologram due to the scratches and the rms types of surface fluctuations. This error cannot be removed by calibration and will limit the final accuracy of the measurements. I cannot estimate the size of this error at this time. It is presumed not to be significant for beam profiles with amplitude changes of less than 20 percent between sampled spots.

4. A fourth source of error comes from mechanical instabilities. Appropriate control can reduce this error. The largest error would come from vibration of the mirror at surface 10.

5. The fifth and final source of error arises from the detection and amplification processes. The amplitude part of the beam profile will have the least error since it is directly measured. The phase measurement error depends on the value of the phase. Briefly, individual measurements at each sampled signal should have precision better than 0.1 percent to be sure the phase precision is better than 1 percent. The actual structure for these phase errors is complex and requires careful analysis.

6. If extensive processing of the signals at surface 11 is available, the error signals from those signals with four beams contributing from the prefilter can improve the accuracy of the phase measurements to better than 1 percent.

Item	Heavy Duty	Electroform Initial	Copies of the Electroform	Discussed in Subsection
Mirror	32,000	14,400	1,400	9.1
Translation	15,200	4,000	4,000	9.2
Hologram (one wavelength only)	4,500	4,200	200	9.5
Support (static)	5,000	5,000	5,000	9.6
Prefilter (unpolished)	4,000	10,000	500	9.4
Subtotal	60,700	37,600	11,100	---
Shop Work (20 percent)	12,200	7,500	7,500	---
Labor for Assembly (about 1 man-year)	100,000	100,000	20,000	---
Grand Total	172,900	145,100	38,600	
Rounded to Reflect Accuracy of Estimate	$200,000	$150,000	$40,000	

Figure 10.1. Summary of estimated costs for construction of a standard for beam profile using the holographic method. We include the optics construction estimates only.

Various Questions Answered:

1. I have been asked, why build the holographic system. Would not the Hartmann plate system without optics be cheaper and just as accurate? To answer this question without direct comparison is not easy. The best we can do here is to list key differences between the two systems and show what happens. Briefly, the holographic system has higher accuracy potential for absolute measurements, but is significantly more complex and expensive. See the appendix for comparison.

2. It is possible to use this instrument without a beam splitter to look at high power beams? Yes. The 200 W/cm^2 limit is a substantial restriction. If the designer allows some form of distortion in location of the spots at surface 11 and causes the splitting process at the hologram into nine beams of each beam to take place anywhere on that hologram, the optics can be changed so that the portion of the Fourier transform of each beam from the prefilter is no longer the same for the other beams. In this case, we no longer have the coherent, N^2, type of contribution at the center of the holographic plate. We may have instead just an incoherent, N, type of contribution. This means that the allowed power density on the holographic plate can be increased by N. For this apparatus, we get a 60 kW/cm^2 restriction which means a potential 40 MW beam within the 10 cm diameter. In this case the prefilter will have to be water cooled and will have special reflection characteristics. The errors due to heating are likely to be significant and will have to be studied to assess their importance. The program, BEAM, can be used to simulate this configuration so we can have estimates of the extent of the distortions. Plasma ignition may occur and affect the accuracy of the measurement. This issue will need careful assessment.

3. What about the polarization? This apparatus can be calibrated for each state of linear polarization It is most likely that the values for the responsivity of the apparatus will change with these two polarization states. I do not know exactly how much change can take place because of this polarization dependence. We need to perform some preliminary measurements to get an estimate of its importance. Because the angles of reflection are small (θ = 0.14 rad) and because we expect the absorption in the mirrors to be less than 2 percent, it is expected at this time that polarization effects are insignificant compared to the errors due to rms scattering and due to the detection and amplification processes. The hologram will also induce some polarization dependence which is also expected to be insignificant compared to the errors just mentioned. This condition is expected because this hologram is a weak grating.

4. What about the detection and electronics part of this apparatus? There are significant construction costs for a detection system with 10 ns time response. Accepting a slower time response could allow use of present TV scanning equipment at much lower costs.

11. ACKNOWLEDGMENTS

I wish to thank F. Michael Maish of the Scientific Computing Division for helping me use its 32-bit Interdata computer system. I generated the computer code and simulation data from this machine. This effort could not have been done without this facility.

I further wish to thank Robert L. Hinebaugh, Major L. Fecteau, and Dr. Felix Schweizer of CCG for their kind support of this effort.

I have had many useful technical discussions with Dr. Matt Young, Dr. Stephen Jarvis, and Mr. Aaron Sanders relative to this system.

I wish to thank Phyllis J. O'Rourke and Shelley Etzel for their fine typing of this complex paper.

I thank Paul Werner for his prototype work, in which we identified the problems for construction of the bumpy surface hologram. This activity sharpened our understanding of what is needed to get useful, computer-generated holograms.

I thank Matt Weinburg for running the required simulations reported in this paper.

12. REFERENCES

[1] Johnson, Eric G., Jr., Laser Beam Profile Measurements Using Spatial Sampling, Fourier Optics, and Holography, NBS (U.S.), Tech. Note 1009, 96 pages (Jan. 1979).

[2] Panofsky, W. K. H., and Philips, M., Classical Electricity and Magnetism,pp. 176-182 (Addison-Wesley Publishing Co., 1955).

[3] Coburn, N., Vector and Tensor Analysis, pp. 80-83 (The Macmillan Company, 1955).

[4] Morse, P. M., and Feshback, H., Methods of Theoretical Physics, Vols. I and II, pp. 805-806 and 810-811 (McGraw-Hill, 1953).

[5] Born, M., and Wolf, E., Principles of Optics, pp. 203-232 and 460-490 (Pergamon Press, Third Edition, 1965).

[6] Cathey, W. T., Optical Information Processing and Holography, pp. 1-73 (John Wiley and Sons, 1973).

[7] Focke, J., Total illumination in an aberration-free diffraction image, Optica Acta 3, 161 (1956).

[8] Boshnyak, B. M., and Korolav, A. N., Synthesis of astimgatism-free condensers consisting of sperical mirrors, Opt. Spektrosk 43, 354, and Opt. Spectrosc., U.S.S.R., 43, 204 (1977).

[9] See [6] pages 106-109 for Fourier Transform Formulae and pages 116-118 for Imaging Formulae.

[10] Hudson, Richard D., Jr., Infrared System Engineering (John Wiley and Sons, 1969).

[11] Danielson, B. L., Beers, Y., Laser Attenuators for the Production of Low Power Beams in the Visible and 1.06 μm Regions, NBS (U.S.), Tech. Note 677, 25 pages (Jan. 1976).

[12] O'Neil, R. W.. Kleiman, H., Marquet, L. C., Kilcline, C. W., and Norham, D., Beam diagnostics for high energy pulsed CO_2 laser, Applied Optics 13, 314 (1974).

[13] Brown, B. R., and Lohman, A. W., Complex spatial filtering with binary masks, Applied Optics 5, 967 (1966).

[14] Gallagher, Neal C., Jr., Angue, John C., Coffield, Frederick E., Edwards, Robert V., and Mann, J. Adin, Jr., Binary phase digital reflection holograms: Fabrication and potential applications, Applied Optics 16, 413 (1977).

[15] Haskell, Richard, Synthetic holograms and kinoforms, Optical Engineering 14, 195 (1975).

[16] Haskell, R. E., and Culver, B. C., New coding techniques for computer generated holograms, Applied Optics 11, 1712 (1972).

[17] Harris, Richard E., A pattern generating code, written to produced gyrex machine code on the CDC 6600. Contact the Cyroelectronics section of the Electromagnetic Technology Division, Boulder, Colorado.

[18] See Optical Spectra, page 26 (Aug. 1978) and pages 30-34 (Sept. 1978).

[19] Denny, Cy, of the Spawr Optical Research, private communications.

[20] Spawr, Walter J., Pierce, Richard L., Metal mirror selection guide, SOR Report No. 74-004, Spawr Optical Research, Inc. (1976).

[21] Biddle, Philip E., of the NBS Machine Shop at Boulder, Colorado, and Werner, Paul, of the Optical Electronic Metrology Section in the Electromagnetic Technology Division, private communications.

[22] Pickel, Jeff, of Pickel Industries, Inc., private communications.

[23] See various manufacturers' cost lists for such units.

[24] Brown, Hugh B., Markevitch, Bob V., Radar signal optical processor, paper presented at Effective Utilization of Optics in Radar Systems, conference sponsored by BMDATC/SPIE, Huntsville, Ala. (Sept. 27-29, 1977).

[25] Bleha, W. P., Lipton, L. T., Wierner-Avnear, E., Ginberg, J., Reif, P. G., Casasent, David, Brown, H. B., and Markevitch, B. V., Application of the liquid crystal light value to real time optical data processing, Optical Engineering 17, 371 (1978).

[26] See [25] for concepts. Further development would be necessary to apply this unit to this apparatus.

[27] See [5], page 444.

[28] Gillespie, R. W., Wick, R. V., and Saxman, A. C., Laser Wavefront Profiling Techniques for Pulse Radiation NTIS Code ΔAD-A011 944/6ST Report(1975).

[29] Workum, Captain John Van, Plascyk, James A., and Skolnick, Michael L., Laser wavefront analyzer for diagnosing high-energy lasers, SPIE 141, Adaptive Optical Components (1978).

[30] Hardy, John W., and Hudgin, Richard H., A comparison of wavefront sensing systems, SPIE 141, 67 (1978).

[31] Wetzstein, Hanns J., A tutorial review of key system aspects of wavefront measurements, control and conjugation, SPIE 141, 32 (1978).

[32] Hardy, John W., Active optics: A new technology for the control of light, Proc. of the IEEE 66, 651 (1978).

13. APPENDIX--THE HARTMANN PLATE METHOD

I define a conceptually perfect system for measuring beam profile using only the Hartmann plate and the necessary electronics at the required far field of each hole in this plate [28]. To allow as close a comparison as possible to the holographic method, the key constraints applied to it are also imposed on the Hartmann plate [1].

Before addressing the details of this comparision, I make five points:

1. This discussion examines only how to make the most accurate beam profile measuring unit that can respond to time changes in the profile that are faster than 1 ms. For those changes slower than 1 ms, the wavefront analyzer unit has superior characteristics [29]. Assuming this unit can preserve its calibration, it appears

to be the best for high accuracy measurements of phase front because there are no significant limitations in the spatial sampling of the wavefront.

2. For the time changes faster than 1 ms, the Hartmann plate is definitely better than the holographic method if the rms variations along the phase front between each sampled point exceed π. The holographic method cannot identify uniquely the relative phase between sampling holes if this phase exceeds π. This ambiguity means that the Hartmann method should be used with laser beams that have rapidly changing phase structure, i.e., moderate beam quality as well as moderate directional control.

   If the structure of the beam profile is known in advance, then some modified version of the holographic system could be better than the Hartmann plate because the number of detectors could be substantially reduced (see discussion of field instrument in reference [1]).

3. The ultimate accuracy of the holographic method is controlled by the noise of the electronics. All other potential errors appear to be removable by calibration. As already discussed in the conclusion and section 7, the noise of the electronics implies that the phase error can approach 1% even if we have measurements with 0.1% accuracy of the power at each spot. In addition, we have seen [1] that the dynamic range for the phase must be restricted to $0 \leq \alpha \leq \pi$, if we are to have uniqueness. These facts represent what the Hartmann plate method should accomplish to be equal to or better than holographic method. Therefore, I require the Hartmann plate to have 1 percent accuracy and a dynamic range of π for the phase measurement. In this case, the phase will range: $-\pi/2 \leq \alpha \leq \pi/2$.

4. The sampling holes at the plate are the same as those in the prefilter, namely 1 mm diameter. This diameter represents the current capability for direct and consistent drilling in the substrate. If the diameter must be made smaller, then both methods can be adjusted to reflect the change. The critical conclusions in this exercise are unchanged by the reduction of this sampling diameter.

5. To compare the two methods we design the Hartmann apparatus to the above accuracy and sampling conditions. This exercise shows that the Hartmann technique has intrinsically a lower spatial sampling than the holographic method for comparable accuracy. For simplicity, I ignore the noise of the electronics for the Hartmann system. If such information becomes available on that noise before the appropriate beam profile devices have been selected, then that data should be used.

I now discuss the Hartmann plate. I follow these four steps:

1. I use the far-field criteria of [1], namely:

$$k \left(\frac{d_1}{2}\right)^2 / z \leq \pi/10$$

with $k = 2\pi/\lambda$ to fix some distances. This implies $\lambda z \geq 5(\mathrm{mm})^2$ with $d_1 = 1$ mm. Thus, $z \geq 0.5$ m for $\lambda = 10.6$ µm, and $z \geq 5$ m for $\lambda = 1.06$ µm. In this analysis, we use $\lambda z = 5(\mathrm{mm})^2$ as the smallest allowed distance for the far field of each hole.

2. The phase equation relates to the displacement of the Airy disc at the far field as $\alpha = kd_1 x/z$. We only look at the x coordinate for this discussion. The maximum displacement has $\alpha = \pi/2$, and implies $x \equiv x_1 = 1.25$ mm. We estimate the accuracy for measuring this position with a square array of detectors. Each detector has a net dimension of 10 μm for each coordinate. This spatial quanta implies a position accuracy of 0.5 percent for the ± 1.25 mm range. We conclude that the accuracy of the Hartmann system is comparable to that of the holographic apparatus (using the above far-field criteria). We continue this evaluation to see what this comparable accuracy implies.

3. The diameter, d_2, of the Airy disk at this distance is $d_2 = 2.44\ \lambda z/d_1 = 12.2$ mm.

4. The dynamic range, s, of each sampling cell in the far field is given as $s = 2x_1 + d_2 = 14.7$ mm.

The cell size deduced in step 4 is only possible if there are shields separating each cell to prevent overlap of the Airy patterns. If the shields cannot properly work, then the size of each cell must be increased. For example, allowing at least three rings of the Airy pattern in the cell dimension instead of the single ring causes a new s, namely:

$$s = 2x_1 + (3.24/1.22)d_2 = 2.5 + 32.4 = 34.9 \text{ mm.}$$

These cell diameter results imply the allowed sampling interval for the Hartmann plate equal 15 to 35 mm. Remember, s = 5 mm for the holographic method. Thus the Hartmann method has 1/3 to 1/7 as much detail as that for the holographic method.

If we want comparable sampling frequencies for both the Hartmann and the holographic methods, then we must use lenses in the Hartmann system. We need one lens for each sampling hole. That action allows us to get the far field at the focal plane of each lens and hence reduces the sampling interval. Remember, $s = 5 \text{ mm} = (\lambda z)(0.5 + n)$ where n is the factor designating the number of rings within the sampling area. The table below summarizes the results.

	one ring	three rings
λz =	1.7 (mm)^2	0.72 (mm)^2
n =	2.44	6.48
x =	0.43 mm	0.18 mm
resolution error		
using 10 μm =	1.2 percent	2.5 percent for full scale

These results show that the Hartmann technique is about 1/2 to 1/3 as accurate as the holographic method. (See references [30], [31], and [32] for additional perspective.)

The ability to check the calibration status in real time of an apparatus is one important difference between the Hartmann and holographic unit. The Hartmann unit cannot be so checked but the holographic unit can be.

To calibrate the Hartmann unit requires (1) a known wavefront that can illuminate at least two holes in each coordinate, (2) the assumption that the unknown and known laser beams do not distort the unit during a measurement, and (3) a means to displace the calibration beam for illuminating other holes in the plate without shifting in the direction of the phase front. This calibration process is not precise because the results have no direct estimates of errors.

In contrast, the holographic unit permits a real-time confirmation of the errors. The measurements of signals where four beams contribute provide significant redundancy of information about the beam profile. By subtracting a calculated response using the measured results from the appropriate single and two beam signals to predict the expected signal at a chosen location where four beams contribute from the measured response at the same position, we have one data point for a consistancy test in beam profile measurements. Extending this procedure to all measured signals in real time gives us direct error estimates in the beam profile during a laser pulse.

In summary, the Hartmann unit does not generate the required error signals; therefore, it is not an appropriate device for a standard. Under measurement situations where the conditions for errors in measurement are known (namely, the Hartmann plate which has been calibrated by the holographic method), then the Hartmann unit could be used for beam profile measurements.

NBS-114A (REV. 9-78)

U.S. DEPT. OF COMM. BIBLIOGRAPHIC DATA SHEET	1. PUBLICATION OR REPORT NO.	2. Gov't. Accession No.	3. Recipient's Accession No.
	NBS TN-1015		

4. TITLE AND SUBTITLE

Design of a Reflection Apparatus for Laser Beam Profile Measurements

5. Publication Date

July 1979

6. Performing Organization Code

7. AUTHOR(S)

Eric G. Johnson, Jr.

8. Performing Organ. Report No.

9. PERFORMING ORGANIZATION NAME AND ADDRESS

NATIONAL BUREAU OF STANDARDS
DEPARTMENT OF COMMERCE
WASHINGTON, DC 20234

10. Project/Task/Work Unit No.

11. Contract/Grant No.

Contract 78-109

12. SPONSORING ORGANIZATION NAME AND COMPLETE ADDRESS *(Street, City, State, ZIP)*

Sponsored in part by: DoD
Calibration Coordination Group

13. Type of Report & Period Covered

14. Sponsoring Agency Code

15. SUPPLEMENTARY NOTES

☐ Document describes a computer program; SF-185, FIPS Software Summary, is attached.

16. ABSTRACT *(A 200-word or less factual summary of most significant information. If document includes a significant bibliography or literature survey, mention it here.)*

Measurement of both the irradiance and phase front (the beam profile) in real time from the output of a laser has interest for control of that beam and for efficient energy and economic design of the source and the resulting optical systems. The National Bureau of Standards (NBS) has begun a program to build a unit that can measure, at numerous wavelengths from 1.06 μm to 10.6 μm, a selected spatial sample of the beam profile. This device would have the following features: (1) The different carrier wavelengths use the same apparatus by changing two mirrors. (2) The beam profile is sampled simultaneously with no time-shift distortions. (3) The output data streams documenting the sampled beam profile are continuous and are distorted only by the finite number and the time constants of the detectors. (4) The phase-front information is generated before the detectors create the data streams. (5) The apparatus uses mirrors and a reflection hologram that is computer generated. (6) The unit is calibrated piecewise over the range of relative phase and irradiances for each pair of neighboring sampling holes which are 5 mm apart. (7) The resulting calibrated unit can measure profiles near 10 cm in diameter with phase-front variations of less than 5 wavelengths. (8) The expected response time for measurements as controlled by the electronics is of the order of several tens of nanoseconds.

The design analysis reported here includes: (1) the theory which uses Fourier optics concepts with off-axis reflections and rough surfaces to provide the basis for accurate computer simulation of laser beams; (2) the program, BEAM, which generates the expected behavior of the apparatus under variation of laser wavelength, physical dimensions for curvatures, hologram structure, and changes in positions of the various components; (3) the simulation results which demonstrate the expected characteristics for the apparatus; and (4) the key element in the apparatus, namely the reflection hologram, which requires discussion of the design, construction, and testing of this element.

The Hartmann plate method is described briefly so that a comparison between it and the holographic method can be made. The comparison shows why the holographic method is best for a standard for irradiance and phase-front measurements.

17. KEY WORDS *(six to twelve entries; alphabetical order; capitalize only the first letter of the first key word unless a proper name; separated by semicolons)*

Key words: Beam profile; calibrated system; holography; irradiance; laser diagnostics; phase front.

18. AVAILABILITY ☒ Unlimited

☐ For Official Distribution. Do Not Release to NTIS

☒ Order From Sup. of Doc., U.S. Government Printing Office, Washington, DC 20402, SD Stock No. SN003-003- 02103-2

☐ Order From National Technical Information Service (NTIS), Springfield, VA. 22161

19. SECURITY CLASS (THIS REPORT)	21. NO. OF PRINTED PAGES
UNCLASSIFIED	122
20. SECURITY CLASS (THIS PAGE)	**22. Price**
UNCLASSIFIED	$4.00

☆ U.S. GOVERNMENT PRINTING OFFICE: 1979-0-677-072/1297 USCOMM-DC

NBS TECHNICAL PUBLICATIONS

PERIODICALS

JOURNAL OF RESEARCH—The Journal of Research of the National Bureau of Standards reports NBS research and development in those disciplines of the physical and engineering sciences in which the Bureau is active. These include physics, chemistry, engineering, mathematics, and computer sciences. Papers cover a broad range of subjects, with major emphasis on measurement methodology, and the basic technology underlying standardization. Also included from time to time are survey articles on topics closely related to the Bureau's technical and scientific programs. As a special service to subscribers each issue contains complete citations to all recent NBS publications in NBS and non-NBS media. Issued six times a year. Annual subscription: domestic $17.00; foreign $21.25. Single copy, $3.00 domestic; $3.75 foreign.

Note: The Journal was formerly published in two sections: Section A "Physics and Chemistry" and Section B "Mathematical Sciences."

DIMENSIONS/NBS (formerly Technical News Bulletin)—This monthly magazine is published to inform scientists, engineers, businessmen, industry, teachers, students, and consumers of the latest advances in science and technology, with primary emphasis on the work at NBS. The magazine highlights and reviews such issues as energy research, fire protection, building technology, metric conversion, pollution abatement, health and safety, and consumer product performance. In addition, it reports the results of Bureau programs in measurement standards and techniques, properties of matter and materials, engineering standards and services, instrumentation, and automatic data processing.

Annual subscription: Domestic, $11.00; Foreign $13.75

NONPERIODICALS

Monographs—Major contributions to the technical literature on various subjects related to the Bureau's scientific and technical activities.

Handbooks—Recommended codes of engineering and industrial practice (including safety codes) developed in cooperation with interested industries, professional organizations, and regulatory bodies.

Special Publications—Include proceedings of conferences sponsored by NBS, NBS annual reports, and other special publications appropriate to this grouping such as wall charts, pocket cards, and bibliographies.

Applied Mathematics Series—Mathematical tables, manuals, and studies of special interest to physicists, engineers, chemists, biologists, mathematicians, computer programmers, and others engaged in scientific and technical work.

National Standard Reference Data Series—Provides quantitative data on the physical and chemical properties of materials, compiled from the world's literature and critically evaluated. Developed under a world-wide program coordinated by NBS. Program under authority of National Standard Data Act (Public Law 90-396).

NOTE: At present the principal publication outlet for these data is the Journal of Physical and Chemical Reference Data (JPCRD) published quarterly for NBS by the American Chemical Society (ACS) and the American Institute of Physics (AIP). Subscriptions, reprints, and supplements available from ACS, 1155 Sixteenth St. N.W., Wash., D.C. 20056.

Building Science Series—Disseminates technical information developed at the Bureau on building materials, components, systems, and whole structures. The series presents research results, test methods, and performance criteria related to the structural and environmental functions and the durability and safety characteristics of building elements and systems.

Technical Notes—Studies or reports which are complete in themselves but restrictive in their treatment of a subject. Analogous to monographs but not so comprehensive in scope or definitive in treatment of the subject area. Often serve as a vehicle for final reports of work performed at NBS under the sponsorship of other government agencies.

Voluntary Product Standards—Developed under procedures published by the Department of Commerce in Part 10, Title 15, of the Code of Federal Regulations. The purpose of the standards is to establish nationally recognized requirements for products, and to provide all concerned interests with a basis for common understanding of the characteristics of the products. NBS administers this program as a supplement to the activities of the private sector standardizing organizations.

Consumer Information Series—Practical information, based on NBS research and experience, covering areas of interest to the consumer. Easily understandable language and illustrations provide useful background knowledge for shopping in today's technological marketplace.

Order **above** *NBS publications from: Superintendent of Documents, Government Printing Office, Washington, D.C. 20402.*

Order **following** *NBS publications—NBSIR's and FIPS from the National Technical Information Services, Springfield, Va. 22161.*

Federal Information Processing Standards Publications (FIPS PUB)—Publications in this series collectively constitute the Federal Information Processing Standards Register. Register serves as the official source of information in the Federal Government regarding standards issued by NBS pursuant to the Federal Property and Administrative Services Act of 1949 as amended, Public Law 89-306 (79 Stat. 1127), and as implemented by Executive Order 11717 (38 FR 12315, dated May 11, 1973) and Part 6 of Title 15 CFR (Code of Federal Regulations).

NBS Interagency Reports (NBSIR)—A special series of interim or final reports on work performed by NBS for outside sponsors (both government and non-government). In general, initial distribution is handled by the sponsor; public distribution is by the National Technical Information Services (Springfield, Va. 22161) in paper copy or microfiche form.

BIBLIOGRAPHIC SUBSCRIPTION SERVICES

The following current-awareness and literature-survey bibliographies are issued periodically by the Bureau:

Cryogenic Data Center Current Awareness Service. A literature survey issued biweekly. Annual subscription: Domestic, $25.00; Foreign, $30.00.

Liquified Natural Gas. A literature survey issued quarterly. Annual subscription: $20.00.

Superconducting Devices and Materials. A literature survey issued quarterly. Annual subscription: $30.00. Send subscription orders and remittances for the preceding bibliographic services to National Bureau of Standards, Cryogenic Data Center (275.02) Boulder, Colorado 80302.

U.S. DEPARTMENT OF COMMERCE
National Bureau of Standards
Washington, D.C. 20234

OFFICIAL BUSINESS

Penalty for Private Use, $300

POSTAGE AND FEES PAID
U.S. DEPARTMENT OF COMMERCE
COM-215

U.S.MAIL

SPECIAL FOURTH-CLASS RATE
BOOK